Aus dem Medizinische Zentrum für Hygiene und Infektionsbiologie
Institut für Virologie
Geschäftsführender Direktor: Prof. Dr. Hans-Dieter Klenk
des Fachbereichs Medizin der Philipps-Universität Marburg

Function of the Viral Matrix Proteins VP40 and VP24 for the Life Cycle of Ebola Virus

Inaugural-Dissertation zur Erlangung des Doktorgrades der Humanbiologie
dem Fachbereich Humanmedizin der Philipps Universität Marburg
vorgelegt von

Thomas Hoenen aus Aachen

Marburg, 2006

Angenommen vom Fachbereich Humanmedizin der Philipps-Universität Marburg am 5.1.2007.

Gedruckt mit Genehmigung des Fachbereichs.

Dekan: Prof. Dr. Maisch
Referent: Prof. Dr. Becker
Koreferent: Prof. Dr. Garten

This thesis is dedicated to

Monika Ochel and **Wolfgang Reinert**

who have most influenced me to become a scientist.

Contents

1 Introduction

1.1 Taxonomy and classification

Ebola viruses (EBOV) and the closely related Marburg viruses (MARV) make up the family *Filoviridae* in the order *Mononegavirales* [50] (Figure 1). The genus *Ebolavirus* is divided into 4 species: *Zaire ebolavirus* (ZEBOV), *Reston ebolavirus* (REBOV), *Sudan ebolavirus* (SEBOV) and *Cote d'Ivoire ebolavirus* (CIEBOV). With the exception of REBOV they all cause severe hemorrhagic fevers in humans with high case fatality rates. Since there is currently no approved treatment or vaccination available, and due to their high lethality, filoviruses are classified as biosafety level (BSL) 4 agents [53], as well as category A biothreat agents [21]. Information given in this thesis, unless otherwise stated, relates to ZEBOV (strain Mayinga).

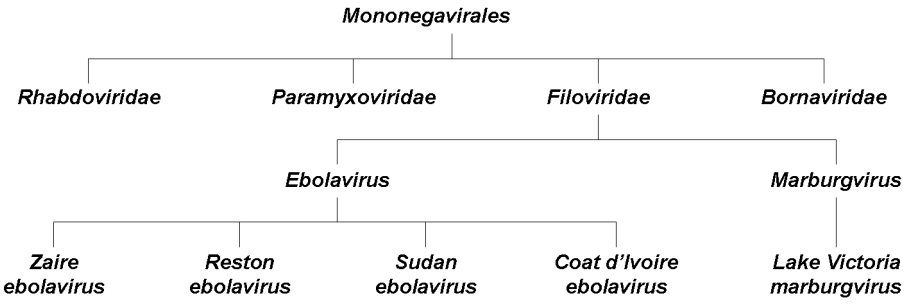

Figure 1: **Taxonomy of Filoviruses.**

1.2 Genome organization

Ebola viruses contain a non-segmented single-stranded negative-sense RNA genome of approximately 19 kB length [168]. The RNA is non-infectious and does not contain a poly-A tail [157]. The gene order is conserved among filoviruses and is 3' - leader - NP - VP35 - VP40 - sGP/GP - VP30 - VP24 - L - trailer - 5' (Figure 2) [54, 168]. At the 3' and 5' ends of the genome nontranscribed regions can be found (leader and trailer), which are partially complementary to each other, a common feature among *Mononegavirales* [53]. These ends contain the signals minimally required for replication, transcription and packaging of the viral genomic RNA (vRNA) and replication of the viral antigenomic RNA (cRNA) [139]. Transcriptional start and stop signals for each gene are conserved among filoviruses

and have the consensus sequence 3'-CUNCNUNUAAUU-5' and 3'-UAAUUCUUUUU-5', respectively [53, 168]. The genes are either separated by intergenic regions or have overlapping start and stop signals (Figure 2) [168]. One among filoviruses unique feature of EBOV is that the fourth gene encodes for at least two proteins, the second of which is expressed after insertion of an additional adenosine into the mRNA at a stretch of seven adenosines (transcriptional editing, see section 1.4.4) [171, 199].

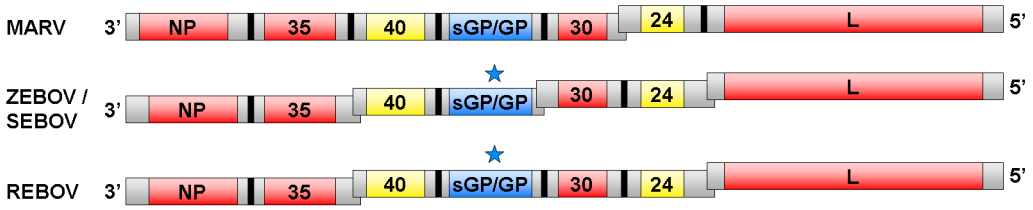

Figure 2: **Genome organization of Filoviruses.** The gene orders of fully sequenced filovirus genomes are presented. Intergenic regions are shown in black, non-coding regions in grey and open reading frames in red for genes encoding nucleocapsid proteins, yellow for genes encoding matrix proteins or blue for the gene encoding the viral glycoproteins. Steps indicate the position of gene overlaps and asterisks indicate the position of the RNA editing site in the EBOV genomes. Adapted from [78] with kind permission of the author.

1.3 Virion morphology

EBOV particles usually form long filamentous rods with a uniform diameter of approximately 80 nm and a mean length of approximately 1250 nm (Figure 3) [70]. Virions formed like the number 6 and circular forms also appear, but are comparatively rare [70]. The centre of the particles is made up of the ribonucleoprotein (RNP) complex (Figure 4), which consists of the nucleoprotein (NP), the virion protein (VP) 35, VP30, the RNA-dependent RNA polymerase (L) and the vRNA, and has a diameter of about 50 nm [70]. Virions are enveloped by a host cell derived lipid bilayer, in which the surface glycoprotein (GP) is inserted as 5 to 10 nm long spikes. The space between the viral envelope and the RNP complex is the so called matrix space, in which VP40 and VP24 are located [45, 110].

1.4 Viral proteins

1.4.1 Nucleoprotein

The nucleoprotein (NP) is the product of the first gene and, with 739 amino acids, the longest nucleoprotein of any member of *Mononegavirales* (Figure 5) [169]. NP has a calcu-

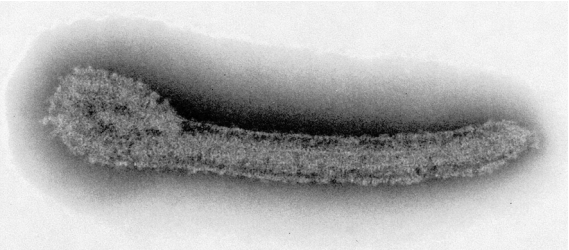

Figure 3: **Electron micrograph of an EBOV particle.** Virus particle was visualized following negative staining. Figure kindly provided by Dr. Larissa Kolesnikova.

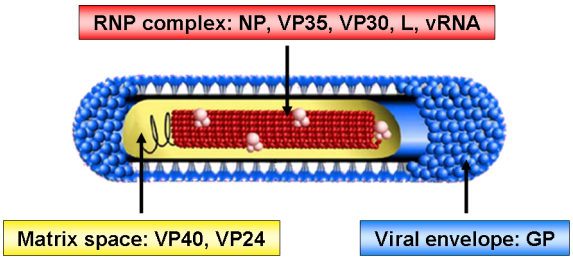

Figure 4: **Schematic drawing of an EBOV particle.** The nucleocapsid complex is drawn in red, the matrix space in yellow and the viral envelope with the surface glycoprotein GP in blue. Figure kindly provided by Dr. Sandra Bamberg.

lated molecular weight of 83 kDa [169] and an apparent molecular weight of 104 kDa when subjected to SDS-PAGE [110], and is an important component of the RNP complex. The protein can be divided into a hydrophobic N-terminal half and a hydrophilic C-terminal half [169]. EBOV NP, as well as MARV NP, is phosphroylated, and in both cases only the phosphorylated form is found inside virions while, at least for MARV, both phosphorylated and unphosphorylated NP can be found inside cells [14, 45]. Several reports suggest that EBOV NP is also glycosylated, although the exact type of glycosylation remains unknown [97, 211].

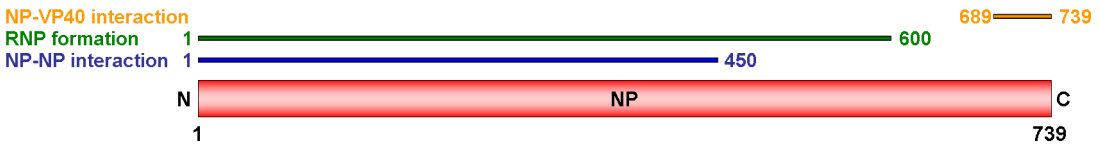

Figure 5: **Schematic drawing of NP.** The self-interaction domain is marked in blue, the region necessary for RNP formation in green and the putative interaction domain with VP40 in orange.

After infection, filoviral NP is localized in characteristic inclusion bodies in the cytoplasm of cells [19, 70], and singular expression of either EBOV or MARV NP leads to formation of similar inclusion bodies [16, 134]. Interestingly, when filoviral NP is coexpressed with either VP35 or VP30, it recruits these proteins into the inclusion bodies, which indicates interaction between NP and VP35 as well as between NP and VP30 [16, 134, 135]. For EBOV NP the interaction with VP35 has been confirmed by coimmunoprecipitation, and it has been shown that this interaction is dependent on posttranslational modification of NP [97].

EBOV NP is able to interact with itself, and the interaction domain has been mapped

to the amino acids 1 to 450 [211]. Upon single expression, NP forms tubular structures inside cells with a diameter of 25 nm, while coexpression of NP, VP35 and VP24 leads to the formation of nucleocapsid-like structures [97, 147, 211]. EBOV NP is thought to encapsidate the viral RNA, and for MARV NP this has been shown experimentally [131]. It is also necessary for transcription and replication of viral RNA [139]. Further, NP seems to interact with VP40, which might be important during morphogenesis, and it has been suggested that the 50 C-terminal amino acids of NP are important for this interaction, although this finding is debated (see also section 4.4.5) [121]. Interestingly, the region from amino acid 601 to 739 is not required for RNP complex formation or for replication and transcription of the viral genome [211].

1.4.2 Virion protein 35

The second gene of the EBOV genome encodes VP35, a 340 amino acid long protein with an apparent molecular weight of approximately 37 kDa (Figure 6). Due to its position in the genome, it has been suggested to be an analogue of the phosphoprotein (P) of other members of *Mononegavirales* [139]. However, in contrast to these proteins VP35 is only weakly phosphorylated in the case of MARV VP35 [15], while for EBOV VP35 no phosphorylation could be detected [45]. On the other hand, VP35 seems to serve as the polymerase cofactor [139], which is the classical function for P proteins of *Mononegavirales* [216]. Confirming this role is the finding that VP35 and L interact with each other for both EBOV and MARV [16, 20]. Recently, it has also been reported that VP35 is able to interact with both VP40 and viral RNA, and has been suggested to be responsible for specific packaging of vRNA into budding virions [108]. Beside these interactions and the previously mentioned interaction with NP (see section 1.4.1), VP35 is also able to interact with itself via a coiled-coil motif and to form homotrimers [135, 158], which have been shown to be essential for the function of VP35 in transcription and replication [135].

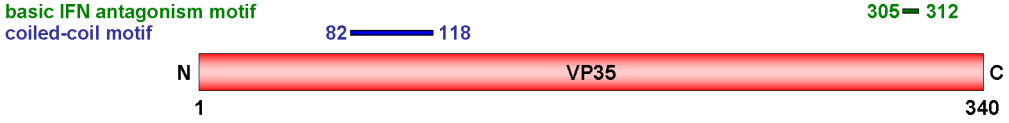

Figure 6: **Schematic drawing of VP35.** The homo-oligomerization domain is marked in blue, the region necessary for IFN antagonism and putative dsRNA binding in green.

Another function for VP35 is its interferon (IFN) antagonism by blocking of virus-induced interferon production [12]. VP35 blocks virus-induced phosphorylation and activation of the IFN regulatory factor 3 (IRF-3), activation of which induces an antiviral state in the cell [10]. For IFN antagonism trimerization as well as a C-terminal basic region from amino acid 305 to 312 is important [90, 158]. Based on homology to the NS1 protein of influenza it has been suggested that this region might be involved in dsRNA binding [90], a finding that was recently experimentally confirmed [29].

1.4.3 Virion protein 40

VP40 is encoded by the the third gene of the EBOV genome and is 326 amino acids long (Figure 7). It has a calculated molecular weight of 35 kDa and an apparent molecular weight of 39 kDa. The X-ray crystal structure of this protein has been determined [39, 40], and it could be shown that VP40 consists of two domains which are connected by a flexible linker (Figure 8). Each domain consists of 2 antiparallel β-sheets with three β-strands each (Figure 9), and it has been suggested that both domains arose from a common ancestor by gene duplication [40]. The C-terminal domain has been shown to associate with lipid membranes [104, 162], and this interaction induces a conformational change in VP40 which leads to oligomerization [179]. It has been proposed that upon membrane binding the C-terminal domain moves away from the N-terminal domain, which exposes the region responsible for oligomerization in the N-terminal domain [162, 179].

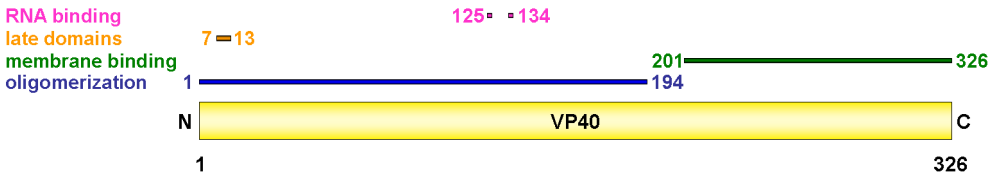

Figure 7: **Schematic drawing of VP40.** The N-terminal oligomerization domain is marked in blue, the C-terminal membrane binding domain in green. The two overlapping late-domains are marked in orange, and the amino acids responsible for RNA binding in pink.

There are two oligomeric forms of VP40, which have been identified by electron microscopy and/or X-ray crystalization, namely hexamers [162, 179] and octamers [76, 192]. Both forms are made up of antiparallel dimers, and it has been suggested that stable dimers also exist on their own [192]. The crystal structure for VP40 octamers has been determined [76], and it has been shown that VP40 octamers form ring-like structures with a central

pore of 17Å (Figure 10). Interestingly, these octamers bind RNA containing an 5'-UGA-3' trinucleotide in a specific manner (Figure 11) [76], and it was shown that this interaction is mediated by the amino acids F125 and R134 and is essential for octamerization [96]. The exact functions of RNA-binding and VP40 octamerization, as well as a function for VP40 hexamers, is so far unknown [89, 103]. However, recently, we were able to show that VP40 octamers are indispensable in the viral life cycle [96].

The classical function of matrix proteins for negative-sense RNA viruses and retroviruses

Figure 8: **Crystal structure of VP40.** VP40 is drawn in ribbon representation. Flexible regions for which a structure could not be determined are omitted.

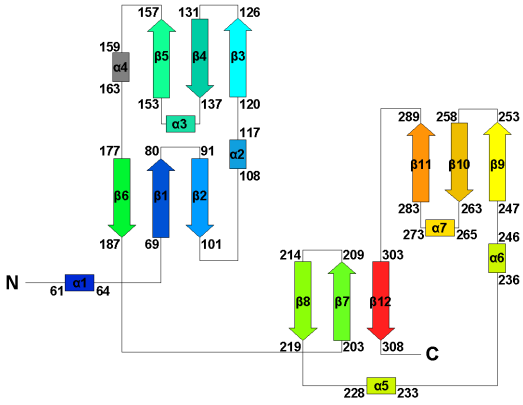

Figure 9: **Topology cartoon of VP40.** α-helices are drawn as boxes, β-strands as arrows. The colour of each secondary structure element matches its colour in Figure 8.

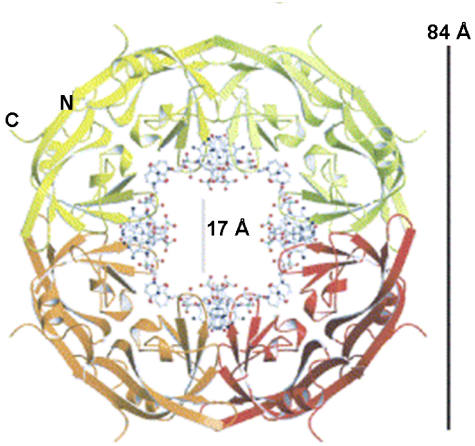

Figure 10: **Crystal structure of the VP40 octamer.** VP40 is drawn in ribbon representation. RNA at the dimer-dimer interfaces is drawn as an all-atom model. Reproduced from [76] with kind permission of the publisher.

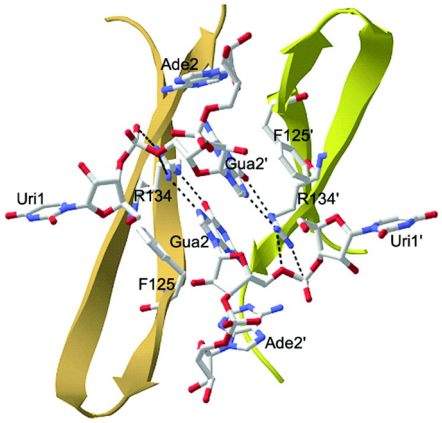

Figure 11: **RNA-binding site in the VP40 octamer.** Close-up of two adjacent VP40 monomers in ribbon representation (orange and green) with the bound RNA as an all-atom model. The amino acids important for RNA binding (F125, R134) are indicated. Polar interaction mediated by R134 are indicated by broken lines.

is to facilitate budding of progeny virions [173]. VP40 is able to induce the formation of VLPs which show the characteristic thread-like appearance of filoviruses, illustrating this function [104, 122, 148, 194]. Budding activity has been mapped to two overlapping late domain motifs at the N-terminus of VP40, 7-PTAPPEY-13, disruption of which strongly diminuished production of VLPs *in vitro* [91, 104, 122]. Late-domain motifs, which were first described in HIV, are essential for budding of a number of negative-sense RNA viruses and retroviruses [63, 173], and mediate interaction with components of the ensomal sorting complexes required for transport (ESCRT) (reviewed in [4]). In particular, the P[T/S]AP motif of EBOV has been shown to interact with TSG101 [122, 130, 193], while the PPXY motif interacts with the ubiquitin ligase Nedd4 [91, 193, 223]. Interestingly, only oligomeric VP40 is able to interact with Nedd4 [193], suggesting a role for oligomerization in virus budding. In an uninfected cell the ESCRT complexes facilitate the formation of multivesicular bodies (MVBs), which play an important role in degradation of transmembrane proteins [4]. It has been suggested that EBOV "hijacks" these cellular complexes to the host cell membrane where they participate in membrane evagination and particle release [103]. Alternatively, budding might occur into MVBs, as has been shown to take place for MARV [112]. Interestingly, a recent study has demonstrated that late domains are not absolutely required for EBOV replication in tissue culture by using a recombinant EBOV with mutated late domain motifs. This suggests that there might be an alternative pathway for virus budding [142]. Also, other proteins such as GP and NP, while not sufficient for the formation of filamentous VLPs on their own, have been shown to increase budding efficiency [108, 121] and, therefore, might play a role in budding independent of late domains.

1.4.4 Glycoprotein

The EBOV surface glycoprotein $GP_{1,2}$ is encoded by the fourth gene of the EBOV genome in two reading frames and, therefore, requires transcriptional editing for expression (Figure 12) [171, 199]. This editing occurs at a stretch of 7 adenosines and involves the insertion of an 8th adenosine into the mRNA, thus shifting the reading frame [171, 199]. In addition to the membrane-anchored $GP_{1,2}$ there are three soluble forms of the glycoprotein: (i) the soluble glycoprotein sGP [172], which is expressed in the absence of transcriptional editing, (ii) Δ-peptide, the smaller cleavage fragment of the precursor of the soluble gly-

coprotein [56], and (iii) $GP_{1,2\Delta}$, the product of cleavage of surface expressed $GP_{1,2}$ by the metalloprotease TACE [41]. Since transcriptional editing occurs in approximately 20% of transcripts, the majority of produced glycoprotein is sGP [171, 199], which can be detected in the blood of acutely infected patients in high concentrations [171]. A fifth glycoprotein species, soluble GP_1, which is probably released from $GP_{1,2}$ by breakdown of the disulfide bridge between GP_1 and GP_2 has been detected in tissue culture supernatant of infected HeLa cells [205], but since it can not be detected in supernatant of several other infected cell lines nor in infected animals, a biological role for this protein has been questioned [41]. Also, a sixth glycoprotein (ssGP) has been detected *in vitro*, which is produced after either insertion of two or deletion of one adenosine residues, but its relevance in an infection is completely unknown [199, 206].

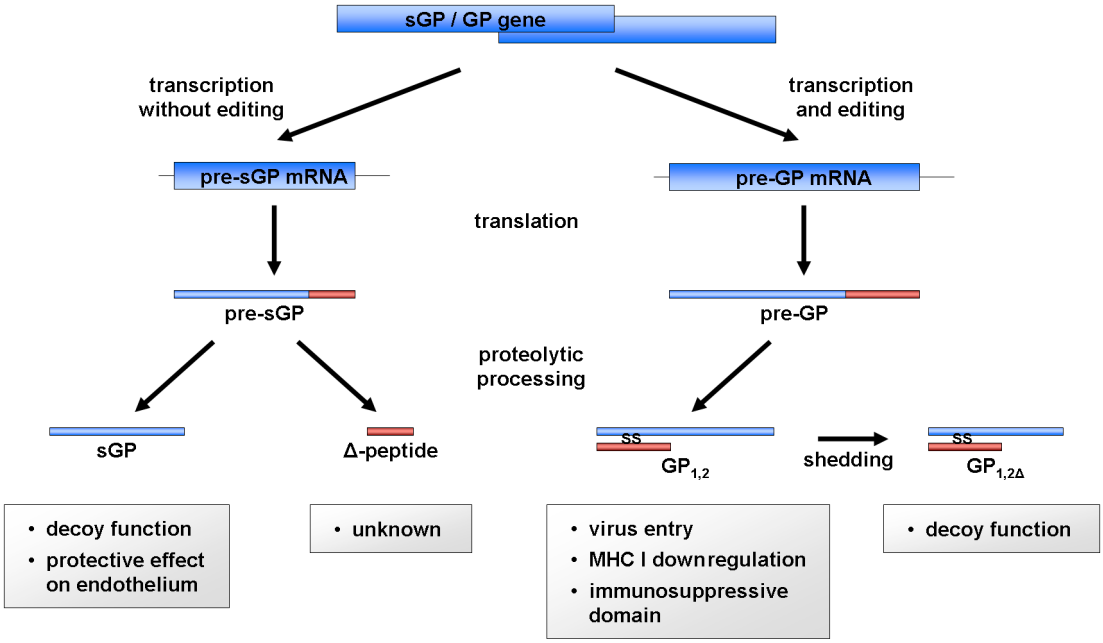

Figure 12: **Expression strategy of GP.** sGP and Δ-peptide are produced by cleavage of a precursor glycoprotein translated from uneditted mRNA. If transcriptional editing occurs, pre-GP is expressed, which is proteolytically processed into $GP_{1,2}$. Further processing into $GP_{1,2\Delta}$ by an extracellular metalloproteinase (shedding) can occur. Proposed roles of the different forms of GP are indicated. Adapted from [94] with kind permission of the author.

$GP_{1,2}$ consists of 676 aminoacids and has a calculated molecular weight of 74 kDa and an apparent molecular weight of 150 kDa (Figure 13) [172]. Responsible for this difference between predicted and apparent molecular weight is extensive N- and O-glycosylation of $GP_{1,2}$ [45, 55]. Further posttranslational modifications include proteolytic removal of the

signal peptide in the endoplasmic reticulum (ER) [202] and acylation in the pre-Golgi [101], as well as furin cleavage of the GP precursor protein into GP_1 and GP_2 [202], which are connected by a disulfide bridge between amino acids C53 and C609 [106]. Further proteolytic cleavage of $GP_{1,2}$ most likely occurs during viral entry by the endosomal proteases Cathepsin B and L [32, 178]. $GP_{1,2}$ is a type I membrane protein and anchored in the viral envelope by a transmembrane domain at the C-terminus of GP_2 [168, 171, 172]. GP_1 has been postulated to be responsible for receptor binding, and the binding site has been mapped to the 152 N-terminal amino acids using GP-pseudotyped retroviruses [129]. GP_2 contains a fusion domain close to its N-terminus [65, 100, 163, 214], which is responsible for fusion of the viral envelope with the target cell membrane. The overall structure of GP_2, as determined by X-ray crystallization, is similar to that of Influenza HA2 and HIV gp41, which suggests a similar mechanism for fusion [214, 215]. One other structural feature of $GP_{1,2}$ is a putative immunosuppressive domain close to the C-terminus of GP_2 [200]. Peptides simulating its structure were shown to inhibit blastogenic lymphocyte proliferation and activity of NK cells *in vitro* [98, 99]; however, a role for this motif in pathogenesis in the context of the whole glycoprotein remains to be shown.

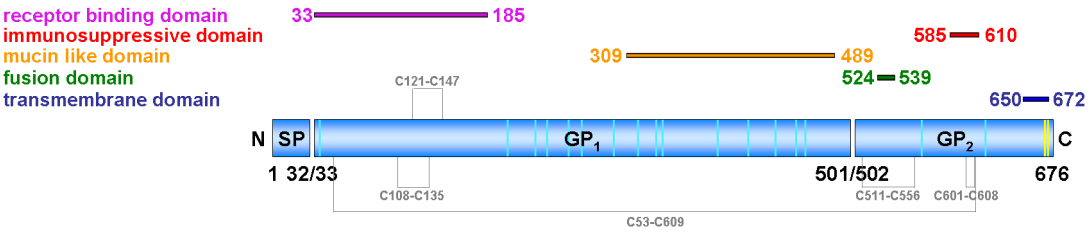

Figure 13: **Schematic drawing of $GP_{1,2}$.** Signal peptide (SP), GP_1 and GP_2 are shown. Predicted N-terminal glycosylation sites according to Uniprot [5] (accession number Q05320) are drawn as turqoise boxes, acylation sites as yellow boxes. The transmembrane region is marked in blue, the fusion domain in green, the mucin-like domain in orange, the putative immunosuppressive domain in red and the putative receptor binding domain in purple. Disulfide bridges are illustrated by gray lines, and the cysteine residues comprised in them are indicated.

The main function of $GP_{1,2}$, which forms trimers on the surface of virions [172], has been shown to be receptor binding and fusion [31, 190, 219, 221]. Several proteins have been suggested to act as cellular receptors for EBOV, and it has been recently suggested that EBOV uses not a single entry mechanism, but a variety of C-type lectins for efficient attachment to host cell types, which would explain its broad cell tropism [92, 189].

It has been suggested that the viral glycoproteins also play a central role in pathogenesis

of EHF (Figure 3) [56]. $GP_{1,2}$ has been hypothesized to be the main viral determinant of vascular cell cytotoxicity and injury, and that hemorrhage is a consequence of replication and $GP_{1,2}$-expression induced damage of endothelial cells [222]; however, this concept has since been challenged [30, 181, 1, 74, 94]. Similar to $GP_{1,2}$, sGP and $GP_{1,2\Delta}$ have also been suggested to take part in pathogenesis, particularly in the impairment of the immune system [111, 221, 41, 101]. Recently, another novel role for sGP in pathogenesis has been proposed [209]. It could be shown that TNF-α is able to impair the barrier function of endothelial cells *in vitro*, and that sGP is able to reverse this effect [209]. Further studies will be necessary to elucidate the significance of this protective role of sGP *in vivo*.

1.4.5 Virion protein 30

The fifth gene of EBOV encodes for VP30, which with 288 amino acids and a molecular weight of 33 kDa is the smallest protein in the RNP complex (Figure 14). In an EBOV minigenome system it is not necessary for replication, but indispensable for transcription, so that its role has been defined as a transcriptional activator [139]. Intriguingly, it has been shown that VP30 contains an unconventional zinc finger in the region between the amin acids 68 and 95 [133]. This zinc finger is necessary for transcription, but not for binding of NP by VP30 [133]. Also necessary for the function of VP30 as a transcription factor is its oligomerization [88]. This oligomerization is mediated by the region between amino acids 94 and 112, in which a cluster of 4 leucine residues can be found, which is essential for VP30-VP30 interaction [88]. VP30 is strongly phosphorylated [45], and the phosphorylation sites have been determined as two serine clusters and one threonine within the 52 N-terminal amino acids [134]. Interestingly, phosphorylated VP30 is found in NP inclusion bodies, while non-phosphorylated VP30 is distributed throughout the cytoplasm [134]. It also could be shown that phosphorylation of VP30 inhibits viral transcription and, therefore, it has been hypothesized that phosphorylation of VP30 constitutes a molecular switch between viral transcription and assembly of nucleocapsids for progeny virion production [134]. However, a possible role of VP30 in RNP assembly has not been studied yet.

The exact mechanism by which VP30 acts as a transcriptional factor is not completely understood. However, it has been shown that the dependence of transcription on VP30 is determined by a RNA secondary structure at the start of the NP gene, and it has

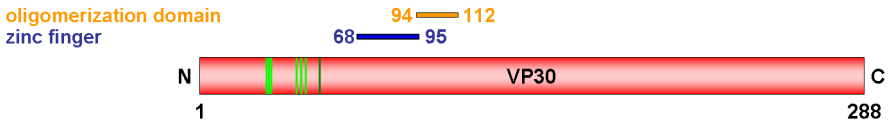

Figure 14: **Schematic drawing of VP30.** Phosphorylated serine residues are drawn as light green boxes, the phosphorylated threonine as dark green box. The zinc finger region is marked in blue, and the oligomerization domain in orange.

been hypothesized that VP30 is necessary to enable the polymerase complex to pass this hairpin [213]. Transcription of subsequent genes is VP30 independent [213]. Interestingly, MARV VP30 is not necessary for transcription of a MARV minigenome by MARV RNP components [137], although secondary structure predictions show a hairpin at the beginning of the NP gene at the same relative position as the one found in EBOV [Hoenen *et al.*, unpublished results]. Also, transcription of an EBOV minigenome by MARV RNP components is VP30 independent, while transcription of an MARV minigenome by EBOV RNP components is VP30 dependent [A. Groseth, personal communication]. Thus, it seems that VP30 dependence of transcription is also a function of genus-specific properties of the RNP complex, and not only due to the presence of a hairpin structure at the beginning of the NP gene.

1.4.6 Virion protein 24

VP24, the product of the sixth gene, is the least well understood protein of EBOV. It is 251 amino acids long and has a calculated molecular weight of 28 kDa. After singular expression in mammalian cells it is able to form tetramers [84]. For MARV, it has been shown that VP24 is localized in inclusion bodies and that for this localization interactions with NP are crucial [8].

Until recently, the function of VP24 remained enigmatic; however, in 2006 Reid *et al.* reported that VP24 is involved in IFN antagonism by binding a nuclear localization signal receptor (karyopherin α1), which is involved in the nuclear import of activated signal transducer and activator of transcription (STAT)-1, a protein important for IFN signaling, thereby blocking nuclear accumulation of activated STAT-1 [159]. It also has been suggested that VP24 might block IFN signaling by inhibition of p38 phosphorylation [82], which has been shown to be central in the mitogen activated protein kinase p38 IFN signaling pathway [152]. Further, VP24 has been shown to be important for the adaptation

of EBOV to rodent hosts [43, 201].

Since VP24 is found in the matrix space of virions [110], it has been termed a minor matrix protein; however, functional data which show a role in morphogenesis and budding, as is typical for viral matrix proteins, are conflicting. While it was reported that VP24 is able to induce its own release in the form of VLPs [84], shortly afterwards a study was published that showed that VP24 does not influence the budding of VLPs [121], a finding that was later confirmed for MARV [8]. Also, while several groups have suggested that NP, VP35 and VP24 are necessary for the formation of nucleocapsid-like structures based on electron microscopic evidence [97, 211], functional studies using an infectious VLP system (see section 1.10.3) suggested that VP24 is not necessary for packaging and transfer of viral RNA into target cells, and thus for nucleocapsid formation [212]. Recently, it was reported for MARV VP24 that it plays an important role for the release of infectious progeny virus; however, the exact mechanism for this is not known [8]. Therefore, further studies of the role of VP24 in morphogenesis and budding are necessary.

1.4.7 Viral polymerase

The last product of the viral genome is the viral polymerase, which due to its size is called L (for large). It is 2212 amino acids long and has a calculated molecular weight of 253 kDa (Figure 15). L has been shown to be absolutely required for replication and transcription of viral RNA [139]. For both EBOV and MARV, sequence analysis has revealed three conserved domains which can be found in polymerases of *Mononegavirales* [138, 153, 203]. These domains are (i) an RNA binding element (motif A, amino acids 553 to 571), (ii) a putative RNA template recognition and/or phosphodiester bond formation domain (motif B, amino acids 738 to 744) and (iii) an ATP and/or purine ribonucleotide triphosphate binding domain (motif C, amino acids 1815 to 1841) [138]. Additionally, highly conserved cysteine residues are present, which might stabilise the secondary structures important for

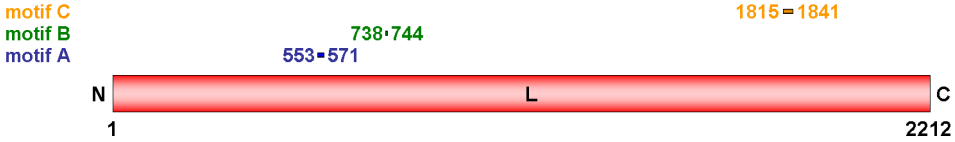

Figure 15: **Schematic drawing of L.** Motif A (RNA binding element) is marked in blue, motif B (RNA remplate recognition) in green, and motif C (ATP binding domain) in orange.

active site formation [138].

1.5 Current model of the viral life cycle

The life cycle of viruses can be divided into 3 major parts: (i) entry, (ii) transcription and replication of the viral genome, and (iii) assembly and budding.

Viral entry can be broken down into receptor binding, virus internalization and postinternalization trafficking, membrane penetration/fusion and finally virus uncoating [180]. For EBOV only details for receptor binding and fusion are known, while the other steps are not well understood. EBOV binds to its cellular receptors (possibly C-type lectins) via the N-terminal region of GP_1 (see section 1.4.4). It then enters the target cell in an pH-dependent fashion, which implies that the virions undergo endocytosis [180]. In the endosomes $GP_{1,2}$ is processed by cathepsin B and L and probably also another cellular factor, which results in a fusion active form of $GP_{1,2}$ [32, 178]. Fusion occurs by a mechanism that is most likely common in enveloped RNA viruses, and which involves binding of the fusion peptide located in GP_2 to the target cell membrane and extensive structural rearrangement of GP, which pulls the viral and cellular membranes together to allow for fusion (Figure 16) [214, 215]. After fusion the RNP complex is delivered into the cytoplasm, where transcription and replication of viral RNA takes place.

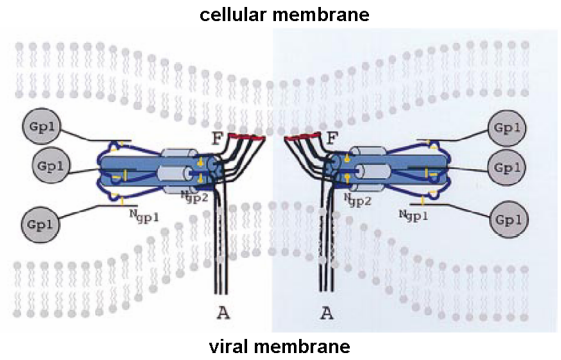

Figure 16: **Model of fusion mediated by GP.** An hypothetical intermediate step of fusion is depicted. Fusion peptides are labelled with F and membrane anchors with A. The N-termini of GP_1 and GP_2 are inidicated, and disulphide bonds are colored yellow. Reproduced from [214] with kind permission of the publisher.

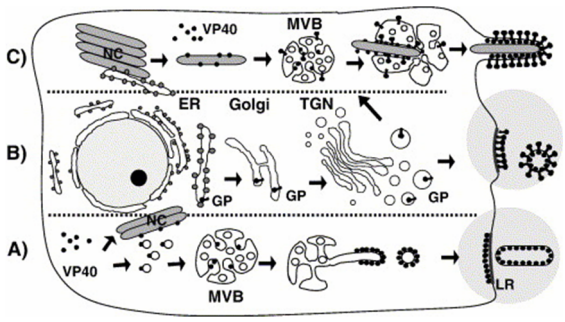

Figure 17: **Intracellular transport of filovirus proteins.** A) VP40 is transported to the plasma membrane via the retrograde endosomal pathway. B) GP is transported by the secretory pathway and then redirected to MVBs where the viral envelope is formed. C) Nucleocapsids (NC) are transported to the site of budding by an unknown mechanism. Lipid rafts (LR) might serve as assembly platform vor virus particles. Reproduced from [89, 113] with kind permission of the authors.

Since EBOV is a negative-sense RNA virus, initial transcription has to be mediated exclusively by the RNP components which were delivered into the target cells inside of virus particles. Transcription by the viral polymerase complex (L and VP35) produces 8 monocistronic mRNA species which are capped and polyadenylated [136]. The current model for transcription is that there is only a single initiation site for transcription located in the leader of the genome, and that the polymerase complex transcribes the genes sequentially in their 3' to 5' order [136, 216]. In analogy to VSV, it is believed that at each gene junction reinitiation occurs only with a less than 100% efficiency, so that there is a gradient in mRNA levels, with NP being transcribed at the highest level and L at the lowest level [36, 136, 167]. Transcription in EBOV is dependent on VP30, which has been implied to be necessary for overcoming a transcriptional block caused by a hairpin in the 3' non-coding region of NP [213]. It has been further proposed that the switch from transcription to replication is controlled by the availability of NP [216]. According to this model high levels of NP allow encapsidation of the nascent viral RNA and lead to production of positive-sense cRNA, which then serves as template for vRNA production. Interestingly, for rabies virus it has been shown that the matrix protein regulates the switch between transcription and replication; however, a similar role for VP40 has not yet been established [57, 58].

The transcribed mRNAs are translated into the viral proteins, which are located in the cytoplasm. The exception is GP, which is cotranslationally translocated into the ER [113]. GP is transported along the secretory pathway and posttranslationally modified as described in section 1.4.4 (Figure 17), and then relocates to MVBs [89, 112]. The RNP proteins NP, VP35, VP30 and L form inclusion bodies, which serve as assembly sites for nucleocapsids [89, 113]. It is unclear what role VP24 plays in nucleocapsid assembly (see section 1.4.6). Similarly, details of the transport of nucleocapsids to the sites of budding are not known. In contrast, for VP40 it has been suggested that it is transported to the plasma membrane via the retrograde late endosomal pathway through MVBs [89, 112, 114]. Therefore, MVBs have been suggested to act as assembly platforms for the filoviral envelope [112]. Budding occurs through the plasma membrane [70], and it has been suggested that lipid rafts serve as sites of budding [13]. Evidence based on VLP production suggests that the cellular ESCRT complex is involved in facilitating budding (see section 1.4.3); however, recent data using a recombinant EBOV in which the interaction domain with ESCRT compontents was mutated suggest that alternative mechanisms exist [142].

1.6 Epidemiology

Since its identification in 1976 there have been 1848 reported cases of Ebola hemorrhagic fever (EHF), including 1288 deaths (Table 1), with all outbreaks having occurred in the tropical African ecosystem and located between the latitudes of 5° north and 5° south. The epidemiology of human infections in nature is unknown. However, the time between the occurrence of index cases and the recognition of the subsequent large outbreaks, in addition to the possibility of asymptomatic infections, suggests that sporadic cases of unrecognized filovirus infections can pass unnoticed [94, 107].

Year	Virus	Country	Human Cases	Fatality [a]
1976	ZEBOV	DRC [b]	318	88%
1976	SEBOV	Sudan	284	53%
1977	ZEBOV	DRC [b]	1	100%
1979	SEBOV	Sudan	34	65%
1989	REBOV	USA [c]	0 [d]	0%
1990	REBOV	USA [c]	0 [d]	0%
1992	REBOV	Italy	0 [d]	0%
1994	ZEBOV	Gabon	52	60%
1994	CIEBOV	Ivory Coast	1	0%
1995	CIEBOV	Liberia	1	0%
1995	ZEBOV	DRC [b]	315	79%
1996	ZEBOV	Gabon	37	57%
1996 - 1997	ZEBOV	Gabon	60	75%
1996	ZEBOV	South Africa	2	50%
1996	REBOV	USA [c]	0 [d]	0%
1996	REBOV	Phillipines	0 [d]	0%
2000 - 2001	SEBOV	Uganda	425	53%
2001 - 2002	ZEBOV	Gabon	65	82%
2001 - 2002	ZEBOV	RC [e]	59	75%
2002 - 2003	ZEBOV	RC [e]	143	90%
2003	ZEBOV	RC [e]	35	83%
2004	SEBOV	Sudan	17	41%
2005	EBOV	RC [e]	12	75%

[a] Fatality rate among human cases
[b] Democratic Republic of the Congo
[c] United States of America
[d] Outbreak among imported Macaques
[e] Republic of the Congo

Table 1: **Ebola outbreaks.** Adapted from [94].

Transmission of the disease generally results from close contact with blood, secretions or tissues from patients or infected animals (e.g. gorillas, chimpanzees) [51]. It has been

noted that many infections occured as a result of injections using contaminated syringes, and that infections acquired in this fashion appear to be invariably fatal. Transmission of EBOV through mucosal exposure has also been shown to occur experimentally in non-human primates (NHPs) and, while it has never been directly shown in humans, it is believed to be possible through contact between contaminated hands and the mucosa or eyes [51]. Finally, there have been a number of cases in which transmission is suspected to have occurred via a person-to-person airborne route [161]. However, this does not appear to be a major contributing mechanism since all epidemics to date have been successfully controlled using isolation techniques without specific airborne precautions.

The source of EBOV has remained elusive since its initial discovery. However, a recent survey of small vertebrate animals collected during EBOV outbreaks in 2001 and 2003 in Gabon and the Republic of Congo has found evidence of apparent asymptomatic infection in three species of fruit bats [154]. This supports earlier experimental data demonstrating replication of EBOV in bats [188]. Further laboratory and ecological investigations will be required to determine the relevance of these findings.

1.7 Clinical presentation

EBOV infection in humans and NHPs, the gold standard animal model, results in a particularly virulent viral hemorrhagic fever known as Ebola hemorrhagic fever (EHF). Following an incubation time typically lasting between 4 and 10 days [166] a fever of >38.3°C abruptly develops. Additional early symptoms are relatively non-specific and may include chills, muscle pain, nausea, vomiting, abdominal pain and/or diarrhea [26, 62, 187]. Swelling of the lymph nodes, kidneys or brain, as well as necrosis of the liver, lymph organs, kidneys, testis and ovaries can occur. All patients will show impaired coagulation to some extent, which can manifest as conjunctival hemorrhage, bruising, impaired clotting at venipuncture sites and/or the presence of blood in the urine or feces. In fatal cases, gross pathological changes include visceral organ necrosis and hemorrhage into the skin, mucous membranes, visceral organs or the lumen of the stomach and/or intestines [187]. While approximately 50% of individuals develop a maculopapular rash on the trunk and shoulders, massive bleeding is fairly rare and, when it occurs, is mainly restricted to the gastrointestinal tract [59]. Severe nausea, vomiting and prostration, as well as increased respiration rate, anuria and decreased body temperature all indicate impending shock and

suggest a poor prognosis [26]. Case fatality rates associated with EHF infection range from 50% to 90% and mainly depend on the virus species, with ZEBOV being the most virulent [71, 166]. In addition, the virus load between fatal and non-fatal cases differs by about 2 $\log_{10}$, with virus loads in peripheral blood samples reaching peak titres of 3.4×10^9 genome copies per ml blood in fatal and 4.3×10^7 genome copies per ml blood in non-fatal cases [170, 197]. In fatal cases very high virus loads (i.e. $\geq 10^8$ genome copies per ml) are reached as early as 2 days after the beginning of symptoms [197], and death usually occurs between 6 and 16 days after the onset of symptoms [166]. Additionally, among survivors a protracted period of convalescence is typical with a number of sequelae having been reported, including deafness, athralgia, pericarditis, orchitis and psychosis [26]. Virus can persist in immunologically privileged sites, and has been isolated from seminal fluid for up to 82 days after onset of symptoms and detected by RT-PCR for up to 101 days [160].

1.8 Pathogenesis

1.8.1 Impairment of innate and adaptive immunity

A central role for the innate immune system in EHF has been demonstrated by many findings (Figure 18). In humans, as well as in NHPs, inflammatory responses accompanied by substantial cytokine production can be detected as a result of EBOV infection [92, 119]. Also, the interferon (IFN) response, which is part of the innate immune response against virus infection [83], has been found to be very important for the outcome of disease in the mouse model [25]. While adult immunocompetent mice are resistant to EBOV-WT, they die within a week if infected with EBOV-WT and treated with neutralizing anti-IFN antibodies. Also, mice lacking either the IFN-α/β receptor or STAT-1 are susceptible to EBOV-WT [25]. In contrast, severe combined immunodeficient (SCID) mice lacking both humoral and cellular adaptive immune responses succumb only very slowly to infection with EBOV-WT and show a disease picture that does not at all resemble infection in humans or NHPs [25]. *In vitro*, EBOV has been shown to selectively suppress responses to IFN-α and IFN-γ as well as the production of IFN-α in response to double stranded RNA [81, 86, 87].

The primary target cells for EBOV are macrophages, monocytes and dendritic cells (DCs)

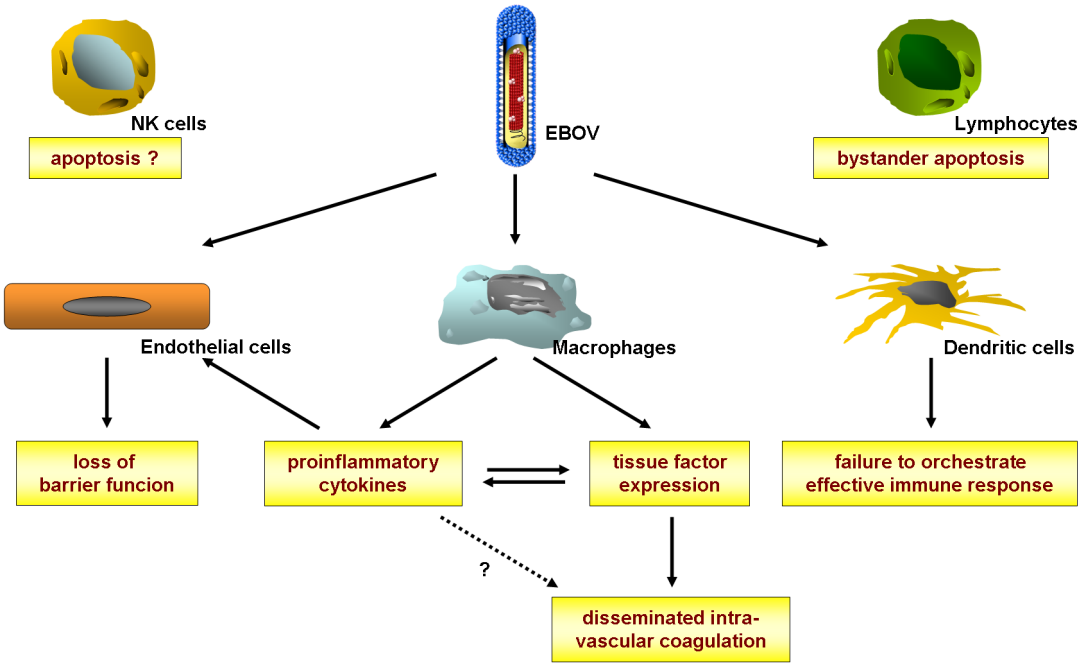

Figure 18: **Overview of the mechanisms involved in EBOV pathogenesis.** Primary target cells for EBOV are macrophages and DCs. Infection of DCs inhibits their function. Macrophages are activated and produce proinflammatory cytokines and tissue factor. Endothelial cells are infected by EBOV and activated by the produced cytokines, which leads to a loss of their function as endothelial barrier. The expression of tissue factor and probably also produced cytokines contribute to disseminated intravascular coagulation. Lymphocytes and NK cells are not infected by EBOV, but undergo bystander apoptosis. Adapted from [94].

[175, 224, 69, 164], which play important roles in the innate immune system. To what extent infection of monocytes and macrophages impairs the function of these cells has not been extensively studied. In contrast, for DCs, which play a crucial role for both innate and adaptive immunity, it has been clearly shown *in vitro* that after infection with EBOV they fail to fulfill these roles [23, 128]. Since non-infectious EBOV VLPs are able to elicit DC-responses, it appears that infectious virus actively interferes with the function of DCs [24]. Similarly, in a NHP model DCs show no increase in the expression of CD80 or CD86 following infection, confirming the *in vitro* data [156]. Further, EBOV is able to induce the proapoptotic tumor necrosis factor related aptoptosis inducing ligand (TRAIL) in DCs both *in vitro* and *in vivo* [69, 93]. However, there is no evidence of apoptosis in EBOV infected DCs *in vivo* [69].

One other class of innate immune cells affected by EBOV infection are natural killer (NK) cells (Figure 18). These cells respond in an antigen-independent manner to viral infections and kill infected cells though the release of perforin and granzymes, as well as

by inducing apoptosis [195]. Although they do not seem to be infected by EBOV, their number dramatically drops during the course of an EBOV infection in NHPs, and they virtually disappear by day 4 p.i., most likely due to apoptosis [7, 66, 156].

The role of adaptive immunity in EBOV infection is more difficult to assess than that of innate immunity, since it is difficult to obtain relevant data from the current animal models. NHPs succumb to disease 6 to 9 days p.i., while in humans the longer incubation period and the longer course of disease may allow an adaptive immune response to be mounted [127]. To date, the limited data available from human infections show profound differences in the adaptive immune responses of fatal and non-fatal cases, thus indicating an important role for the adaptive immune system during EBOV infection [7, 170].

1.8.2 Vascular dysfunction

Vascular dysfunction and loss of endothelial barrier function is considered to be a major contributor to the fatal outcome of EBOV infections [177]. It has been suggested that this dysfunction is caused by activation rather than direct infection of the endothelium [176]. It could be shown that treatment with tumor necrosis factor (TNF)-α, which is found at increased levels in fatal EHF cases [198], as well as with the supernatants of monocyte/macrophage cultures infected with the closely related Marburg virus, increases the permeability of cultured human endothelial cell monolayers [49, 198, 209, U. Ströher, personal communication]. Also, VLP-associated GP is able to activate endothelial cells and cause a breakdown of their barrier function, further supporting this hypothesis (Figure 18) [209].

Another proinflammatory mediator that is likely to contribute to endothelial dysfunction is nitric oxide (NO), which is a potent endogeneous vasodilatator and involved in the development of vasodilatory shock [116]. In EBOV infected NHPs elevated nitrate levels, indicating increased production of NO, can be detected starting at day 3 p.i. [69, 93]. Also, in humans, highly increased levels of NO can be found in the blood, where they correlate with fatal outcome of EHF [6, 170]. Beside its impact on endothelial barrier function, TNF-α is able to induce the expression of tissue factor (TF) on endothelial cells (Figure 18) [141, 18] and impairs the function of the anticoagulant protein C pathway by downregulating thrombomodulin [120]. In EBOV infected NHPs, plasma levels of protein C dramatically drop shortly after infection (2 days p.i.) and increased mRNA levels for TF can be

detected starting at day 3 after infection [73]. TF is present on infected macrophages and endothelial cells, as well as on the surface of membrane microparticles that can be found in copious amounts in the blood of infected NHPs. *In vitro*, EBOV is able to directly induce the expression of TF on the surface of macrophages (Figure 18) [73]. These increased levels of TF, whether induced by TNF-α or by direct infection of macrophages, lead to the development of disseminated intravascular coagulation (DIC), which is a prominent feature of EHF and characterized by the systemic activation of the blood coagulation system leading to fibrin deposition and microvascular thrombi [120]. Inhibition of TF increases the survival of EBOV infected NHPs, which further demonstrates the significance of TF for pathogenesis [67].

The procoagulant state induced by filovirus infection not only directly harms the host by causing DIC, but also enhances inflammation by a number of mechanisms, which then in turn further provokes activation of coagulation [92, 120]. This two-way interaction between coagulation and inflammation is demonstrated by the fact that EBOV infected NHPs treated with an inhibitor of TF also show decreased levels of interleukin (IL)-6 and macrophage chemotactic protein (MCP)-1 [67].

1.9 Treatment and vaccines

1.9.1 Treatment

At present, the treatment of EHF is mainly supportive in nature and involves a combination of intravenous fluid replacement, the administration of analgesics and standard nursing measures [52]. Despite the lack of any specific antiviral drugs approved for the treatment of EHF, a number of experimental approaches have shown promise in recent years. In particular, since over-expression of TF has been shown to play such a profound role in the development of DIC, the possibility of inhibiting this pathway as a therapeutic measure has been considered. Despite the general contraindication towards the use of anticoagulants in the treatment of hemorrhagic fever disease [21], Geisbert *et al.* could show that treatment with the recombinant nematode anticoagulant protein c2 (rNAPc2), administered as late as 24 hours p.i., resulted in a 33% survival in an otherwise uniformly fatal EBOV-infected NHP model [67]. In addition, the survival time in remaining animals was significantly prolonged indicating that, while this therapy may not be sufficient

on its own, it could be a valuable tool in the treatment of EHF, and potentially other hemorrhagic diseases that involve over-expression of pro-coagulant molecules.

Another avenue of treatment that has been successfully applied to viral hemorrhagic fevers is the use of passive immunization [21]; however, its applicability to the treatment of EHF remains unclear [94].

1.9.2 Vaccines

Early attempts to produce vaccines for EBOV focused on the use of inactivated virus and were universally unsuccessful [51, 72]. More recently, several vaccine strategies using recombinant viruses and/or DNA vaccination have been developed. While these were successful in protecting rodents from EBOV, almost all were still unsuccessful in protecting NHPs [72]. VLPs have also been successfully used to vaccinate mice and guinea pigs, but have not yet been evaluated in NHPs [210]. The first vaccine to have proven efficacy in NHPs was a DNA prime/adenovirus boost approach [186, 185]. More recently, another candidate system based on a recombinant vesicular stomatitis virus (VSV) has been shown to protect NHPs 28 days after a single vaccination and is also able to protect mice as well as NHPs when given 30 minutes after challenge [109, S. Jones *et al.*, personal communication].

1.10 Reverse genetics systems for Ebola virus

Reverse genetics systems have contributed considerably to our knowledge of the molecular biology of EBOV [42]. As the term "reverse genetics" indicates, these system facilitate the introduction of mutations into the virus genome and the subsequent study of the resulting phenotypes, in contrast to classical genetics, where a given phenotype is analysed for the genotype causing it. One can broadly group reverse genetics systems in two categories: (i) infectious clone systems, which can be used to create recombinant viruses, and (ii) artificial replication systems (minigenome systems and infectious VLP (iVLP) systems), which allow the study of certain aspects of the viral life cycle.

1.10.1 Infectious clone systems

The first infectious clone system was established in 1981 for a positive-sense RNA virus, the early success of these systems being due to the fact that, for these viruses, the vRNA

itself is infectious [155]. For negative-sense RNA viruses, the vRNA has to be transcribed by the viral RNP components in order to start the viral life cycle, which explains why the first rescue of a recombinant negative-sense RNA virus, Influenza A, was not achieved until almost 10 years later [47, 124]. Helper-virus infection was used to provide the necessary RNP components, which has the disadvantage of requiring a strong selection system to distinguish the modified virus from the wild-type (WT) helper virus [145]. The first rescue of a recombinant negative-sense RNA virus completely from cDNA was achieved by Conzelmann and colleagues in 1994 [174]. Viral RNA was transcribed from a plasmid using the T7 RNA polymerase (T7) provided by infection with a recombinant vaccinia virus [64]. Since T7 incorporates additional nucleotides at the 3' ends of transcripts, a hepatitis delta virus ribozyme (HDVrib) was used to provide an authentic 3' end to the RNA [150]. Critical for the success of this system was to provide cRNA, most likely because it avoided the problem of hybridization between initial NP-uncomplexed negative-sense vRNA and positive-sense mRNA encoding for the viral proteins [42, 145, 174]. Although rescue of negative-sense RNA viruses from cDNA encoding a negative-sense vRNA has since been reported, efficiency for this is generally lower than by using cDNA encoding a positive-sense cRNA [145]. For both EBOV and MARV infectious clone systems are available [48, 143, 204], and have been used to answer a number of questions, including the roles of glycoprotein cleavage [143] and sGP production [204], the role of both the phylogenetic origin of RNP components and VP30 in transcription and replication [48, 191], and the importance of VP40-octamerization and the presence of late-domain motifs in the viral life cycle [96, 142]. Also, recombinant EBOVs expressing enhanced green fluorescent protein (eGFP) from an additional open reading frame have been generated and shown to be valuable research tools [95, 196].

1.10.2 Minigenome systems

In contrast to infectious clone systems minigenome systems do not produce infectious progeny virus, which allows the study of BSL4 organisms under BSL2 conditions, if no helper virus infection is used. Minigenome systems can be used to study certain parts of the viral life cycle, especially transcription and replication, and often precede the development of an infectious clone system because they can be used to establish optimal rescue conditions, particularly the ratios of RNP components necessary for efficient tran-

scription and replication [42, 145]. Minigenome systems employ a miniature version of the viral genome in which the coding regions have been replaced by an open reading frame (ORF) for a reporter protein (e.g. chloramphenicol acetyl transferase (CAT), eGFP or luciferase), but in which the authentic 3' and 5' non-coding regions are still present (Figure 19). These minigenomes are expressed from a plasmid by an RNA polymerase, usually T7 or RNA polymerase-I (Pol-I), and authenticity of the 3' end is ensured by an HDVrib in case of T7-driven transcription. The resulting negative-sense vRNA analogue is recognized as a suitable target for replication and transcription by cotransfected RNP components, because the minimally required signals for these processes are contained in the leader and trailer region of the vRNA [37]. mRNA that is produced by the viral RNP complex is expressed, which leads to reporter activity reflecting both viral transcription and replication.

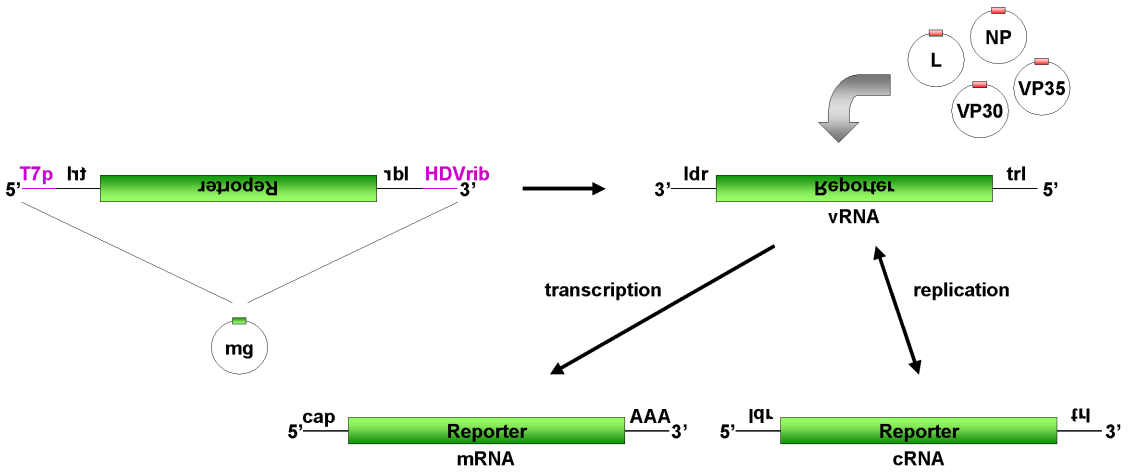

Figure 19: **T7 driven-minigenome system.** A reporter flanked by the viral leader and trailor is cloned in antisense orientation under the control of a T7 promoter. T7-driven transcription results in a negative-sense vRNA, which serves a template for specific transcription and replication by the viral RNP components NP, VP35, VP30 and L, resulting in mRNA production and reporter activity.

Minigenome systems have been set up for a number of negative-sense viruses [42, 145], and are available for ZEBOV, REBOV and MARV [20, 77, 137, 139]. These systems have been used to determine the proteins required for transcription and replication [137, 139], the influence of the phylogenetic origin of RNP components on transcription and replication and a possible relationship to the different virulence observed between different filovirus species [77], the role of VP30 for transcription and replication [134, 213], the role of VP35-oligomerization for transcription and replication [133], but also for screening of antivirals

[79]. Interestingly, one of the available systems for REBOV uses Pol-I instead of T7 [77], which because of the nuclear localization of Pol-I and the cytoplasmic localization of EBOV replication seems, at first, counterintuitive. However, it has been shown for several negative-sense RNA viruses with cytoplasmic replication that it is possible to drive minigenome systems for these viruses with Pol-I [60, 61], and in the case of REBOV it could be shown that this is not only technically simpler, but also more efficient than a T7-driven system [77].

1.10.3 Infectious virus-like particle (iVLP) systems

In order to study more aspects of the viral life cycle, minigenome systems have been extended to so-called "iVLP systems" (Figure 20) [212]. In these systems cells (called p0) are transfected with a minigenome and plasmids coding for all structural proteins of the virus of interest, which leads to the production of iVLPs which resemble WT virions, but contain a minigenome instead of a full-length vRNA. These iVLPs are able to enter target cells (called p1) and deliver their minigenome, which is then replicated and transcribed by RNP components either previously transfected into these target cells or provided by helper virus infection. Therefore, iVLP system not only allow to study transcription and replication, but also virion morphogenesis, budding and entry into target cells. If RNP components in p1 are provided without helper virus infection, these systems can be used under BSL2 conditions, since the iVLPs are only able to undergo one infectious round, because they lack the genetic information for the production of progeny particles. One step that could not be studied in the iVLP systems prior to this work was the initial transcription in target cells by RNP components brought into the target cells by the iVLPs themselves, a step indispensable in the viral life cycle, since the RNP components pretransfected into the target cells take over this step [95]. Therefore, in iVLP systems with pretransfected target cells it is impossible to determine whether or not the RNP complex inside the iVLPs is functional.

The first iVLP system for negative-sense RNA viruses was set up by in 1995 for VSV [182]. Since then, a number of systems have been developed, including systems for Lymphocytic Choriomenigitis virus, Influenza virus, Borna disease virus and Thogoto virus [118, 144, 151, 207]. For EBOV an iVLP system was first established by Watanabe *et al.* in 2004 and used to study the role of VP24 in morphogenesis and budding [212]. Also, this system

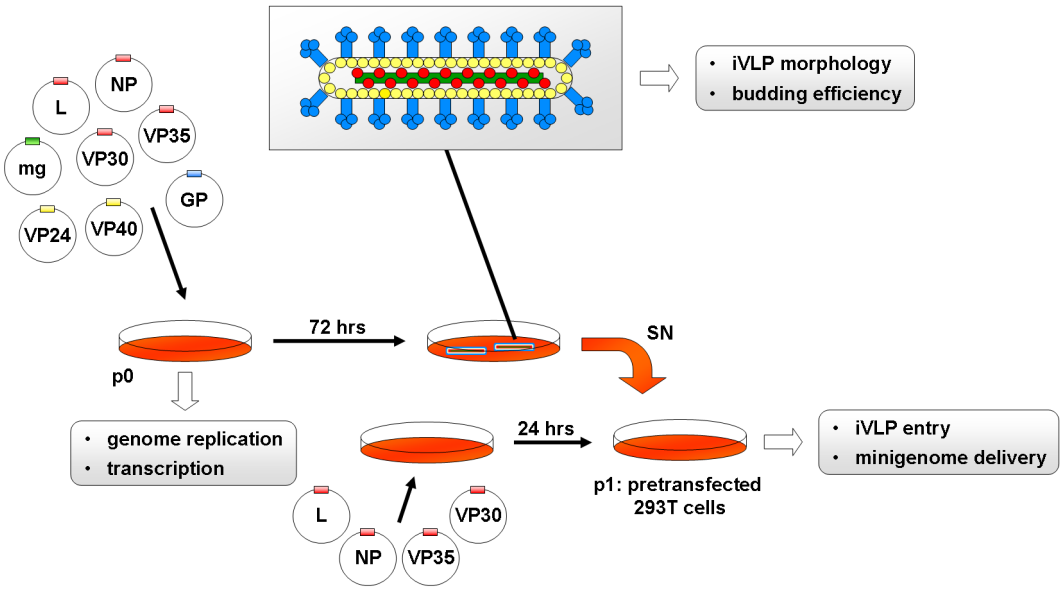

Figure 20: **iVLP system with pretranfected target cells.** Cells (p0) are transfected with plasmids encoding a minigenome and all EBOV structural proteins. These cells produce iVLPs that resemble WT virions, but carry a minigenome instead of a full-length vRNA. After passage of the iVLPs onto target cells (p1) these are infected, the minigenome is delivered into these cells, and subsequently replicated and transcribed by RNP components previously transfected into p1.

has been succesfully used to analyze the mechanism of antivirals against EBOV *in vitro* [183].

1.11 Objectives of this study

The role of VP40 in the viral life cycle is only partially understood and, although recently there have been some publications about possible functions of VP24 (see section 1.4.6), its role in morphogenesis remains enigmatic. We, therefore, decided to further investigate the role of these two matrix proteins in the viral life cycle, with special emphasis on morphogenesis and budding. Of particular interest were the following topics:

- **Role of VP40 octamerization.** The role of VP40 octamers should be investigated using previously characterized octamerization-deficient VP40 mutants. As a readout method we decided to use an iVLP assay with pretransfected target cells. Since initial results using this system did not allow for any conclusions about the role of VP40 octamers, a new iVLP assay with naïve target cells was developed to allow more accurate modelling of the viral life cycle *in vitro*, as well as a system to knock out viral VP40 and substitute it by plasmid derived VP40 *in vivo*.

- **Role of VP40 dimerization.** Similar to the role of VP40 octamers, the role of VP40 dimers should be addressed by constructing dimerization deficient VP40 mutants and testing their effect in the developed systems.

- **VP40-NP interaction.** It should be investigated whether or not VP40 and NP directely interact with each other. As readout methods we chose coimmunoprecipitation and recruitment of NP into VP40 VLPs. Further, the interacting domain of VP40 should be mapped using a series of deletion mutants.

- **Role of VP24 in morphogenesis and budding.** The role of VP24 should be investigated using the established iVLP assays with pretransfected and naïve target cells. Also, in the course of the studies, a packaging assay was developed and used to analyse the role of VP24 in this process.

2 Methods

2.1 Molecular biology methods

2.1.1 Polymerase chain reaction (PCR)

To amplify fragments of DNA, polymerase chain reaction (PCR) can be used [140, 165]. It is facilitated by the use of two specific primers and a thermostable DNA polymerase. The initial step in a PCR is a denaturation step at high temperature (94 to 98°C), in which the two strands of the double stranded DNA template are separated. In a second step the temperature is lowered (typically to 5°C below the theoretical melting temperature of the primers used), which allows for efficient binding of the primers to their complementary target region on the DNA template (annealing). For the third step the temperature is raised to the optimal reaction temperature for the polymerase (typically 68 to 72°C), and extension of the primer occurs complementary to the DNA template (elongation). Repeated cycling through these 3 steps leads to exponential amplification of the region flanked by the two primers. Since the primer sequences are included in the final product, DNA sequences that are not present in the DNA template (e.g. molecular tags) can be added to the ends of the amplified fragment.

PCR was performed using the PfuUltra II Fusion HS polymerase and a touchdown protocol to reduce background due to unspecific binding of primers.

setup:	30 ng	DNA template
	5 μl	10 × PfuUltra II reaction buffer
	1 μl	primer #1 (10 μM)
	1 μl	primer #2 (10 μM)
	1 μl	dNTPs (10 mM each)
	1 μl	PfuUltra II Fusion HS DNA polymerase
	ad 50 μl	dH_2O

cycle conditions:	1×	denaturation	95°C	3 minutes
	10×	denaturation	95°C	30 seconds
		annealing	T_m to $T_m - 5$°C	30 seconds
		elongation	72°C	30 seconds/kB
	35×	denaturation	95°C	30 seconds
		annealing	$T_m - 5$°C	30 seconds
		elongation	72°C	30 seconds/kB
	1×	store at	4°C	∞

2.1.2 Reverse transcriptase polymerase chain reaction

To amplify a DNA fragment from an RNA template, reverse transcriptase PCR (RT-PCR) can be used. This method is similar to a regular PCR (see section 2.1.1); however, before the PCR an additional step is included in which the RNA is transcribed into a cDNA using an RNA-dependent DNA polymerase (reverse transcriptase) and the same primers as used for PCR. After this step the reverse transcriptase is inactivated by denaturation at high temperature, and the transcribed cDNA serves as the template for a regular PCR.

RT-PCR was performed using the Qiagen Onestep RT-PCR kit, which makes use of a hot start DNA polymerase, which is inactive during the initial reverse transcription, and becomes activated by the high temperature used to inactivate the reverse transcriptase. This allows the reaction to be performed in one vial without cleanup of the cDNA and/or addition of DNA polymerase after the reverse transcription step is finished.

setup:	2μl	RNA template
	10 μl	5 × RT-PCR buffer
	1 μl	primer #1 (30 μM)
	1 μl	primer #2 (30 μM)
	2 μl	dNTPs (10 mM each)
	1 μl	enzyme mix
	ad 50 μl	RNAse free dH_2O

cycle conditions:	1×	reverse transcription	50°C	30 minutes
	1×	inactivation	95°C	15 minutes
	10×	denaturation	95°C	30 seconds
		annealing	T_m to $T_m - 5$°C	30 seconds
		elongation	68°C	30 seconds/kB
	35×	denaturation	95°C	30 seconds
		annealing	$T_m - 5$°C	30 seconds
		elongation	68°C	30 seconds/kB
	1×	store at	4°C	∞

2.1.3 Preparative restriction digest

To generate single-stranded DNA overhangs for directed ligation of DNA fragments (see section 2.1.8), and to cut out DNA fragments from vectors for subcloning (see section 2.1.11), DNA was digested with restriction endonucleases. Two types of restriction enzymes were used: (i) type II enzymes, which have palindromic recognition sites and cut within the recognition site, and (ii) type IIs enzymes, which have non palindromic recognition sites and cut several base pairs away from the recognition site. The use of type IIs enzymes allows the generation of user-defined overhangs; and by positioning the recognition site on the side of the cleavage site that is cleaved off, one can clone fragments without leaving any remainders of the restriction site in the final product.

Restriction digest was performed using enzymes from New England Biolabs (NEB) according to the manufacturers instructions. If recommended, BSA was included in the reaction mix to stabilize the enzyme. For determining reaction conditions for double digests, the NEB Double Digest Finder (http://www.neb.com/nebecomm/DoubleDigestCalculator.asp) was used.

setup:	2 μg	DNA
	5 μl	10 × restriction buffer
	5 μl	10 × BSA (if recommended)
	1 μl	restriction enzyme(s)
	ad 50 μl	dH_2O

Samples were incubated for 4 to 8 hours at 37°C, then the enzyme was heat-inactivated

for 20 minutes at 65 °C and the samples were stored until further use at either 4°C or -20°C.

2.1.4 Analytical restriction digest

To check cloned constructs for the presence of the desired insert, the constructs were digested with restriction endonucleases and the generated fragments subjected to agarose gel electrophoresis to check for the correct size. If possible, the FastDigest enzymes from Fermentas were used, otherwise enzymes from NEB were used according to the manufacturers instructions.

setup:	FastDigest		NEB Digest	
	200 ng	DNA	200 ng	DNA
	1 μl	10 × FastDigest buffer	1 μl	10 × restriction buffer
			1 μl	10 × BSA (if recommended)
	1 μl	FastDigest enzyme(s)	0.3 μl	restriction enzymes(s)
	ad 10 μl	dH_2O	ad 10 μl	dH_2O

Samples were incubated for 5 minutes (FastDigest) or 60 minutes (NEB) at 37°C and the products visualized using agarose gel electrophoresis (see section 2.1.5).

2.1.5 Agarose gel electrophoresis

To visualise DNA fragments, they were loaded onto a 1% agarose gel containing 0.01% ethidium bromide, separated by their size using electrophoresis and then visualized on a UV screen. The samples were mixed with 6 × DNA sample loading buffer (final concentration 1 ×), and 10 μl of the samples was loaded. Electrophoresis was performed in tris acetate EDTA (TAE) buffer at a constant voltage of 100 V for 45 minutes, then the gel was placed on a UV screen and the bands documented using a polaroid camera. For visualizing small differences in fragment size, gel electrophoresis was performed in a 2% agarose gel for 4 to 6 hours at 50 V, which allows resolution of bands with a $\geq$ 10 bp size difference and a size of about 1 kB.

2.1.6 Purification of DNA by gel electrophoresis

To purify a DNA fragment of a given size from a pool of different sized fragments, agarose gel elctrophoresis was used (see section 2.1.5). The band of the desired size was cut out with a scalpel, and then extracted using the QIAquick Gel Extraction Kit from Qiagen according to the manufacturers instructions. Briefly, the agarose was dissolved in 3 × its volume QG buffer at 50°C for 10 minutes on a thermo shaker, loaded onto a DNA binding column which contains a silica gel membrane that binds DNA under high salt conditions and a pH≤7.5, washed with buffers to remove agarose traces (QG) and salt (PE) and then eluted with 50 μl dH_2O.

2.1.7 Purification of PCR products

To purify DNA from proteins and salt after an enzymatic reaction, the QIAquick PCR Purification Kit from Qiagen was used according to the manufacturers instructions. Briefly, the sample was mixed with 5 × its volume QB buffer, loaded onto a DNA binding column (see section 2.1.6), washed with several buffers to remove protein traces (QB) and salt (PE) and then eluted with 50 μl dH_2O.

2.1.8 Ligation

To join DNA fragments, usually a cut vector and a DNA fragment (insert) to be inserted into the vector, they were incubated with T4 DNA ligase, which catalyzes the formation of a phosphodiester bond between the 3' hydroxyl group of one nucleotide and the 5' phosphate group of another nucleotide. It is, therefore, essential that the 5' ends of at least one DNA fragment are phosphorylated to allow for the reaction to occur. If only the insert but not the vector is 5' phosphorylated, nicked DNA plasmids are generated which contain single-strand breaks, but which are repaired after transformation into bacteria by bacterial DNA repair enzymes. However, this avoids religation of the vector with itself and, thus, reduces the number of undesired ligation products. Also, to avoid religation usually an excess of insert is used for ligation (ideally at a molar ratio of 3:1 of insert to vector). To control for the amount of uncut and religated vector, a cut control in which the ligase was exchanged against dH_2O and a religation control in which the insert was exchanged against dH_2O were performed.

setup:	5.5 μl	insert
	1.5 μl	vector
	2 μl	5 × T4 DNA ligase buffer
	1 μl	T4 DNA ligase

The samples were incubated for 16 hours at 14°C, and then stored at 4°C until transformation (see section 2.1.17).

2.1.9 Dephosphorylation

To minimise religation of the vector during a ligation (see section 2.1.8), the 5' ends of the cut vector were dephosphorylated using shrimp alkaline phosphatase. 1 μl of phosphatase was added to the sample and incubated for 1 hour at 37°C, then another 1 μl phosphatase was added and the sample incubated for 30 minutes at 52°C. Since alkaline phosphatase is active in any restriction buffer, it usually was added directly to the unpurified digested sample; however, if purified DNA should be dephosphorylated, an appropriate amount of 10 × dephosphorylation buffer was included in the reaction. After dephosphorylation the sample was purified prior to ligation by PCR purification (see section 2.1.7) or gel purification (see section 2.1.6).

2.1.10 Hybridization of oligonucleotides

In order to generate short doublestranded oligonucleotides which can be ligated into a cut vector, single-stranded oligonucleotides were phosphorylated and hybridized. Phosphorylation was performed using the T4 polynucleotide kinase.

setup:	1 μl	primer (100 μM)
	4 μl	5 × T4 DNA ligase buffer
	1 μl	T4 polynucleotide kinase
	14 μl	dH_2O

The samples were incubated for 1 hour at 37°C, and then hybridized. To do so, 1 μl of both phosphorylated primers were combined with 18 μl dH_2O, and the sample was heated for 5 minutes at 99°C in a heating block. Then the heating block was turned off and the

sample was allowed to slowly cool down to RT in the block. The theoretical concentration of the oligonucleotides was 0.25 pmol/μl. The oligonucleotides were then ligated with the cut vector as described in section 2.1.8 using a molar ratio of 3:1 of insert to vector.

2.1.11 Subcloning

To subclone a DNA-fragment (insert) from one vector to another, the insert was first cut out of the source vector using restriction enzymes flanking it and gel purified to isolate it (see sections 2.1.3 and 2.1.6). The target vector was cut with the same enzymes if possible, otherwise with enzymes using different recognition sites but producing compatible overhangs. The target vector was dephosphorylated and purified by either PCR purification, if the cut sites in the target vector were not too far away from each other ($\leq$ 40 bp), or by gel purification (see sections 2.1.9 and 2.1.7 or 2.1.6). Insert and target vector were then ligated and transformed into bacteria, along with the cut control and religation control (see sections 2.1.8 and 2.1.17). Colonies on both the cut and religation control plate indicated incomplete cutting of the target vector, colonies only on the religation control plate incomplete dephosphorylation of the target vector. The number of colonies to pick was estimated using the formula:

$$n = \frac{\ln 0.01}{\ln \frac{c}{l}}$$

with n being the number of colonies to pick, c the number of colonies on the religation control plate and l the number of colonies on the ligation plate. The colonies were then grown in a miniprep culture and plasmid DNA was isolated and analysed using analytical restriction digest (see sections 2.1.18 and 2.1.4). A positive clone was then expanded in a maxiprep culture and the plasmid DNA was isolated for further use (see section 2.1.18).

2.1.12 Cloning of PCR fragments

Amplification of fragments by PCR and subsequent cloning allows for the introduction of additional sequences, e.g. molecular tags or restriction sites not present in the original sequence. After amplification of the fragment by PCR or RT-PCR fragments were PCR purified (see sections 2.1.1, 2.1.2 and 2.1.7). They were then cut with restriction enzymes to produce the overhangs needed for cloning and either gel purified or, if the PCR did not produce any unspecific products, DpnI treated to remove methylated template DNA by adding 1 μl DpnI to the sample and incubating it for 4 hours at 37°C, and subsequently

PCR purified (see sections 2.1.3 and 2.1.6 or 2.1.7). Preparation of the target vector, ligation, subsequent transformation, plasmid propagation and screening were carried out as described in section 2.1.11.

2.1.13 Site-directed mutagenesis

To introduce point mutations into a plasmid, the whole plasmid was amplified using PCR with two complementary primers which contained the mutation to be introduced. The primers were designed so that they contained at least 15 bp left and right of the mutation site, and so that they had a T_m of about 78°C according to the formula

$$T_m = 81.5 + 0.41 \cdot (\%GC) - \frac{675}{N} - \%mismatch$$

with $\%GC$ being the GC-content in percent, N the length of the primer and $\%mismatch$ the percentage of mismatching nucleotides. To calculate the T_m according to this formula, the Stratagene T_m calculator (http://www.stratagene.com/QPCR/tmCalc.aspx) was used. The PCR was performed using the PfuUltra Fusion HS II polymerase.

setup:	30 ng	DNA template
	5 µl	10 × PfuUltra II reaction buffer
	1.25 µl	primer #1 (10 µM)
	1.25 µl	primer #2 (10 µM)
	1 µl	dNTPs (10 mM each)
	1 µl	PfuUltra II Fusion HS DNA polymerase
	ad 50 µl	dH_2O

cycle conditions:	1×	denaturation	95°C	3 minutes
	18×	denaturation	95°C	30 seconds
		annealing	55°C	30 seconds
		elongation	72°C	1 minute/kB
	1×	store at	4°C	∞

To remove the template DNA, 1 µl DpnI was added to the sample after PCR. DpnI digests the methylated bacterial plasmid DNA, but does not cut the non methylated PCR product. The nicked, circular PCR product was then transformed into bacteria, 3 to 12

colonies were picked, grown as minipreps and sent for sequencing to identify positive clones (see sections 2.1.17 and 2.1.18).

2.1.14 Deletional mutagenesis

To introduce deletions into a plasmid, the whole plasmid with the exception of the deletion was amplified by PCR with 21bp long primers flanking and pointing away from the deletion (see section 2.1.1). The PCR product was then DpnI digested and gel purified (see sections 2.1.13 and 2.1.6). After that, the 5' ends of the PCR product were phosphorylated by T4 polynucleotide kinase.

setup:	50 μl	purified PCR product
	13 μl	5 $\times$ T4 DNA ligase buffer
	1 μl	T4 polynucleotide kinase

The sample was incubated for 30 minutes at 37°C, then chilled on ice. 1 μl high concentrated T4 DNA ligase was added and the sample incubated fo 16 hours at 14°C. The religated plasmid was transformed into bacteria, 3 to 12 colonies were picked, grown as miniprep and either sent for sequencing to identify positive clones or subjected to analytical restriction digest and agarose gel electrophoresis (see sections 2.1.17 and 2.1.18 or 2.1.4 and 2.1.5).

2.1.15 Type IIs deletional mutagenesis

To avoid blunt end ligation during deletional mutagenesis, it is possible to modify the protocol by including type IIs restriction sites in the primers (Figure 21). After PCR, the PCR product was purified as described (see section 2.1.14), but then not phosphorylated, but instead digested with the chosen type IIs enzyme (see section 2.1.3). After that, the sample was PCR purified and religated (see section 2.1.7 and 2.1.8). The subsequent procedure is identical to the one described in section 2.1.14.

2.1.16 Preparation of chemically competent bacteria

Chemically competent E. coli (strain XL1-Blue) were prepared by the method of Chung *et al.* [33]. Briefly, an 5 ml overnight culture was prepared by growing E. coli in 5 ml LB

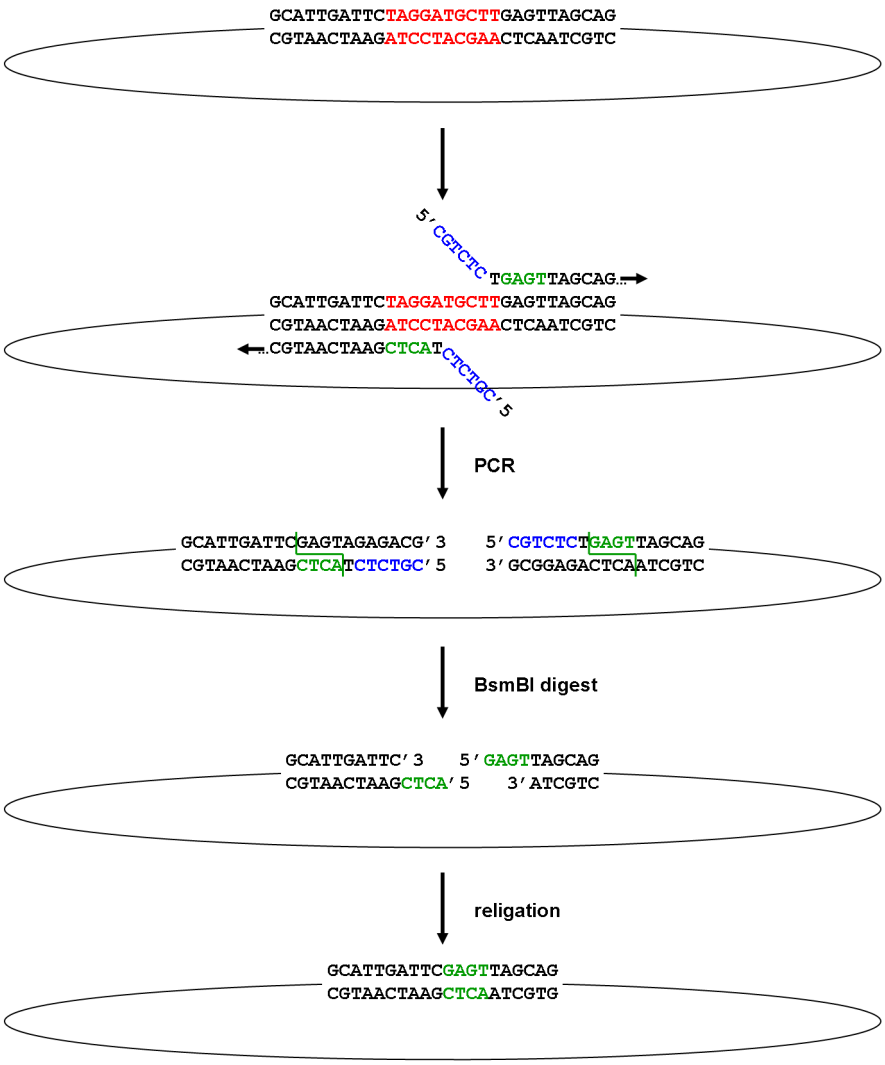

Figure 21: **Type IIs deletional mutagenesis.** The red region is deleted by amplifying the rest of the plasmid by PCR. The primers contain a type IIs recognition site (blue), which leads to cutting at the indicated cut site (green) and generation of the green overhangs. These overhangs are then rejoined by ligation.

medium overnight at 37°C in a shaker following addition of 100 μl of a previous culture. 0.5 ml of this overnight culture was added into 50 ml LB medium and grown at 37°C in a shaker until an optical density of 0.5 was reached (about 2 to 3 hours). After that, the cells were placed for 20 minutes on ice, and then centrifuged for 10 minutes at 2500 $\times$ g and 4°C. Then the cells were resuspended in 5 ml TSS buffer and aliquoted in 100 μl aliquots into pre-chilled vials on dry ice. Chemically competent bacteria were stored at -80°C.

2.1.17 Transformation of chemically competent bacteria

Chemically competent E. coli were thawed on ice. 10 ng of plasmid DNA or 10 μl of ligation product was added to the cells, and the sample was mixed by pipetting it up and down once with a 100 μl pipette. The mix was kept on ice for 20 minutes, then transfered to a 42°C water bath for 45 seconds and put back on ice for 3 additional minutes. After that, 250 μl medium without antibiotics was added and the cells were incubated for 30 to 60 minutes at 37°C . Then 250 μl of the cells was plated on prewarmed LB agar plates with the appropriate antibiotic (Ampicillin 100 μg/ml, Kanamycin 50 μg/ml) and incubated overnight at 37°C.

2.1.18 Preparation of plasmid DNA from bacterial cultures

Bacteria containing plasmid DNA were propagated either as miniprep (5 ml) or maxiprep cultures (100 ml) in LB medium with appropriate antibiotics (Ampicillin 100 μg/ml, Kanamycin 50 μg/ml) for 16 hours at 37°C in a shaker. Plasmids were then isolated according to the manufacturers instructions using the Qiagen QIAprep spin miniprep kit or HiSpeed plasmid maxi kit, respectively. Briefly, the bacteria were pelleted, resuspended in an RNAse A containing buffer, and lysis buffer containing SDS and NaOH was added, which leads to disruption of the bacterial cell walls. The solution was neutralized by adding buffer containing potassium acetate and glacial acetic acid, which leads to renaturation of the plasmid DNA, while the genomic DNA precipitates. The lysate was cleared of cell debris, SDS and genomic DNA either by centrifugation (miniprep) or filtration (maxiprep). Afterwards the plasmid DNA was purified using either spin-columns containing a silica gel membrane (miniprep) or gravity flow columns containg an anion exchange resin (maxiprep). After binding of the DNA to the column under high salt (miniprep) or low salt (maxiprep) conditions, the DNA was washed and then eluted either with 50 μl dH_2O (miniprep) or with a high salt elution buffer (maxiprep). In the case of a maxiprep, the eluate was then concentrated and desalted using isopropanol precipitation and a proprietary Qiaprecipitator module, and finally eluted from this module with 1 ml dH_2O.

2.2 Tissue culture methods

2.2.1 Cultivation of mammalian cells

Mammalian cells were cultivated in $DMEM_{10\%FBS}$ at 37°C and 5% CO_2. For a T75 flask either 25 ml (for VeroE6 cells) or 30 ml (for 293T cells) medium was used. Cells were split when they reach confluency, or for 293T cells when they were about 80 to 90% confluent. In preparation for splitting cells were washed twice with phosphate buffered saline (PBS), and then incubated in 2 ml Trypsin/EDTA until they start to detach. The cells were then washed off the flask with 8 ml $DMEM_{10\%FBS}$, resuspended and an appropriate amount was transferred to a new flask. VeroE6 cells were typically split 1:10 every 3 to 4 days, and 293T cells 1:15 to 1:20 every 3 to 4 days.

2.2.2 Cryopreservation of mammalian cells

For storage mammalian cells can be frozen in the presence of 10% DMSO. 2 ml cryovials were precooled in a cell freezing module to -20°C. One T75 flask of cells with a confluency of 90% was washed and trypsinized as described in section 2.2.1, and then resuspended in 5 ml $DMEM_{10\%FBS}$. The cells were centrifuged for 3 minutes at 120 × g. The supernatant was discarded and the cell pellet was gently resuspended in 1 ml of an ice-cold 4:1 mixture of FBS and $DMEM_{10\%FBS}$. Then 1 ml of an ice-cold 4:1 mixture of FBS and DMSO was added, and the cell suspension was aliquoted into 1 ml aliquots in the precooled cryovials. The cryovials were placed back in the freezing module, which was then put overnight at -80°C. Afterwards, the cells were stored in liquid nitrogen.

2.2.3 Poly-D-lysine coating

To increase the adherence of 293T cells for use in longer experiments, tissue culture plates were coated with poly-D lysine. This reagent increases the number of positively charged sites on the plastic that are available for cell binding. A 0.1 mg/ml solution of poly-D-lysine was prepared by resuspending 5 mg poly-D-lysine hydropbromide in 50 ml sterile dH_2O. 2 ml of this solution was added to each well of a 6 well plate, and the plates were incubated 20 to 60 minutes at 37°C. After that, the plates were washed twice with PBS and then used for seeding of cells as usual. The used poly-D-lysine was collected, stored at -20°C and reused up to 5 times.

2.2.4 Isolation of macrophages from peripheral blood

Blood was collected in Vacutainers containing sodium heparin from a healthy donor. For one well of a 6 well plate 10 ml of blood was used. The blood was diluted 1:2 with PBS and 37.5 ml of the diluted blood was layered on 12.5 ml of Ficoll in a 50 ml vial. The blood was centrifugated for 40 minutes at 400 × g and room temperature (RT) with no brake. During centrifugation, the mononuclear cells formed a white layer above the Ficoll. The serum above this layer was removed, then the mononuclear cells were carefully taken off and washed twice with 45 ml of ice-cold PBS. After each wash step the cells were spun down at 350 × g and 4°C. After the second centrifugation, the cells were resuspended in 8 ml RPMI with 5% human AB serum and 4 ml per well was seeded into Primaria 6 well plates and incubated at 37°C and 5% CO_2. After one hour, the medium was removed and the cells were thoroughly washed three times with PBS to remove the lymphocytes. After that, 4 ml of RPMI with 5% human serum was added to the cells, and they were incubated for 7 days at 37°C and 5% CO_2.

2.2.5 Generation of stable cell lines

To generate a VeroE6 derivative cell line stably expressing a gene, this gene was cloned under the control of a eukaryotic promoter into a vector containing a geneticin resistance gene. VeroE6 cells were electroporated with 10 μg of this plasmid and seeded into a T75 flask (see section 2.2.7). After 3 days the cells were split into $DMEM_{10\%FBS}$ containing 500 μg/ml geneticin. Cells were propagated in $DMEM_{10\%FBS}$ containing geneticin for 2 weeks and regularly split. After 2 weeks, they were split into 10 cm culture dishes at ratios of 1:300, 1:900, 1:2700 and 1:8000, respectively. The dishes were monitored for the growth of isolated cell islets, and the dish with a low to intermediate frequency of cell islets was used for isolation of clones to ensure that the clones were derived from a single cells. Once the islets had a size of 50 to 100 cells, they were picked under the BSC using a 200 μl pipettor. Picking of clones was monitored with an Axiovert microscope. The picked clones were transferred into a 24 well plate containing $DMEM_{10\%FBS}$ without geneticin. After 1 day the medium was exchanged against $DMEM_{10\%FBS}$ containing geneticin. Clones were regrown in a T75 format, and then frozen down (see section 2.2.2). After they had been expanded to a T75 format, they were continously kept in $DMEM_{10\%FBS}$ containing 200 μg/ml geneticine. Cell clones were screened for expression of the introduced gene as

descirbed in section 3.1.7.2.

2.2.6 Transfection of mammalian cells with Fugene

In order to express foreign proteins in 293T cells, these were transfected with Fugene. Fugene is a multi-component lipid-based transfection reagent that complexes with and transports DNA into the cell during transfection.

Transfections were usually performed in 6 well plates with cells having a confluency of $\sim$ 50%. The plasmids for transfection were combined in a 1.5 ml vial outside of a biosafety cabinet (BSC), all other steps were performed inside a BSC. 100 μl OptiMem was added to a 1.5 ml vial and 3 μl Fugene per μg DNA was added. The mix was briefly vortexed, spun down and incubated for 5 minutes at RT. After that, the DNA was added, and the mix was again briefly vortexed and spun down. The transfection mix was incubated for 15 minutes at RT; during that time the cells to be transfected were washed once with $DMEM_{0\%FBS}$, after which 2 ml of $DMEM_{5\%FBS}$ without Penicillin/Streptomycin was added to each well. After that, the DNA/Fugene/OptiMem mixture was given dropwise onto the cells. The cells were incubated for 5 hours at 37°C and 5% CO_2, then 2 ml $DMEM_{5\%FBS}$ was added to the cells. Cells were harvested between 1 and 3 days p.t., depending on the experiment performed. If the cells were harvested after more than 24 hours, the medium was exchanged against 4 ml $DMEM_{5\%FBS}$ after 18 to 24 hours.

2.2.7 Transfection of mammalian cells by electroporation

In order to express foreign proteins in VeroE6 cells, electroporation was used since this method has been shown to be highly efficient for this cell type [9]. After optimization, Viaspan was selected for use as an electroporation medium (see section 3.4.4.1). One day prior to transfection Vero E6 cells were split 1:2 into one T75 flask. On the day of transfection 10 to 20 μg of DNA was incubated in a speedvac to reduce the volume to less than 20 μl. The DNA was then resuspended in 400 μl ViaSpan. The cells were washed twice with 10 ml PBS and trypsinized with 2 ml Trypsin/EDTA. After cells showed the first signs of detaching, they were washed off with 5 ml $DMEM_{10\%FBS}$ and spun down for 5 minutes at 120 $\times$ g and RT. The cell pellet was resuspended in the ViaSpan / DNA mix and put into a 0.4 cm gap cuvette. Then the cells were electroporated in a Biorad

Genepulser XCell with the following settings: exponential decay, U = 230 V, C = 950 μF, $\Omega = \infty$. After electroporation, the cells were resuspended in 8 ml $DMEM_{10\%FBS}$ and then seeded out as usual, with cells of one T75 being seeded out in 8 wells of a six well plate. One day after transfection, the cells were usually confluent. With a pCAGGS-GFP plasmid the efficiency of this method is $\approx 50\%$.

2.2.8 Harvest and lysis of cells

2.2.8.1 Harvest Cells were harvested by scraping into 1 ml PBS. After a 10 minute centrifugation at 3500 × g and 4°C the supernatant was removed from the cells. The cells were then either resuspended in PBS for storage at 4°C or directly lysed.

2.2.8.2 Lysis with passive lysis buffer (PLB) 5 × PLB was diluted with water to a 1 × concentration. The cell pellet from the previous centrifugation step was resuspended in 200 μl lysis buffer by pipetting up and down. If necessary, additional lysis buffer (up to 800 μl) was added to adjust the volume. The samples were incubated for 15 minutes at RT, then briefly vortexed, spun down for 3 minutes at 10000 × g, and the supernatant was transferred into cryovials. The lysate was either stored at -80°C or used immediately for assaying of reporter expression levels.

2.2.8.3 Lysis with sample loading buffer The cell pellet from the previous step was resuspended in an appropriate volume of PBS, then 4 × $\text{sample buffer}_{2\%\ SDS}$ was added for a final concentration of 1 × sample loading buffer, and the sample was vortexed thoroughly. After that, the sample was incubated for 5 to 10 minutes at 95°C, briefly spun down and either placed on ice or stored at -20°C for later use.

2.2.8.4 Lysis by Triton X-100 treatment In order to harvest proteins from mammalian cells without lysis of the nuclei, these were separated from the rest of the cell by differential centrifugation after gentle lysis with Triton X-100. The cell pellet from the previous centrifugation step (see section 2.2.8.1) was resuspended in an appropriate volume of PBS (e.g. 120 μl), and 5% Triton X-100 in PBS was added for a final concentration of 1% (e.g. 30 μl). The sample was incubated for 5 minutes on ice, and the nuclei were spun down for 5 minutes at 830 × g and 4°C. Then the supernatant was transferred to a

new vial, 4 × sample buffer$_{2\%\ SDS}$ was added (e.g. 50 μl) and the sample was vortexed thoroughly. Subsequently, the sample was incubated for 5 to 10 minutes at 95°C, briefly spun down and either put on ice or stored at -20°C.

2.3 Protein biochemistry methods

2.3.1 Sodium dodecyl sulfate polyacrylamide gel electrophoresis (SDS-PAGE)

To separate proteins based on their molecular mass, they were subjected to sodium dodecyl sulfate polyacrylamide gel electrophoresis (SDS-PAGE). In this procedure proteins are complexed with SDS, an anionic detergent, which denatures the proteins and gives them a negative charge proportional to their molecular mass. They are then separated by electrophoresis through a polyacrylamide gel.

For SDS-PAGE the mini-PROTEAN 3 system was used. Gels were prepared according to the following recipe, with the Tetramethylethylenediamine being added immediately before the gel was poured, since it catalyzes polymerization.

	10 ml 10% resolving gel	5 ml 4% stacking gel
dH_2O	4.9 ml	3.2 ml
40% acrylamide	2.5 ml	0.5 ml
1.5M Tris pH 8.8	2.5 ml	-
0.5M Tris pH 6.8	-	1.25 ml
10% SDS	100 μl	50 μl
10% ammonium persulfate	50 μl	25 μl
Tetramethylethylenediamine	10 μl	5 μl

After polymerization the gels were place in a mini-PROTEAN 3 electrophoresis cell and SDS-PAGE buffer was added. Samples in 1 × sample buffer$_{2\%\ SDS}$ were incubated for 5 minutes at 95°C and then put on ice. 12 μl of each sample was loaded onto the gel and electrophoresis was performed at 100V until the bromophenol blue dye front has reached the bottom of the gel.

2.3.2 Western blotting

To specifically detect proteins after SDS-PAGE, they were transferred onto a polyvinylidene fluoride (PVDF) membrane and then detected using specific antibodies. Transfer was performed using a mini Trans-Blot Cell. A 7.5×10 cm piece of PVDF membrane was soaked in methanol for 5 minutes and then placed in transfer buffer. Fibre pads and blotting paper were briefly soaked in transfer buffer as well. The stacking gel was removed from the acrylamide gel, and the clamping frame was assembled as follows: cathode (black), fibre pad, blotting paper, acrylamide gel, PVDF membrane, blotting paper, fibre pad, anode (white). The clamping frame was then placed in the transblot module, and this module, together with an ice pack, into the buffer tank. Transfer buffer was added to the tank until the clamping frame was completely covered, and blotting was performed at either 100 V and 250 mA for 1 hour or 30 V and 40 mA overnight.

After blotting, the membrane was blocked for 1 hour in $PBS_{0.1\%\ Tween}$ with 10% skim milk powder at RT on a rocking platform or overnight in PBS with 10% skim milk powder at 4°C. Then the membrane was rinsed once briefly with $PBS_{0.1\%\ Tween}$ and washed for 5 minutes on a rocking platform with $PBS_{0.1\%\ Tween}$. The primary antibody was diluted in $PBS_{0.1\%\ Tween}$ with 1% skim milk powder in a final volume of 1 ml. A glass plate was covered with parafilm and placed into a wet chamber. The blot membrane was put onto the glass plate with the protein side facing up, and the antibody dilution was added onto the membrane. The following antibodies and dilutions were used:

Antibody	Specificity	Dilution	Species	Type	Reference
2C4	EBOV VP40	1:100	mouse	monoclonal	[123]
B1-C6-6	EBOV NP	1:100	mouse	monoclonal	[95]
α-RES 30	EBOV VP30	1:100	mouse	polyclonal	[95]
α-RES 35	EBOV VP35	1:20	mouse	polyclonal	[95]
αVSV-GP	EBOV GP	1:500	goat	polyclonal	[95]
goat α-EBOV	EBOV	1:400	goat	polyclonal	

A second piece of parafilm was placed on the membrane, the edges weighed down with 1 cent coins and the wet chamber closed. The blots were incubated for 1 hour on a rocking platform. The blots were then washed 3 × for 10 minutes with $PBS_{0.1\%\ Tween}$and

incubated for 1 hour at RT on a rocking platform with the secondary antibody diluted in $PBS_{0.1\%\ Tween}$ with 1% skim milk powder in a final volume of 25 ml. The HRP conjugated secondary antibodies were used in a dilution of 1:50000 (α-mouse) or 1:30000 (α-goat). After incubation with the secondary antibody, the blots were washed 2 × with $PBS_{0.1\%\ Tween}$ and 4 × with PBS for 10 minutes each. 1.5 ml ECL plus reagent A and 37.5 μl reagent B were combined and vortexed. The blot membrane was placed on a parafilm-covered glass plate, the ECL plus reagent added on top and a second piece of parafilm placed over the membrane. After 3 minutes incubation the membrane was put into a Kapak sealpack pouch and taken into a dark room for detection. Hyperfilm ECL was exposed to the blot membranes for 10 seconds to 10 minutes and developed using a Feline 14 X-ray film processor.

2.3.3 Octamerization assay

To detect octamers, cells were harvested and gently lysed using Triton-X100 as described in section 2.2.8.4 with some modifications. After lysis on ice and spinning down of nuclei, samples were transferred to fresh vials and an appropriate volume of 4 × $buffer_{0.5\%\ SDS}$ was added. Samples were not boiled, but immediately loaded onto a polyacrylamide gel and subjected to SDS-PAGE and western blotting (see sections 2.3.1 and 2.3.2).

2.3.4 Silverstaining of SDS-PAGE gels

To visualize proteins in an SDS-PAGE gel without the use of specific antibodies, silverstaining was performed. The principle of silverstaining is that Ag^+ ions complex sulfhydryl and carboxyl groups in proteins, and are then selectively reduced to the metallic silver and, therefore, form visible silver deposits.

The SilverSNAP stain kit II from Pierce was used according to the manufacturers instructions. Briefly, the gel was fixed in 30% ethanol and 10% acetic acid, washed twice in ethanol and twice in H_2O and then sequentially incubated in sensitizer solution, staining solution and developer solution. The developing reaction was stopped by replacing the developer solution with a 5% acetic acid solution.

2.3.5 Coimmunoprecipitation

To assess protein-protein interactions, coimmunoprecipitation can be used. This assay is based on precipitation of one of the proteins of interest with a specific antibody, followed by detection of the other protein of interest in the precipitate by SDS-PAGE and western blotting with another specific antibody (see sections 2.3.1 and 2.3.2). The second protein should only be detectable in the precipitate if the two proteins interact with each other.

Coimmunoprecipitation was performed against the flag-epitope using anti-flag M2 agarose from Sigma according to the manufacturers instructions. 40 μl M2 agarose per sample was washed 3 $\times$ with 1 ml tris buffered saline (TBS) buffer and centrifuged down for 1 minute at 3500 $\times$ g after every wash step. After the last centrifugation, the agarose was resuspended in 40 μl TBS per sample. Cells were harvested as described (see section 2.2.8.1) and redissolved in 200 μl lysis buffer. Another 800 μl lysis buffer was added, and the samples were lysed for 20 minutes at RT. Samples were briefly vortexed and centrifuged for 10 minutes at 12000 $\times$ g at 4°C. All subsequent steps were performed either on ice or at 4°C. 900 μl sample was added to 40 μl washed agarose and the samples were incubated overnight at 4°C on a rotator. The next morning, the agarose was washed 3 $\times$ with 1 ml TBS with 0.4% Sodiumdesoxycholate and 1% NP40. After the final wash step, the supernatant was removed so that the residual volume of the sample was 50 μl, and 20 μl 4 $\times$ sample buffer$_{2\%\ \mathrm{SDS}}$ was added. After that, the samples were icubated for 10 minutes at 95°C and subjected to SDS PAGE (see section 2.3.1) and western blotting (see section 2.3.2).

2.3.6 Mammalian two hybrid assay

As an alternative to coimmunoprecipitation (see section 2.3.5) a mammalian two hybrid assay can be used to analyse protein-protein interactions. In this assay the two proteins of interest are expressed as fusion proteins with a DNA-binding domain and a transactivating domain, respectively. If the two proteins interact with each other, the DNA-binding domain and the transactivating domain are brought in close proximity to each other and function as a transcription factor for a cotransfected reporter gene.

For mammalian two hybrid assay the Checkmate system from Promega was used. This system uses the yeast GAL4 DNA-binding domain (vector pBind) and the VP16 activation

domain (vector pAct) in combination with a Firefly luciferase construct (pG5luc), which contains five GAL4 binding sites upstream of the reporter ORF. As a positive control, two plasmids encoding fusion proteins with mammalian proteins known to interact with each other are provided (pBind-Id and pAct-MyoD). The assay was performed according to the manufacturers instructions. Briefly, 293T cells in poly-D-lysine coated 6-well plates were transfected with 500 ng of each pG5luc and the pBind and pAct constructs (see section 2.2.6). 48 hours p.t., the cells were harvested and lysed in 200 μl 1 $\times$ PLB (see section 2.2.8.2). Firefly activty was then determined using the Dual Luciferase Assay and a Veritas luminometer.

2.3.7 Immunofluorescence analysis

HUH7 cells were cultivated on coverslips ($\oslash$ 12 mm) and transfected as described in section 2.2.6. For fixation, the coverslips were transferred into 1 ml DMEM/4% Paraformaldehyde and stored at 4°C. For staining, coverslips were washed 3 $\times$ with PBS for 3 minutes each. They were then incubated in 0.1M Glycin/PBS for five minutes, and then permealized for 5 minutes in 0.1% Triton X-100/PBS. Coverslips were then washed again for 3 minutes in PBS, and blocked for 10 minutes in blocking buffer$_{\mathrm{IFA}}$ to reduce unspecific staining. 20 μl of primary antibody (2C4, dilution 1:10 in blocking buffer$_{\mathrm{IFA}}$) was placed on a sheet of parafilm, the coverslip was layed face-down onto the drop of antibody solution, and incubated for 1 hour in a wet chamber. Subsequently, coverslips were washed 3 $\times$ in PBS, and then incubated for 1 hour on a 20 μl drop of secondary antibody on parafilm (Rhodamine-coupled α-mouse, dilution 1:100) in a wet chamber in the dark. After another 3 $\times$ washing with PBS coverslips were stained for 30 minutes with 4',6'-diamidino-2-phenylindole, washed 3 $\times$ with PBS, briefly rinsed by dunking them in a beaker with dH_2O and then mounted on a microscope slide using Fluoprep.

2.4 Virus like particle (VLP) assays

2.4.1 Infectious VLP (iVLP) assay with pretransfected target cells

293T cells were seeded out into a poly-D-lysine coated 6 well plate (p0) one day before transfection for a confluency of 50% at the time of transfection (see section 2.2.3). The cells were then transfected with Fugene (see section 2.2.6) with the following plasmids: 125

ng pCAGGS-NP, 125 ng pCAGGS-VP35, 75 ng pCAGGS-VP30, 250 ng 3E5E-luc, 60 ng pCAGGS-VP24, 250 ng pCAGGS-T7, 250 ng pGL2-control, 1000 ng pCAGGS-L, 250 ng pCAGGS-VP40 and 250 ng pCAGGS-GP. As a negative control VP40 was ommitted in one of the samples. 5 hours p.t., 2 ml $DMEM_{10\%FBS}$ was added to the cells. 24 hours p.t., the cells were washed once with $DMEM_{0\%FBS}$ and then incubated in 4 ml $DMEM_{5\%FBS}$. At the same time, 293T cells were seeded into a poly-D-lysine coated 6 well plate (p1) for a confluency of 60% on the next day. 2 days p.t. these cells were transfected with the following plasmids: 125 ng pCAGGS-NP, 125 ng pCAGGS-VP35, 75 ng pCAGGS-VP30, 1000 ng pCAGGS-L and 250 ng pGL2-control.

72 hours p.t., the supernatant from p0 was transferred into a 15 ml vial and spun down for 5 minutes at 800 × g at RT. One well at a time, the supernatant was removed from p1 and 3 ml of the VLP-containing supernatant was immediately added. At the same time, p0 cells were harvested and and lysed in 1000 μl 1 × PLB (see section 2.2.8.1 and 2.2.8.2). The samples were then measured using a Veritas luminometer and the Dual Luciferase Assay, and Renilla activity was normalized to Firefly activity.

6 hours post transfer 1 ml $DMEM_{10\%FBS}$ was added to p1. 24 hours post transfer, the medium was exchanged against 4 ml of fresh $DMEM_{5\%FBS}$. 72 hours post transfer the samples were harvested and lysed in 200 μl 1 × PLB (see section 2.2.8.1 and 2.2.8.2). The samples were then measured using a Veritas luminometer and the Dual Luciferase Assay. Reporter activity of WT-iVLPs was set to 100%.

2.4.2 iVLP assay with naïve target cells

An iVLP assay with naïve target cells was performed similar to an iVLP assay with pretransfected target cells (see section 2.4.1), but with several modifications. p0 cells were transfected and afterwards treated as described. For p1 cells VeroE6 cells instead of 293T cells were used, and were seeded out 2 day p.t. for a confluency of 100% at the next day.

Transfer of the supernatant was performed as described; however, the p1 cells were harvested 48 hours post transfer and lysed in 200 μl 1 × PLB (see section 2.2.8.1 and 2.2.8.2). The samples were then measured using a Veritas luminometer and the Dual Luciferase Assay. Reporter activity of WT-iVLPs was set to 100%.

2.4.3 iVLP packaging assay

To assay packaging of minigenomes into iVLPs independent of transcription and replication in p0, an iVLP assay with pretransfected target cells was performed with several modifications (see section 2.4.1). 293T cells were seeded out into a poly-D-lysine coated 6 well plate (p0) one day before transfection for a confluency of 50% at the time of transfection (see section 2.2.3). The cells were then transfected with Fugene (see section 2.2.6) with the following plasmids: 125 ng pCAGGS-NP, 125 ng pCAGGS-VP35, 75 ng pCAGGS-VP30, 750 ng 3E5E-luc, 60 ng pCAGGS-VP24, 750 ng pCAGGS-T7, 250 ng pGL2-Control, 250 ng pCAGGS-VP40, 250 ng pCAGGS-GP, but no pCAGGS-L. As a negative control VP40 was ommitted in one of the samples. After transfection the p0 cells were treated as described (see section 2.4.1). 1 day p.t. VeroE6 cells were split into two T75 flasks for 100% confluency on the next day. 2 days p.t., these cells were electroporated with the following plasmid combinations: (i) 10 μg pCAGGS-NP, 10 μg pCAGGS-VP35, 4 μg pCAGGS-VP30 and 10 μg pCAGGS-L or (ii) as an additional negative control 10 μg pCAGGS-NP, 10 μg pCAGGS-VP35, 4 μg pCAGGS-VP30, but no pCAGGS-L.

For transfer the supernatant was harvested and iVLPs were purified over a 20% sucrose cushion as described in section 2.4.4. The iVLP pellet was resuspended in 2 ml $DMEM_{5\%FBS}$, and the resuspended iVLPs added to the p1 cells. 24 hours after transfer another 2 ml of $DMEM_{5\%FBS}$ was added, and p1 cells were harvested 72 hours post transfer and lysed in 200 μl 1 $\times$ PLB (see section 2.2.8.1 and 2.2.8.2). The samples were measured using a Veritas luminometer and the Dual Luciferase Assay. Reporter activity of WT-iVLPs was set to 100%.

2.4.4 Purification of (i)VLPs over a sucrose cushion

Cell culture supernatant containing (i)VLPs was cleared twice by centrifugation at 800 $\times$ g at room temperature for 5 minutes. If necessary the supernatant was diluted with PBS to a volume of 10 ml. 3 ml of 20% sucrose was prelaid in a 14 $\times$ 89 mm Ultra-Clear centrifuge tube and carefully overlaid with 9 ml of the sample. The tubes were balanced by adding PBS so that the weight difference between the tubes was less than 10 mg. Then the samples were centrifuged in a SW41 rotor for 2.5 hours at 21000 RPM and 4°C. After centrifugation the supernatant was decanted and, without turning the tube

back upright, the tube was carefully dried without touching the pellet. Subsequently, the pellet was resuspended in an appropriate volume of either (i) $DMEM_{5\%FBS}$ for infection of target cells, (ii) TNE for additional purification over a Nycodenz gradient, (iii) PBS for proteinase K protection assay, or (iv) 4% PFA in PBS for negative staining and electron microscopic analysis.

2.4.5 Nycodenz gradient purification

To separate spherical VLPs from filamentous VLPs, ultracentrifugation over a Nycodenz gradient can be used (L. Kolesnikova, personal communication). This gradient was poured in 14 × 89 mm Ultra-Clear centrifuge tubes and contained from bottom to top the following layers: 2 ml 30% Nycodenz/TNE, 1.33 ml of 20%, 15%, 10%, 7.5%, 5% and 2.5% Nycodenz/TNE. After preparation of the gradient, 2 ml VLPs in TNE were carefully layered on top, and the samples were centrifuged for 20 minutes at 16500 RPM in an SW41 rotor at 4°C. After centrifugation, 2 ml fraction were taken from top to bottom. Spherical VLPs are found in fraction 1 to 3, while filamentous VLPs are located in fraction 4 to 6.

2.4.6 Proteinase K protection assay

In order to ensure that proteins were inside VLPs, these were subjected to a proteinase K protection assay. The sample was split into 3 × 40 μl. To the first sample 12 μl PBS was added, to the second sample 7.2 μl PBS and 4.8 μl proteinase K diluted in PBS (150 μg/ ml), and to the third sample 7.2 μl 0.1% Triton X100 diluted in PBS and 4.8 μl proteinase K diluted in PBS (150 μg/ ml). The samples were incubated for 1 hour at 37°C and then heated for 5 minutes at 99°C. After that, 20 μl 4 × $\text{sample buffer}_{2\%\ \text{SDS}}$ preheated to 99°C was added and the samples were incubated for another 15 minutes at 99°C. They were then briefly spun down and then stored at -20°C until analysis by SDS-PAGE (see section 2.3.1) and western blotting (see section 2.3.2).

Proteins outside the VLPs should be visible only in the first, but not in the second and third sample, since they were not protected by a membrane from the proteinase K. Proteins inside the VLPs should be visible in both first and second sample. The third sample serves as control for the activity of proteinase K.

2.4.7 Statistical analysis

Statistical analysis was performed using the GraphPad InStat software package. A paired t-test was used and differences were deemed significant when the two-tailed p-value was lower than 0.05.

2.5 Virological methods

All infectious work with EBOV was performed in the BSL4 laboratory at the CSCHAH according to the standard operation procedures in place.

2.5.1 Infection of VeroE6 cells with Ebola virus

For infection with EBOV, either a recombinant ZEBOV (strain Mayinga) with an additional ORF between NP and VP35 encoding GFP (ZEBOV-GFP) [95] or REBOV (strain Pennsylvania) [78] was used. VeroE6 cells were infected at a confluency of 60 to 80% in 6 well plates. If different cell lines should be compared, 5×10^5 cells were split 6 hours before infection into 6 well plates in 2 ml $DMEM_{10\%FBS}$, to minimize differences in cell number. Prior to infection cells were washed once with $DMEM_{0\%FBS}$. Infection was performed with 200 FFU ($\simeq$ multiplicity of infection (MOI) 0.0005) for ZEBOV (10 μl virus per 6 ml $DMEM_{0\%FBS}$, virus titer $\sim 5 \cdot 10^5$) or 20000 FFU ($\simeq$ MOI 0.05) for REBOV (500 μl virus per 6 ml $DMEM_{0\%FBS}$, virus titer $\sim 1 \cdot 10^6$) in 250 μl $DMEM_{0\%FBS}$ for 1 hour, with rocking after every 15 minutes. After 1 hour, the inoculum was removed, and the cells washed once with $DMEM_{0\%FBS}$. Cells were then incubated in 2.5 ml $DMEM_{2\%FBS}$ at 37°C and 5% CO_2 for 5 days until harvesting.

2.5.2 Autofluorescent plaque assay

For determining the infectious titer in tissue culture supernatants, supernatant was harvested and cleared from cellular debris by centrifugation at 3500 $\times$ g for 10 minutes. Then a 10 $\times$ dilution series was prepared with virus dilutions 10^{-1} to 10^{-4}. Plaque assay was performed on confluent VeroE6 cells in 24 well plates. Cells were infected as described in section 2.5.1 with 200 μl of each supernatant dilution. After infection for 1 hour, cells were washed 3 $\times$ with $DMEM_{0\%FBS}$, and then overlaid with 1 ml of a 1:1 mixture of 3% CMC and 2 $\times$ EMEM. Then the cells were incubated at 37°C and 5% CO_2 for 5 (ZEBOV) or 6

(REBOV) days. For harvesting, the CMC overlay was removed by washing the cells 3 × with PBS (for the first wash step the PBS was left on the cells for 5 minutes). Then 1 ml 10% formalin was added onto the plates and they were stored overnight at 4°C wrapped in aluminium foil. The next day, the formalin was discarded and the plates were placed into heat-sealable bags, which were filled with fresh 10% formalin, sealed so that only a minimal amount of air was left inside the bag, and surface decontaminated for removal out of BSL4 by immersion in 5% microchem for at least 10 minutes. Bags were opened outside of BSL4 after another incubation at 4°C overnight. For plaque assays for ZEBOV-GFP, GFP plaques were counted using an Axiovert fluorescence microscope, for plaque assays for REBOV, an immuno staining was performed (see section 2.5.3).

2.5.3 Immunoplaque assay

To visualise REBOV plaques, cells were stained using a polyclonal mouse α-REBOV-VP30 serum. Cells were washed 3 × with PBS for 5 minutes each, then permeabilized for 15 minutes with 0.1% Triton X-100 in PBS and again washed 3 × with PBS for 5 minutes each. Then cells were incubated with 200 μl/well of α-REBOV-VP30 1:1000 in PBS for 1 hour at RT. After that, cells were washed 3 × with PBS for 5 minutes each, and then incubated for 1 hour at RT with 200 μl/well of the secondary antibody Alexa goat α-mouse-488 1:200 in PBS. Finally, cells were again washed 3 × with PBS and the plaques were counted using an Axiovert fluorescence microscope.

2.5.4 Flow cytometry analysis of Ebola virus infected cells

For flow cytometry analysisof cells infected with ZEBOV-GFP, cells were harvested and then fixed in PFA. For harvesting, the tissue culture supernatant was removed and the cells were washed once with 0.04% EDTA in PBS. After that, they were incubated for 10 to 15 minutes in 800 μl 0.04% EDTA in PBS and, once detached, added to 8 ml 4% PFA in PBS. Cells were fixed overnight at 4°C wrapped in aluminium foil. The next day, they were centrifuged for 10 minutes at 3500 × g and 4°C, and the old PFA was discarded. The pellet was resuspended in 1000 μl of fresh 4% PFA in PBS and added to 3.5 ml 4% PFA in a 5 ml cryovial. Samples were then surface decontaminated for removal out of BSL4 by immersion in 5% microchem for at least 10 minutes. Samples were stored outside BSL4 for another night at 4°C before transfer to 12x75 mm culture tubes and analysis using a

FACSCalibur flow cytometer. Data were analyzed using the Flowjo software package and Microsoft Excel.

2.5.5 Fluorescence assisted cell sorting

Fluorescence assisted cell sorting (FACS) was performed using a FACSCalibur flow cytometer according to the manufacturer's instructions. For each sample, three 50 ml tubes were coated for 1 hour with 50 ml 4% BSA in PBS at 4 °C. After coating, the BSA/PBS solution was discarded. The sort lines were primed with dH_2O, and then the BSA-coated tubes were installed in the sorting ports. A sort gate was defined for GFP-positive cells, the sort count was set to zero to allow for continuous counting, and cells were sorted in exclusion mode at approximately 300 events/second.

After sorting, cells were concentrated by centrifugation at 2400 × g for 10 minutes in a swinging bucket rotor. The pellets were resuspended in 300 μl PBS each, combined and checked for concentration and purity by flow cytometry (see section 2.5.4). The concentration of cells can be calculated according to the formula $c = n \cdot 5000$, with c being the concentration of cells per ml and n the events per second at low flow rate. If necessary, samples were then further concentrated using another centrifugation step at 3500 × g for 10 minutes. For successful detection of VP40 by western blotting a minimum of 3000 infected cells ($\simeq$ 300000 cells/ml) is necessary. After the second centrifugation step samples were adjusted to the same concentration of infected cells, and then 4 × sample $\text{buffer}_{2\%\ \text{SDS}}$ was added and samples were incubated for 5 minutes at 95°C. Samples were then subjected to SDS-PAGE and western blotting (see section 2.3.1 and 2.3.2).

3 Results

3.1 Role of VP40 octamerization

Our previous studies have indicated that VP40 octamerization is essential for the viral life cycle, and that a single mutation R134A in VP40 abolishes octamerization [96]. However, we were not able to find differences in VLP production between VP40-WT and VP40-R134A. Therefore, one objective of this thesis was to characterize VP40-WT and VP40-R134A and to look for differences that would indicate roles of VP40 octamerization in the viral life cycle.

3.1.1 Intracellular distribution of octamerization-deficient VP40

To analyze the intracellular distribution of VP40-WT and VP40-R134A, HeLa cells were transfected with pCAGGS-VP40-WT and pCAGGS-VP40-R134A. Also, two other mutants, VP40-F125A-R134A and VP40-F125A, were analysed. VP40-F125A-R134 ia also octamerization deficient, and VP40-F125A shows an intermediate phenotype with respect to octamerization. The distribution of proteins was determined using a monoclonal α-VP40 antibody.

While WT-VP40 was mainly distributed in small patches along the plasma membrane, VP40-F125A was detected in larger aggregates along the plasma membrane as well as in the perinuclear region (Figure 22). Similarly, VP40-R134A and VP40-F125A-R134A were mostly found in large aggregates in the perinuclear region and at the plasma membrane. However, the extent of cytoplasmic VP40 distribution of these two mutants seemed to be reduced when compared to WT-VP40 and VP40-F125A.

3.1.2 Morphology of VLPs containing octamerization-deficient VP40

Although we had previously reported that there are no obvious differences in the morphology of VLPs produced by WT-VP40 or octamerization-deficient VP40, as judged by electron microscopy, these results had not been quantified. We, therefore, decided to quantify the diameter of VLPs produced by the different forms of VP40. A large number of electron microscopic photos were obtained and the diameter of VLPs was measured. 1714 measurements were obtained in 100 nm intervals from 152 VLPs. No significant difference

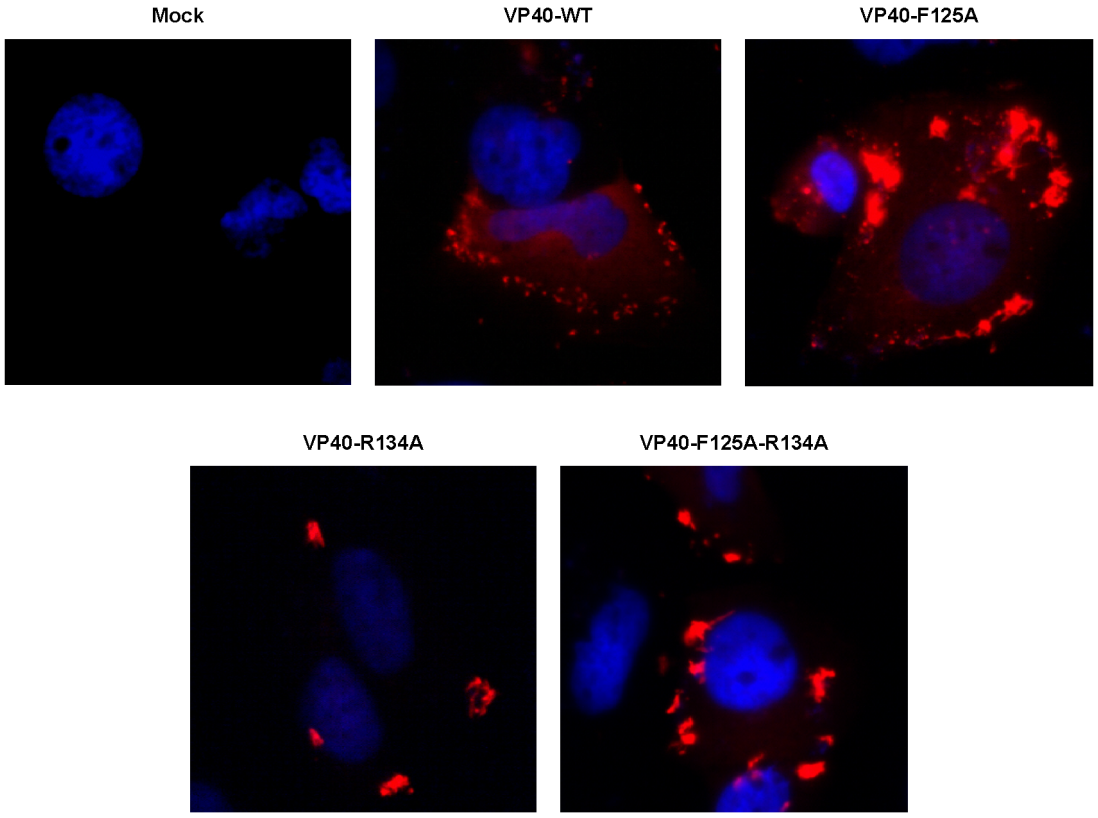

Figure 22: **Intracellular distribution of VP40.** HeLa cells transfected with different VP40 constructs as indicated were stained 24 hours p.t. using a monoclonal α-VP40 antibody and a rhodamine-coupled secondary antibody. Cell nuclei were stained with 4',6'-diamidino-2-phenylindole.

in diameter could be detected between the different VLPs, supporting our earlier finding that they are morphologically indistinguishable (Table 2).

VP40 mutant	diameter	# measurements	# measured VLPs
WT	40.9 nm ± 9.5 nm	378	32
F125A	44.3 ± 8.9 nm	353	37
R134A	44.0 ± 9.5 nm	550	49
F125A-R134A	40.0 ± 7.0 nm	433	34

Table 2: **Diameter of VP40 VLPs.**

3.1.3 Dominant negative effect of VP40-R134A on octamerization

To further characterize the octamerization-deficient VP40-R134A mutant we wanted to know whether or not this mutant would be dominant negative with respect to octamer-

ization. We, therefore, coexpressed a constant amount of HA-tagged VP40-WT and increasing amounts of flag-tagged VP40-R134A and visualized HA-tagged VP40 octamers using western blotting.

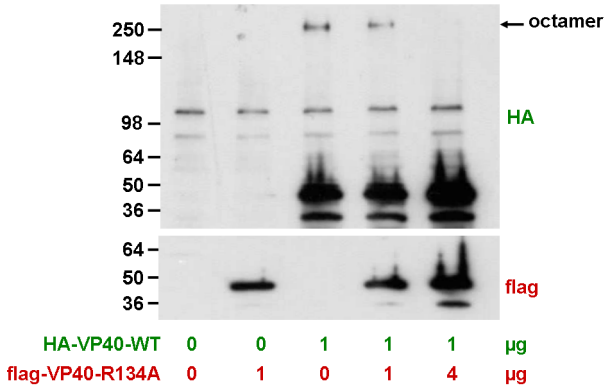

Figure 23: **Dominant negative effect of VP40-R134A.** VP40 octamerization after coexpression of 1 μg HA-tagged VP40-WT and 0, 1 or 4 μg flag-tagged VP40-R134A. Octamerization assay was performed and VP40 was detected using monoclonal antibodies against the flag-tag or the HA-tag.

When we coexpressed VP40-WT and VP40-R134A, the amount of octamers decreased, although the amount of VP40-WT available for octamerization remained constant (Figure 23). Corresponding to the decrease in octameric VP40 an increase in monomeric VP40 was observed. Therefore, we concluded that VP40-R134A is dominant negative *in vitro*.

3.1.4 Role of VP40 octamerization in an iVLP assay with pretransfected target cells

Analysis of VLP production by VP40 allows only the investigation of budding, while other processes in which VP40 is potentially involved, e.g. morphogenesis and incorporation of RNP complexes into virions, but also viral transcription and replication, can not be studied using this system. It was therefore decided to test the effect of octamerization-deficiency in an iVLP assay which had recently been developed for ZEBOV by Watanabe *et al.* [212], and which allows the study of these processes.

3.1.4.1 Role of VP40 octamerization on transcription, translation and vRNA replication To analyze the influence of VP40 on cellular and viral transcription, translation and vRNA replication, we performed an iVLP assay as described in section 2.4.1, but

evaluated only reporter activity in p0 cells. 293T cells (p0) were transfected with plasmids encoding all viral structural proteins, a T7-driven minigenome and T7 RNA polymerase to allow for inital transcription of the minigenome. An expression plasmid encoding firefly luciferase was included in the assay to serve as a transfection control, and to allow normalization of samples to transfection efficiency. Cells that where not transfected with the VP40-encoding plasmid served as a control, and reporter activity in these cells was defined as 100% .

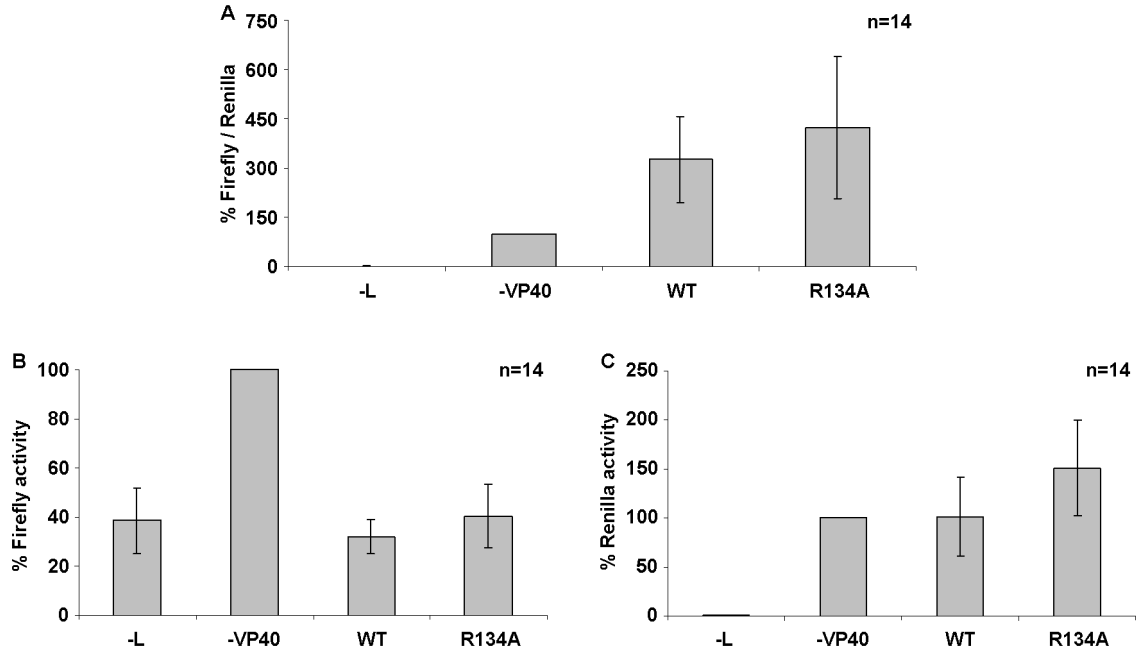

Figure 24: **Influence of VP40-WT and VP40-R134A on transcription and replication.** 293T cells were transfected with plasmids enocding a T7-driven minigenome and T7 RNA polymerase, as well as plasmids encoding all viral proteins and Firefly luciferase to allow for normalization of transfection efficiency. Either no VP40, VP40-WT or VP40-R134A was included. As a negative control, L was omitted. 72 hours p.t., reporter activity was measured. Activity in cells without VP40 was defined as 100%. (A) Renilla reporter activity normalized to Firefly reporter activity. (B) Firefly reporter activity. (C) Renilla reporter activity.

Reporter activity in p0 was dependent on L (Figure 24A). To our surprise, minigenome encoded Renilla activity in presence of VP40 was increased about 3 ×, when we looked at reporter activity normalized to Firefly activity (Figure 24A). Also, we observed a higher reporter activity in presence of VP40-R134A compared to VP40-WT (327% ± 131% vs. 422% ± 216%; n=14). In a paired t-test this difference was significant (p=0.046). However, if VP40 has an influence on cellular transcription or translation, this would influence the level of Firefly luciferase used for normalization and, thus, distort the results. We, there-

fore decided to examine the activities of Firefly and Renilla luciferase separately from each other. When we compared only Firefly activity in the presence or absence of VP40, we saw that it was about 3 × lower in the presence of VP40 (Figure 24B). Interestingly, VP40-WT and VP40-R134A had a significantly different influence on Firefly activity (32% ± 7% vs. 40% ± 13%; n=14; p=0.0053). In contrast VP40-WT did not influence Renilla activity (101% ± 40%; n=14) (Figure 24C). However, VP40-R134A showed a higher Renilla activity (151% ± 49%; n=14; p=0.0041), which was significantly different from the Renilla activity in the presence of VP40-WT. We, therefore, concluded that VP40 seems to influence cellular transcription and/or translation, but does not influence minigenome transcription and replication.

3.1.4.2 Role of VP40 octamerization on minigenome transfer To analyze the influence of VP40 octamerization on morphogenesis, budding and entry, the iVLP assay with pretransfected target cells was performed as described in section 2.4.1. 293T cells (p0) were transfected and after 3 days the supernatant of these cells was transferred to 293T target cells (p1), which had been pretransfected with all RNP components. While reporter activity in p0 reflects replication and transcription of the minigenome, reporter activity in p1 is also dependent on delivery of minigenomes into the target cells and, therefore, additionally reflects packaging, morphogenesis, budding and entry. Reporter activity in p1 was dependent on the presence of VP40 in p0; the negative signal without VP40 in p0 was 1.4% ± 1.2% of the positive signal when WT iVLPs were transferred (Figure 25). Changing VP40 against VP40-R134A did not induce a significant change in reporter activity in p1.

3.1.5 Development of an iVLP assay with naïve target cells

To date all iVLP systems rely on RNP components in p1, which are provided by either transfection or helper virus infection. Since, in theory, delivery of one minigenome is enough to initiate replication and transcription, these systems produce high signals. However, they do not model the initial transcription of negative-sense RNA in target cells by the RNP components packaged in the virion, a step indispensable in a real infection. We, therefore, decided to develop an iVLP system that is independent of the presence of RNP components in p1.

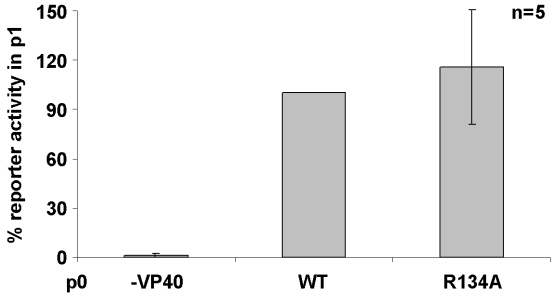

Figure 25: **VP40-R134A in an iVLP assay with pretransfected target cells.** iVLPs were produced with either VP40-WT or VP40-R134A. 3 days p.t. the iVLP-containing supernatant of p0 was transferred to 293T target cells (p1) pretransfected with all RNP components. After 3 days reporter activity, reflecting delivery of the minigenome and, therefore, packaging, budding and entry, was determined in these cells.

3.1.5.1 Timecourse of reporter activity in p1 In a first pilot experiment the protocol for an iVLP assay with pretransfected target cells was adopted; however, naïve 293T and VeroE6 cells were used as target cells. In this first experiment naïve VeroE6 cells were much more susceptible to transfection than naïve 293T cells; however, in both cases absolute signals were very low when compared to those obtained using an iVLP assay with pretransfected target cells (data not shown). We, therefore, decided to perform timecourse experiments to determine the optimal timepoint for analyzing p1 cells for reporter activity.

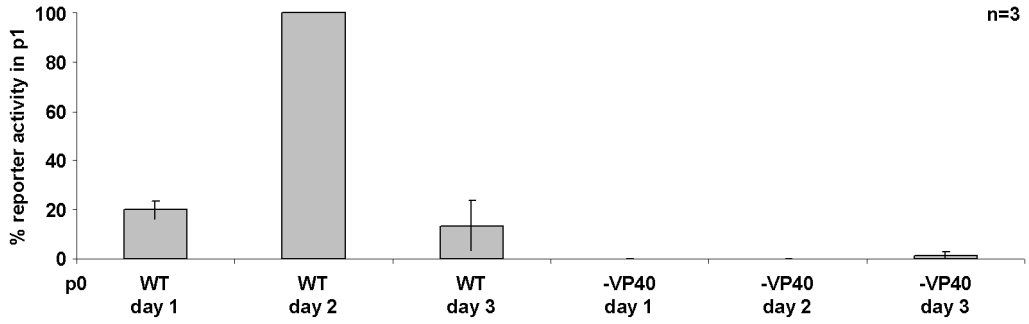

Figure 26: **iVLPs assay with naïve target cells: timecourse.** iVLPs were produced and used to infect naïve VeroE6 cells. p1 cells were harvested at days 1, 2 and 3 p.i. and reporter activity was determined.

Interestingly, reporter activity increased from day 1 to day 2, but then dropped down again (Figure 26). This can be explained by the fact that after entry and uncoating initial transcription takes place, which leads to the accumulation of reporter protein. However, since RNP components as well as minigenome are only available in very small amounts, and most likely no replication of the minigenome takes place (see section 1.5), this process

comes to a stop after some time, and the previously produced reporter protein is turned over via the degradation pathways in the target cells.

3.1.5.2 Infection of different target cell types To further optimize the system, different target cell types were tested. In particular, we compared 293T cells, which have been used in previous iVLP assays as target cells, VeroE6 cells, which are usually used in our laboratory to propagate EBOV, and human macrophages, which are known to be natural target cells for EBOV.

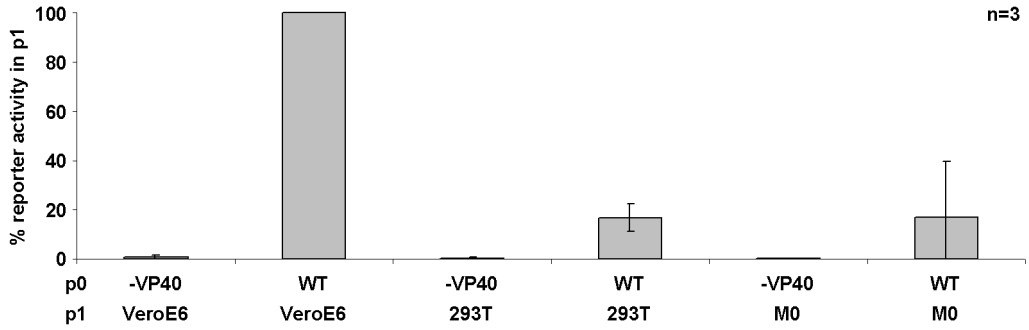

Figure 27: **iVLPs assay with naïve target cells: cell lines.** iVLPs were produced and used to infect VeroE6 and 293T cells as well as human macrophages (M0). After 2 days reporter activity was determined.

As already observed in our pilot experiment, infection of 293T cells with iVLPs resulted in an about 6 × lower signal than infection of Vero E6 cells (17% ± 6%; n=3). Also, infection of human primary macrophages produced lower reporter levels than infection of VeroE6 cells; however, only macrophages from one donor were tested.

3.1.5.3 Further characterization of the iVLP assay with naïve target cells To ensure that reporter activity in p1 was not due to unspecific transfer of reporter protein inside iVLPs, the iVLP producing p0 cells were cotransfected with a plasmid encoding Firefly luciferase under the control of an eukaryotic promoter. If reporter activity in p1 was due to unspecific transfer of reporter protein from p0 to p1, there should be no drop in the ratio of Firefly to Renilla from p0 to p1, since unspecific packaging of Renilla and Firefly luciferase would be expected to occur equally.

We observed a drop in the ratio of Firefly luciferase to Renilla luciferase of about 12 × (4.6‰± 1.5‰vs. 0.4‰± 0.1‰; n=4). This indicates that reporter activity in p1 is not

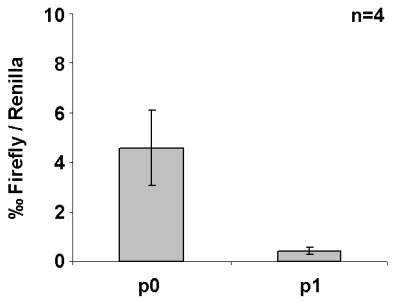

Figure 28: **Specific transfer of minigenome in an iVLP assay with naïve target cells.** To ensure that reporter activity in p1 is not due to unspecific transfer of reporter protein, the ratio of minigenome encoded Renilla luciferase and plasmid encoded Firefly control luciferase was determined in p0 and p1.

due to unspecific transfer of reporter protein, but rather caused by transfer of minigenome and subsequent transcription of minigenome and translation of the reporter mRNA in p1.

We also compared the absolute signal strength between iVLP assays with pretransfected and naïve target cells (Table 3). It is interesting to note that a positive signal in an iVLP assay with pretransfected 293T target cells is about 100 × higher than a positive signal in an iVLP assay with naïve VeroE6 target cells. Also, a negative signal in an iVLP assay with pretransfected target cells is of similar strength than a positive signal in an iVLP assay with naïve target cells.

cell type	sample	pretransfected p1	naïve p1
293T	-40	$1.8 \times 10^5 \pm 5.7 \times 10^4$	$7.4 \times 10^2 \pm 3.6 \times 10^2$
293T	WT	$9.3 \times 10^6 \pm 1.8 \times 10^5$	$1.8 \times 10^4 \pm 8.3 \times 10^3$
Vero	-40	nd	$7.1 \times 10^2 \pm 4.9 \times 10^2$
Vero	WT	$2.5 \times 10^6 \pm$ nd	$1.3 \times 10^5 \pm 8.4 \times 10^4$

Table 3: **Absolute signals in iVLP assays.** Signals are given in RLU/s/well. nd = not determined.

Finally, we wanted to demonstrate that filamentous particles and not spherical particles, which are usually found in high amounts in VLP preparations, are responsible for transfer of minigenomes. We, therefore produced iVLPs and purified them over a sucrose cushion and a Nycodenz gradient (see sections 2.4.4 and 2.4.5). We then pooled fractions 1-3 and 4-6, which contain the spherical and filamentous particles, respectively (see section 2.4.5), pelleted the iVLPs by ultracentrifugation for 1 hour at 21000 × g in an SW41 rotor, resuspended the pellet in 4 ml $DMEM_{5\%FBS}$ and used this suspension to infect naïve VeroE6 cells.

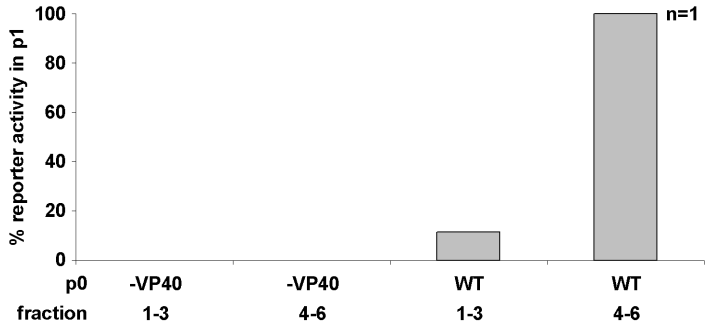

Figure 29: **iVLP assay with Nycodenz gradient separated iVLPs.** iVLPs were produced and purified over a sucrose cushion and a Nycodenz gradient. Fractions 1-3 (spherical particles) or 4-6 (filamentous particles) were used to infect naïve VeroE6 cells.

The reporter signal in cells infected with particles from fractions 4-6 was about 10 × higher than the signal in cells infected with particles from fractions 1-3, showing that filamentous particles are responsible for the transfer of reporter activity (Figure 29).

3.1.6 Role of VP40 octamerization in an iVLP assay with naïve target cells

With the iVLP assay with naïve target cells set up, we analyzed the influence of VP40-octamerization on minigenome transfer and initial transcription in p1 in this system.

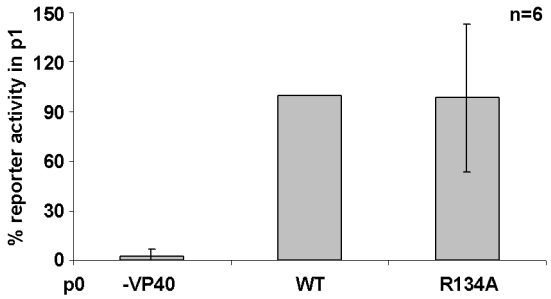

Figure 30: **VP40-R134A in an iVLP assay with naïve target cells.** iVLPs were produced with either VP40-WT or VP40-R134A and used to infect naïve VeroE6 target cells. After 2 days reporter activity, reflecting morphogenesis of functional nucleocapsids, packaging, budding, entry and initial transcription, was determined in these cells.

We were not able to detect a significant difference in reporter activity conferred by iVLPs produced with VP40-WT or VP40-R134A (Figure 30), suggesting that VP40 octamerization is not necessary for the assembly of functional RNP complexes able to perform initial transcription in target cells.

3.1.7 Development of a stable cell line supressing viral VP40

Since we were not able to detect any differences between VP40-WT and VP40-R134A using iVLP systems, we decided to analyze the impact of impaired octamerization on the viral life cycle in a real virus infection. However, we faced the problem that a recombinant virus carrying the R134A mutation was not rescuable, since octamerization is essential for the viral life cycle [96]. We, therefore, decided to knock out viral VP40 using a non-coding region (NCR) directed siRNA, and substitute either WT-VP40 or VP40-R134A carrying a flag-tag *in trans* by transfection of the corresponding plasmids, which do not contain the NCR. As an siRNA system we decided to generate a stable cell line expressing a small hairpin RNA under the control of a human H1 RNA polymerase III promoter, which is then cleaved into siRNA molecules by the cellular enzyme Dicer, since this approach had previously been succesfully used in our laboratory [79].

3.1.7.1 Cloning and testing of siRNA constructs siRNA target sequences were selected using the Invivogen siRNA wizard (http://www.sirnawizard.com). In total 3 siRNA were designed, 2 directed against the NCR of ZEBOV-VP40 (Z0 and Z1) (Figure 31A), and 1 directed against the NCR of MARV-VP40 (M0) as a control. siRNA-expressing constructs were cloned as described in appendix A.13; also, an VP40 expression plasmid which contained the VP40-NCR (pCAGGS-VP40-STP) was constructed to allow testing of siRNA *in vitro*.

To test the constructed siRNA-expressing plasmids, they were cotransfected with pCAGGS-VP40-STP, and after 24 hours the cells were harvested and a western blot against VP40 was performed. When we compared the two constructs expressing siRNAs against ZEBOV-VP40, we observed that Z0 was more potent in reducing the amount of expressed VP40-STP than Z1 (Figure 31B). Also, Z0 was specifically directed against the VP40-NCR, since it did not reduce expression of VP40-WT, which does not contain the NCR. Also, a control siRNA directed against the MARV-VP40-NCR did not reduce expression of VP40-STP, showing that the reduction observed in presence of Z0 is not due unspecific effects of siRNA being present (Figure 31C).

3.1.7.2 Generation of a stable cell cell line expressing an siRNA directed against the non-coding region of VP40 (653#9) We then proceeded to generate

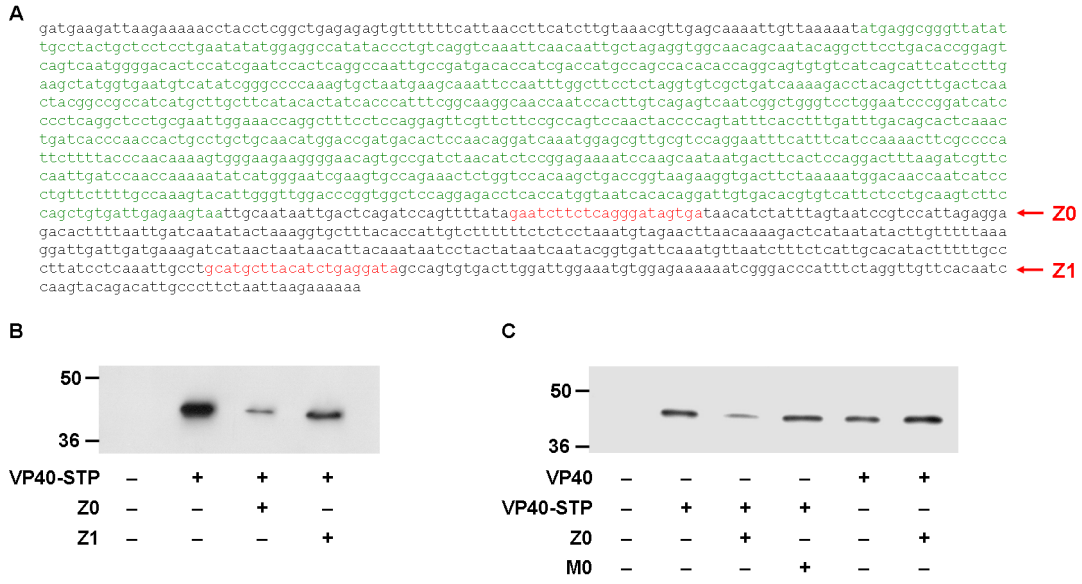

Figure 31: **VP40-NCR siRNAs *in vitro*.** (A) Location of siRNA targets. The VP40-transcript including NCRs is shown. The ORF for VP40 is marked in green, the target sequences for Z0 and Z1 in red. (B) Comparison of Z0 and Z1. 250 ng pCAGGS-VP40-STP was cotransfected with 1 μg of siRNA encoding plasmid Z0 or Z1. After 24 hours, cells were harvested and subjected to western blotting using a monoclonal α-VP40 antibody. (C) Specificity of siRNA targeting. To ensure that Z0 does not unspecifically impair expression of VP40-STP, a control experiment was performed in which pCAGGS-VP40-WT was cotransfected with the Z0 expressing plasmid. As an additional control, the plasmid expressing the siRNA M0 which should not have an effect on VP40-STP expression was coexpressed with pCAGGS-VP40-STP.

a cell line stably expressing the construct encoding Z0, which had the plasmid number 653. Generation of the VeroE6-derived cell line was performed as descibed in section 2.2.5. 24 cell clones were picked, expanded and then seeded at three different ratios into 6-well plates for transfection. On the day of transfection, wells with approximately 50% confluency were selected and cotransfected with pCAGGS-NP and pCAGGS-VP40-STP. After 48 hours cells were harvested and the samples subjected to western blotting using monoclonal antibodies directed against VP40 and NP. The ratio of VP40 to NP was evaluated, and samples of 8 cell clones which showed the most promising results, i.e. low levels of VP40 compared to levels of NP, were loaded again onto an SDS-PAGE gel. The amount of lysate loaded was chosen so that NP levels were expected to be similar in each lane, in order to compensate for differences in cell number at the time of harvest, as well as differences in tranfectibility and expression rate between the cell lines. After SDS-PAGE the samples were again subjected to western blotting. From the 8 cell lines that were selected for this second round of western blotting, clones 3, 7, 8, 9, 16 and 20 showed highest reduction in VP40-levels and were chosen for further testing (Figure 32).

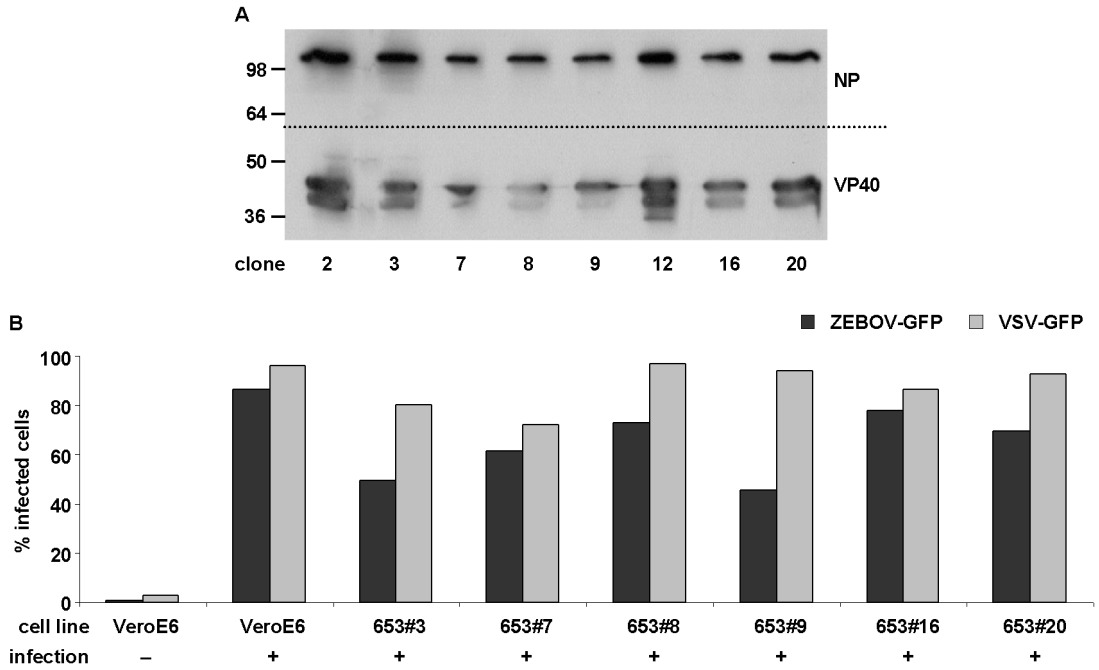

Figure 32: **Testing of cell line 653 clones.** (A) Cell clones were grown to approximately 50% confluencey and transfected with 500 ng pCAGGS-NP and 500 ng pCAGGS-VP40-STP. 48 hours p.t. cells were harvested, and subjected to SDS-PAGE and western blotting with monoclonal antibodies directed against NP and VP40. The amount of sample loaded was adjusted for equal NP expression. (B) 6 Clones were grown to confluency and then infected with either ZEBOV-GFP (MOI 0.05) or VSV-GFP (MOI 0.005). Cells were harvested 2 days (VSV-GFP) or 4 days (ZEBOV-GFP) p.i., and analyzed by flow cytometry.

As a next step we tested the 6 selected clones for supression of ZEBOV infection. Each cell line clone was grown to confluency, and infected with ZEBOV-GFP at an MOI of 0.05 as described in section 2.5.1. As a control, in parallel each cell line clone was infected with VSV-GFP to detect general defects in the cell line making it resistent to infection with negative strand viruses (e.g. defects in the cellular translation machinery). Cells infected with VSV-GFP were harvested after 2 days, cells infected with ZEBOV-GFP after 4 days, and subsequently analyzed using flow cytometry. From the cell line clones tested, cell line 653#9 showed the highest reduction in the number of ZEBOV-GFP infected cells (46% vs. 87% infected cells for VeroE6 cells), while there was no difference using this cell line for infection with VSV-ZEBOV compared to VeroE6 cells (Figure 31B). Therefore, we decided to use cell line 653#9 for our further experiments.

3.1.7.3 Characterization of filovirus infection in cell line 653#9 We then decided to compare the growth kinetics of ZEBOV-GFP in VeroE6 and 653#9 cells at dif-

ferent MOIs, in order to find conditions under which the greatest difference in infectivity between these cell lines is observed, which would provide us with the highest sensitivity for further experiments. 500000 cells VeroE6 or 653#9 were seeded into 6-well plates and after 6 hours infected with ZEBOV-GFP at MOIs of 0.05 and 0.0005. Supernatant and cells were harvested daily from day 2 to day 6, and the number of infected cells was determined by flow cytometry. Also, the viral titer in the supernatant was determined by autofluorescent plaque assay (see section 2.5.2).

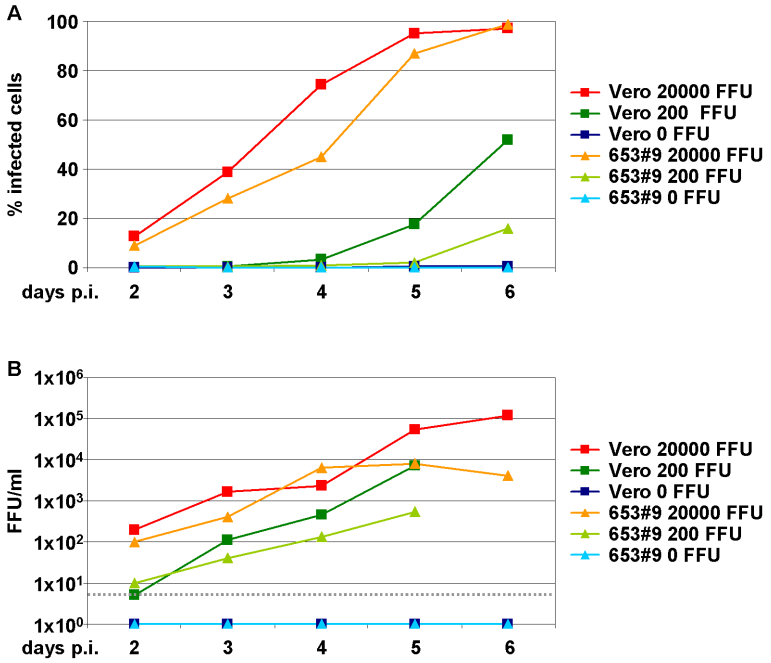

Figure 33: **Growth of ZEBOV-GFP in 653#9.** VeroE6 and 653#9 cells were infected with 20000 or 200 FFU ZEBOV-GFP (MOI 0.05 or 0.0005). (A) The number of infected cells was determined using flow cytometry. (B) The infectious titer was determined using plaque assay. The detection limit is indicated as gray dotted line.

After 5 days for both VeroE6 and 653#9 cells almost all cells were infected when a high MOI was used (Figure 33A). 4 days after infection at a high MOI 45% of 653#9 cells were infected, vs. 74% of VeroE6 cells, which correspondes to a 1.6 fold decrease in number of infected cells. For infection at low MOI, the biggest difference in the number of infected cells was observed after 5 days, when 18% of VeroE6 cells, but only 2% of 953#9 cells were infected, corresponding to an 9 fold decrease in the number of infected cells. This difference was also observed in infectious titer in the supernatant, which was 8×10^3 for VeroE6 cells, and 5.5×10^2 for 653#9 cells, a 14 fold reduction in infectious titer. We, therefore, decided to perform further experiments at a low MOI of 0.0005, and to harvest

cells for analysis by flow cytometry analysis after 5 days.

To ensure that the impairment of ZEBOV-infection is really due to a specific effect of the siRNA, we infected both VeroE6 cells and 653#9 cells with REBOV at an MOI of 0.0005 and harvested supernatant for plaque assay after 5 days. REBOV does not have the target sequence for the siRNA in its VP40-NCR; however, since it is a very close relative of ZEBOV, any target-sequence unspecific effect of the siRNA, which might be impairing ZEBOV infection, should also be detectable in a REBOV infection. Since there is currently no infectious clone system and, therefore, also no recombinant REBOV-GFP, available, we did not perform flow cytometry analysis of infected cells, but performed an immunoplaque assay with the supernatants as described in section 2.5.3. While we observed a strong decrease in infectious titer between VeroE6 cells and 653#9 cells when infected with ZEBOV-GFP, no significant difference could be detected when using REBOV for infection (Figure 34). This shows that the impairment of virus growth is specific for ZEBOV.

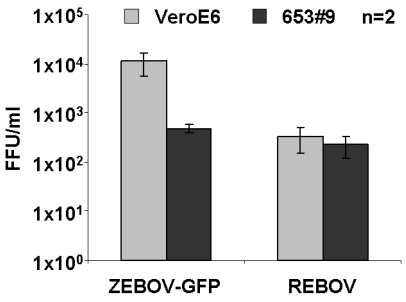

Figure 34: **REBOV and ZEBOV infection of VeroE6 and 653#9 cells.** VeroE6 and 653#9 cells were infected with ZEBOV-GFP or REBOV at an MOI of 0.0005 (200 FFU). Infectious titers in the supernatant after 5 days were determined using either plaque (ZEBOV-GFP) or immunoplaque (REBOV) assay. The detection limit was 5×10^1 FFU/ml.

3.1.8 Rescue of infection in 653#9 cells by VP40 expression *in trans*

After we had confirmed that the stable cell line 653#9 specifically inhibits ZEBOV infection by inhibiting expression of viral VP40, we decided to try to rescue ZEBOV-infection by providing either VP40-WT or VP40-R134A *in trans* from plasmids lacking the VP40-NCR, and thus the siRNA target. The comparison of rescue by VP40-WT and VP40-R134A should then allow confirmation of the importance of VP40 octamerization for the viral life cycle.

As electroporation in the BSL4 laboratory in Winnipeg is not possible since no electroporator is present, we decided to transfect VeroE6 with chemical transfection reagents (see also section 3.4.4.1). After several optimization steps we decided to used an increased ratio of Fugene:DNA (6 to 1). VeroE6 cells or 653#9 cells were then infected with 200 FFU ZEBOV-GFP (MOI 0.0005). One hour p.i., the cells were washed once and then transfected with 800 ng of either pCDNA3.1-flag-VP40-WT or pCDNA3.1-flag-VP40-R134A. As a control, empty plasmid was transfected. Cells were harvested 5 days p.i. and the percentage of infected cells was determined by flow cytometry.

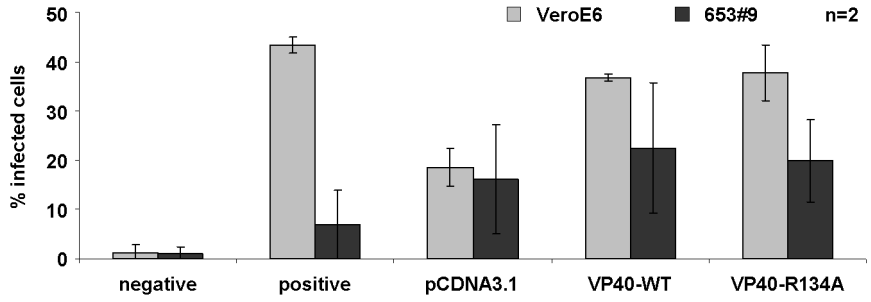

Figure 35: **Rescue of infection in 653#9 cells.** 653#9 and VeroE6 cells were infected with 200 FFU ZEBOV-GFP (MOI 0.0005). Cells were either not transfected (negative and positive controls) or transfected one hour p.i. with 800 ng of either empty plasmid (pCDNA3.1), pCDNA3.1-flag-VP40-WT or pCDNA3.1-flag-VP40-R134A. Cells were harvested 5 days p.i., and the number of infected cells was determined by flow cytometry.

Transfection of both VP40-WT or VP40-R134A seems to be able to restore infectivity in 653#9 cells (Figure 35). However, transfection of empty plasmid also increased the percentage of infected cells, suggesting that this rescue is not due to specific effects of the transfected proteins. Therefore, alternative methods of transfection or changes in the transfection protocol need to be considered for future experiments.

3.2 Role of VP40 dimerization

Besides octamers VP40 is also able to form hexamers [162, 179]. Unfortunately, there is no crystal structure for hexamers available, and the only theoretical model that was published has since been withdrawn from the protein data bank [146]. However, the available data suggest that the building blocks for both hexamers and octamers are antiparallel dimers [192]. Therefore, we decided to design a dimerization incompetent mutant based on the structural data available for VP40 octamers, in the hopes that this mutant would also not be able to from hexamers and, thus, be completely oligomerization-deficient.

3.2.1 Design, cloning and expression of dimerization-deficient VP40 mutants

Based on the crystal structure, we identified two key residues in dimer formation, namely W95 and E160 (Figure 36). Constructs expressing point mutants in which these amino acids were exchanged against alanine were designed for expression in mammalian cells using pCAGGS as a backbone, as well as in pBind and pAct to allow assessment of oligomerization using a mammalian two hybrid assay (see section 2.3.6). Cloning of the constructs was performed as described in appendix A.13. Constructs were checked for expression in 293T cells (Figure 37).

3.2.2 Dimerization in a mammalian two hybrid assay

To assess whether the cloned VP40 mutants are still able to dimerize, they were analyzed using a mammalian two hybrid assay as described in section 2.3.6. Surprisingly, in our first experiments we were unable to detect any VP40 oligomerization even with VP40-WT (Figure 38), although the constructs were expressed. Since oligomeric VP40 has been shown to bind membranes, we concluded that this membrane binding might interfere with nuclear localization of the VP40-fusion proteins, which is necessary in a mammalian two hybrid assay for transactivation of reporter transcription. Therefore, we decided to remove the C-terminal membrane-binding domain and to express just the N-terminal oligomerization domain of VP40, and check for interaction.

We observed that VP40-ΔC194 is able to oligomerize, with reporter activity levels being around 28% of the positive control (Figure 38). Both single mutants VP40-ΔC194-W95A and VP40-ΔC194-E160A showed impaired interaction (9% $\pm$ 3% and 12% $\pm$ 4%; n=3),

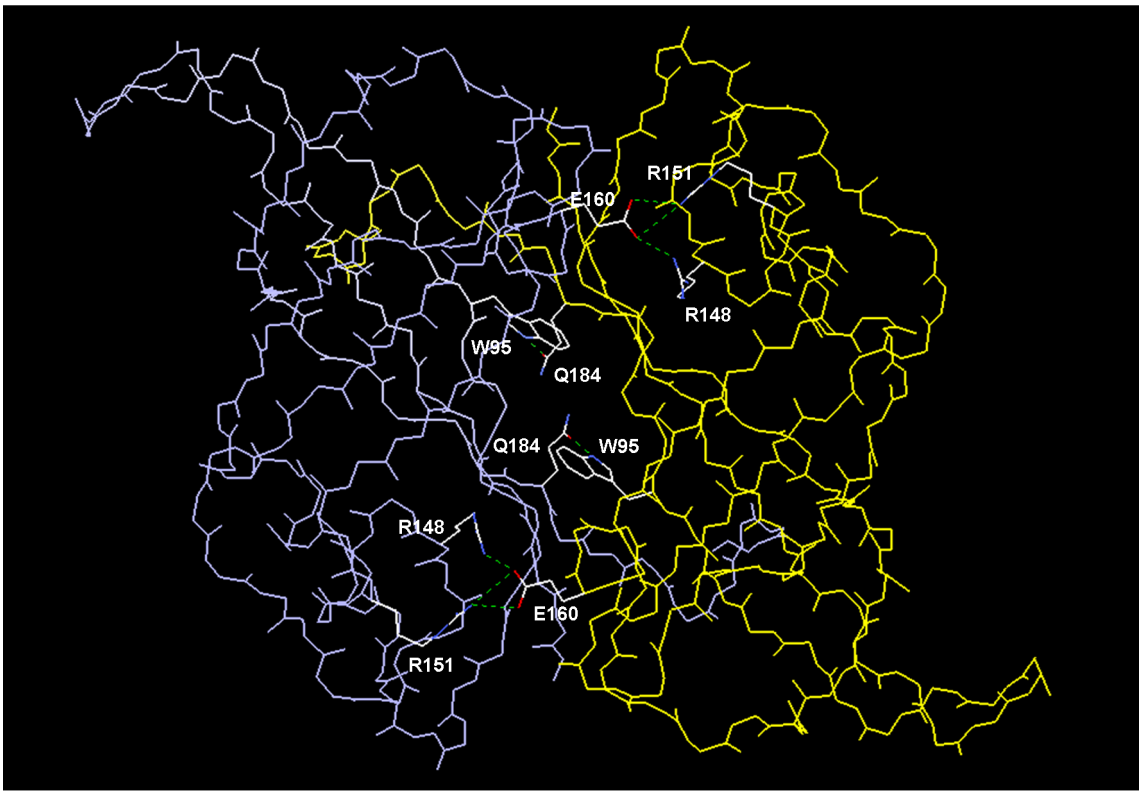

Figure 36: **VP40 dimer.** One dimer of a VP40 octamer is shown. The backbone of one VP40 monomer is shown in purple, the backbone of the other VP40 monomer in yellow. The sidechains of amino acids responsible for intradimeric interaction are shown as an all atom model. Interaction forces between aminoacids E160/R148, E160/R151 and W95/Q184 are indicated as green dotted lines.

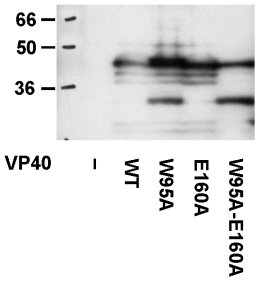

Figure 37: **Expression of VP40 dimerization-mutants.** 1 μg of pCAGGS-VP40-WT, pCAGGS-VP40-W95A, pCAGGS-VP40-E160A or pCAGGS-VP40-W95A-E160A were transfected into 293T cells. As a negative control empty pCAGGS plasmid was transfected. 24 hours p.t., cells were harvested and subjected to SDS-PAGE and western blotting using a polyclonal goat serum against EBOV.

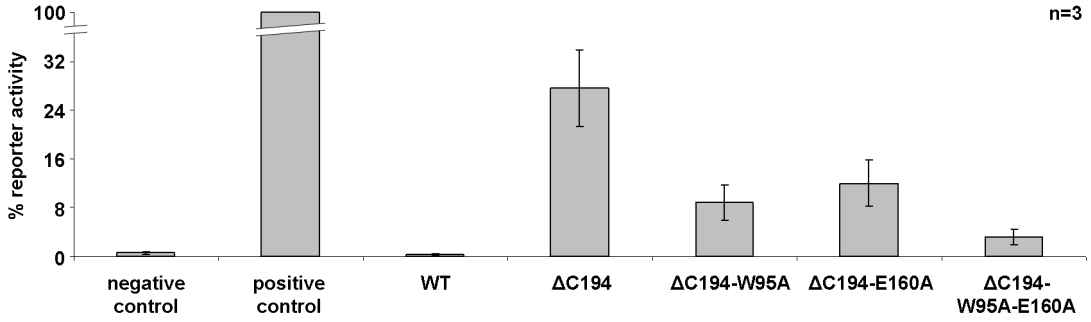

Figure 38: **VP40 dimerization in a mammalian two hybrid assay.** Fusion proteins consisting of VP40 and either a DNA-binding domain or a transactivator domain were cotransfected with a reporter plasmid. Two days p.t., cells were harvested and reporter activity indicating the formation of a functional transcription factor by interaction of the two fusion proteins was determined. As a positive control fusion proteins containing the MyoD and Id proteins, which are known to interact with each other, were used; as a negative control cells cotransfected with reporter plasmid and plasmids expressing the DNA-binding domain and transactivator domain without any interaction domain were used.

while for the double mutant VP40-ΔC194-W95A-E160A almost no interaction could be detected (3% ± 1%; n=3).

3.2.3 Influence of VP40 dimerization on transcription, translation and vRNA replication

Since our previous results had suggested an influence of VP40 on cellular transcription and/or translation, we decided to analyze the influence of dimerization-impaired VP40 on these processes as described in section 3.1.4.1. 293T cells (p0) were transfected with plasmids encoding all viral structural proteins, a T7-driven minigenome and T7 RNA polymerase, as well as an expression plasmid encoding firefly luciferase to allow for normalization of samples to transfection efficiency. Reporter activity was determined 3 days p.t. As a positive control cells that were not transfected with the VP40-encoding plasmid were used, and reporter activity in these cells was defined as 100% .

For Renilla activity, we did not observe any differences between the dimerization impaired VP40 mutants and VP40-WT (Figure 39C). Interestingly, when we compared the Firefly activity, the fully dimerization-incompetent mutant VP40-W95A-E160A showed a significantly higher activity than VP40-WT (65% ± 4% vs. 32% ± 10%; n=3; p=0.0039), while the partially dimerization-impaired mutants did not show any difference (Figure 39B).

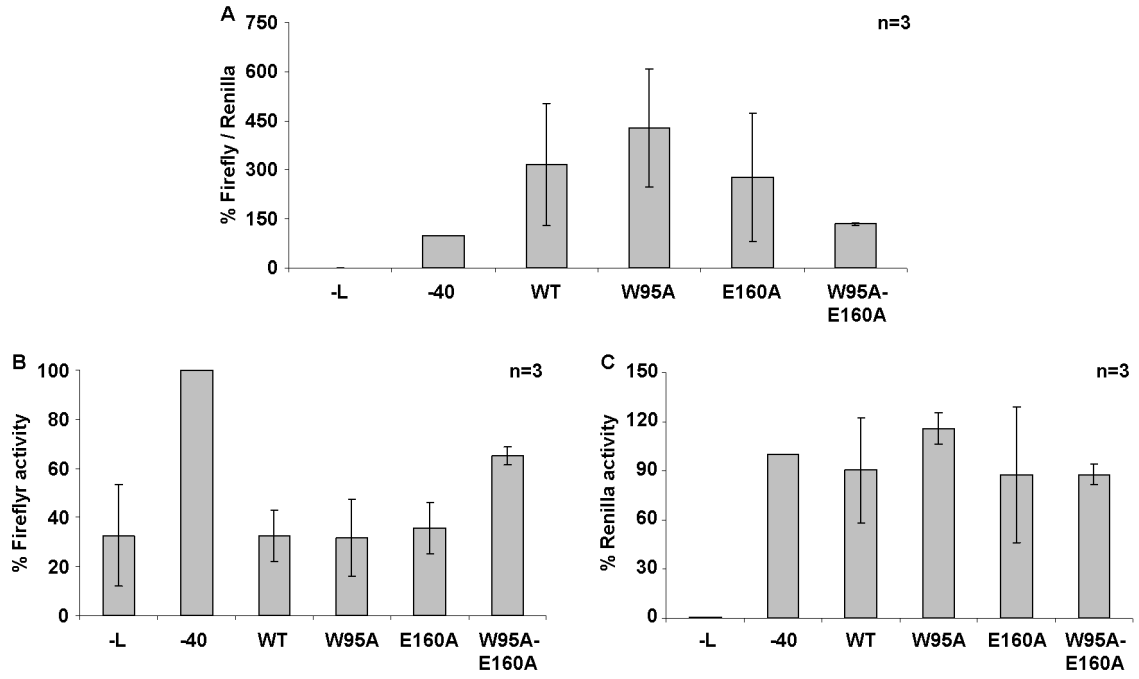

Figure 39: **Influence of VP40 dimerization on transcription and replication.** 293T cells were transfected with plasmids enocding a T7-driven minigenome, T7 RNA polymerase, Firefly luciferase to allow for normalization of transfection efficiency, and all viral proteins. Either no VP40, VP40-WT or one of the VP40 dimerization mutants was included. As a negative control, L was omitted. 72 hours p.t., reporter activity was measured. Activity in cells without VP40 was defined as 100%. (A) Renilla reporter activity normalized to Firefly reporter activity. (B) Firefly reporter activity. (C) Renilla reporter activity.

3.2.4 Role of dimerization in an iVLP assay

We next analyzed the role of VP40 dimerization in an iVLP assay with pretransfected target cells. When iVLPs were produced in the presence of the single mutants W95A or E160A, we did not observe a significant difference in reporter activity in p1 compared to VP40-WT (Figures 40). In contrast, when we included the dimerization incompetent VP40-W95A-E160A in p0, reporter activity in p1 dropped to 9%. Since this result can be caused either by the absence of iVLPs produced by VP40-W95A-E160, or by the production of non-functional iVLPs (e.g. lacking a nucleocapsid due to impaired interaction between VP40 and NP), we then further analysed the iVLPs produced in presence of VP40-W95A-E160A. While iVLPs produced by VP40-W95A or VP40-E160A could be shown to contain membrane-enclosed VP40, we were not able to detect VP40 or NP in form of iVLPs in the supernatant of cells transfected with VP40-W95A-E160A (Figure 41), which indicates that the block in the production of functional iVLPs is at the level of

budding, or even earlier in the viral life cycle, such as intracellular transport of VP40.

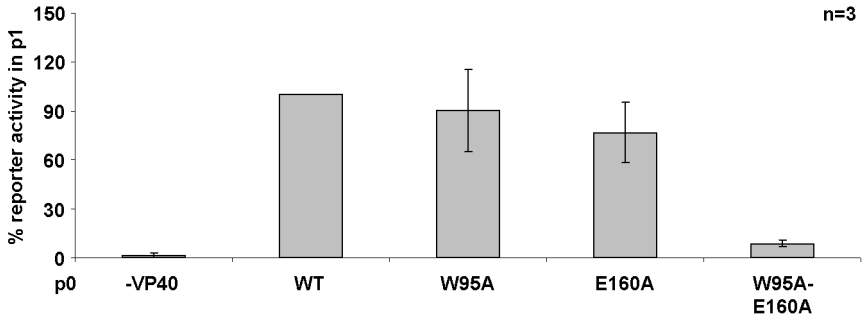

Figure 40: **Effect of VP40 dimerization in an iVLP assay.** iVLPs were produced with VP40-WT or the dimerization mutants VP40-W95A, VP40-E160A or VP40-W95A-E160A. 3 days p.t., the iVLP-containing supernatant of p0 was transferred to 293T target cells (p1) pretransfected with all RNP components. After 3 days reporter activity, reflecting delivery of the minigenome and, therefore, packaging, budding and entry, was determined in these cells.

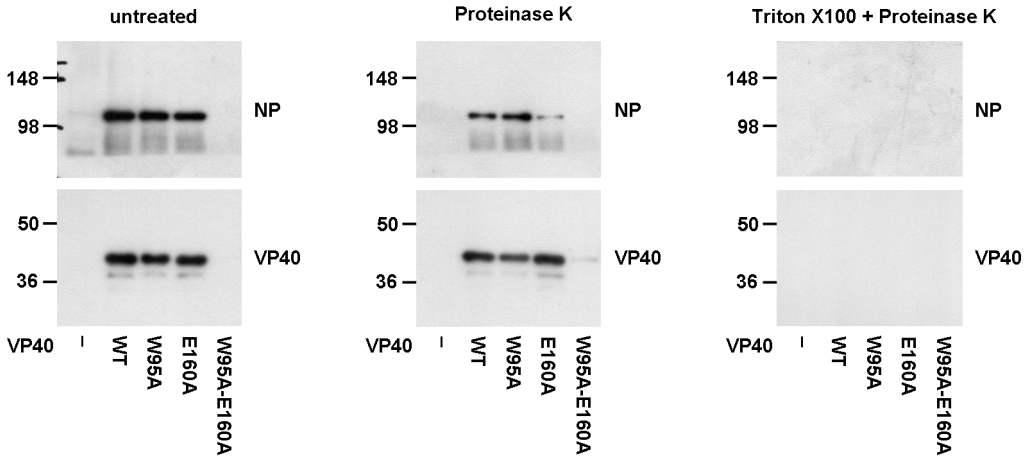

Figure 41: **Analysis of VLPs produced with dimerization-deficient VP40.** iVLPs were produced in the presence of VP40-WT or dimerization-impaired VP40. Supernatant was cleared from cellular debris and subjected to a proteinase K protection assay. VP40 and NP were detected by western blotting using monoclonal antibodies.

3.3 Interaction of VP40 and NP

As central player in morphogenesis, VP40 has been suggested to interact with NP, which can be found in VP40-induced VLPs [121]. We, therefore, decided to investigate whether VP40 can directly interact with NP and to characterize this potential interaction. In particular, we were interested to map the interacting domain on VP40. Also, we decided to use the generated mutants to investigate other aspects of VP40, in particular its effect on viral genome transcription and replication, as well as on cellular transcription and/or translation.

3.3.1 Design, cloning and expression of VP40 deletion mutants

3.3.1.1 Design Since the crystal structure of VP40 has been determined, we decided to try to use this information in designing VP40 deletion mutants. VP40 contains 2 domains, an N-terminal oligomerization domain (amino acids 1 to 194) and a C-terminal membrane binding domain (amino acids 201 to 326), which are connected by a flexible linker (see section 1.4.3). Both domains are made up of a β-sandwich consisting of 6 β-strands. The first 61 amino acids of the protein are unstructured, amino acids 61 to 65 make up a short α-helix, and the N-terminal β-sandwich starts at amino acid 69. The C-terminal β-sandwich is located between the amino acids 212 to 308. Another important feature of VP40 are two overlapping late domain motifs found between amino acids 7 and 13. Based on these data 3 N-terminal and 3 C-terminal deletion mutants were designed (Table 4). Also, we decided to try to remove individual secondary structure elements (Table 4).

For all mutants a homology model was created using Swiss-Model in first approach mode. For the mutants VP40-$\Delta\beta$0708 and VP40-$\Delta\beta$0910 the alignment of the model was adjusted manually, and the projects resubmitted to Swiss-Model in optimize mode. The created models were checked for plausibility, with special attention to region surrounding the deletion (Figure 42). The only model that showed problems with respect to plausibility was the one for VP40-$\Delta\beta$11, in which a collision between N- and C-terminal domain was predicted. However, this collision likely does not constitute a problem as it can be resolved with a very small movement of the C-terminal domain, and since the N- and C-terminal domains are known to be mobile in relation to each other in VP40-WT.

Construct	Amino acids	Description
VP40-ΔN14	14-326	late domains missing
VP40-ΔN61	61-326	unstructured 61 N-terminal amino acids missing
VP40-ΔN65	65-326	61 N-terminal amino acids and 1st α-helix missing
VP40-ΔC308	1-308	C-terminal amino acids after 2nd β-sandwich missing
VP40-ΔC212	1-212	2nd β-sandwich and amino acids after it missing
VP40-ΔC194	1-194	only N-terminal domain
VP40-Δα01	1-60, 65-326	1st α-helix missing
VP40-Δβ0102	1-67, 104-326	1st and 2nd β-strand missing
VP40-Δα02	1-107, 118-326	2nd α-helix missing
VP40-Δβ0304	1-118, 139-326	3rd and 4th β-strand missing
VP40-Δα03	1-146, 152-326	3rd α-helix missing
VP40-Δα03L	1-141, 154-326	3rd α-helix and flanking loop missing
VP40-Δα04	1-158, 169-326	4th α-helix missing
VP40-Δβ06	1-176, 188-326	6th β-strand missing
VP40-Δβ0708	1-202, 220-326	7th and 8th β-strand missing
VP40-Δα0506	1-227, 247-326	5th and 6th α-helix missing
VP40-Δβ0910	1-246, 264-326	9th and 10th β-strand missing
VP40-Δα07	1-264, 274-326	7th α-helix missing
VP40-Δβ11	1-282, 290-326	11th β-strand missing
VP40-Δβ12	1-302, 309-326	12th β-strand missing
VP40-ΔL1112	1-289, 303-326	loop between β-strand 11 and 12 missing

Table 4: **VP40 deletion mutants**

Since homology modelling uses a known structure to predict the structures of proteins with similar primary sequence, and uses the known structure as a scaffold for the new structure, all models for the deletion mutants are based on the assumption that they will fold in a similar fashion to VP40-WT. Whether this really is the case is impossible to predict from the models. However, problems with the plausibility of the models would indicate if there is no theoretical way to fold the deletion mutants in a way similar to VP40-WT. Homology modelling, therefore, only allows to draw conclusions regarding which mutants most likely will not fold properly, but not which one will fold properly, and functional data must be considered in light of this potential limitation.

3.3.1.2 Cloning and expression Constructs were cloned as described in appendix A.13. To check for expression, they were transfected into 293T cells as, described in section 2.2.6, and after 24 hours cells were harvested, lysed and samples subjected to SDS-PAGE and western blotting using a monoclonal antibody directed against VP40 (see section 2.2.8, 2.3.1 and 2.3.2).

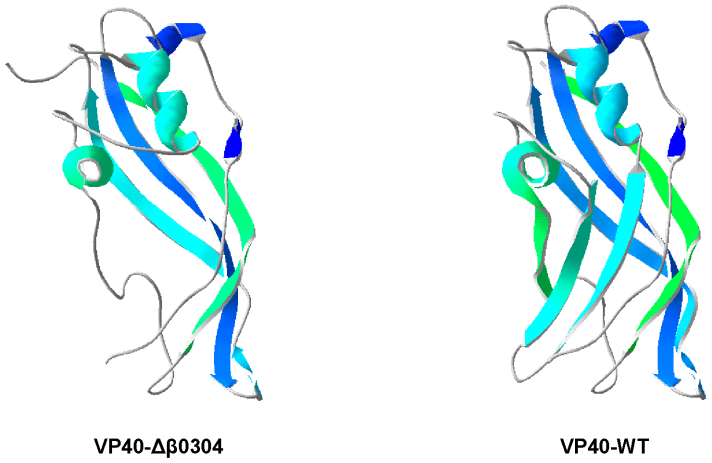

Figure 42: **Example for a VP40 homology model.** Both the homology model for VP-40-Δβ0304 and VP40-WT are displayed. In the homology model, the two β-strands at the bottom left front of VP40 have been removed, and a possible loop structure connecting the two flanking α-helices has been calculated.

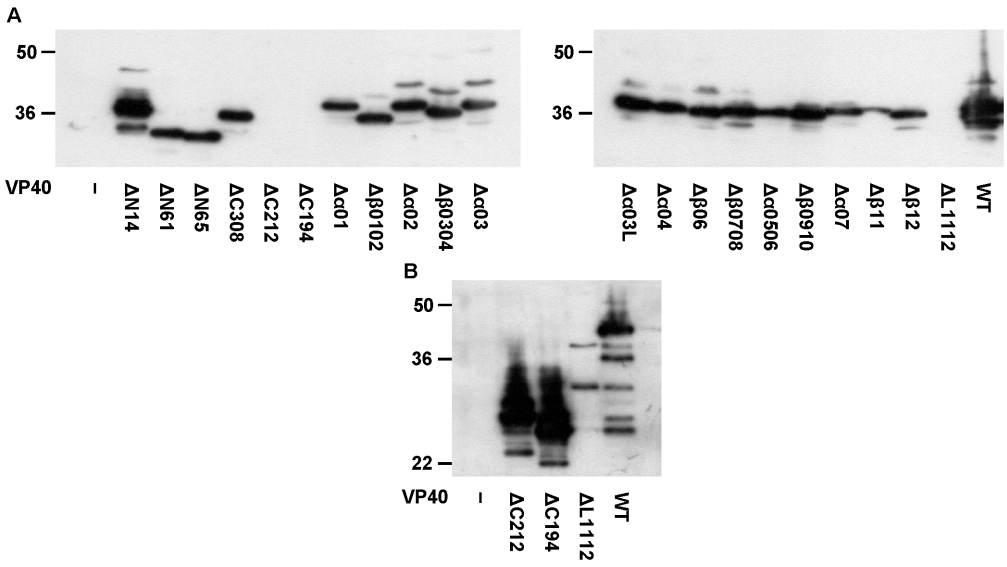

Figure 43: **Expression of VP40 constructs.** 293T cells were transfected with VP40 constructs, harvested 24 hours p.t. and subjected to SDS-PAGE and western blotting using either a monoclonal antibody or a polyclonal goat serum against VP40. (A) Western blot using the monoclonal antibody 2C4. (B) Western blot using a polyclonal goat anti ZEBOV serum.

All VP40 constructs except VP40-ΔC212, VP40-ΔC194 and VP40-ΔL1112 lead to expression of VP40-mutants detectable with the monoclonal antibody 2C4 (Figure 43A). We, therefore, concluded that this monoclonal antibody recognizes an epitope between amino acid 290 and 302, which corresponds to a long, surface-exposed loop in VP40 (Figure 44). The three constructs not detectable with 2C4 could be detected using a polyclonal goat serum against ZEBOV (Figure 43B). Interestingly, the goat serum detected several bands for VP40-WT, the strongest of which corresponds to the main band detected by the monoclonal antibody 2C4. Since all VP40 mutants were expressed, we decided to use all constructs in further analyses.

Figure 44: **Binding region for 2C4.** VP40 is shown in ribbon representation. The region which contains the epitope recognized by the monoclonal antibody 2C4 (amino acids 290 to 302) is drawn in an all atom representation.

3.3.2 Influence of VP40 mutants on viral transcription and replication

Since we had observed a clear influence of VP40 on cellular transcription or translation, we decided to test the VP40 deletion mutants for this effect (see also section 3.1.4.1). Firefly and Renilla activity were analyzed separately from each other, and reporter activity in the absence of VP40 was defined as 100%.

For Firefly activity, almost all mutants caused an intermediate phenotype, with Firefly signals between 40% and 70% of activity without VP40 (Figure 45A). However, VP40-Δβ06 produced a Firefly activity as low as VP40-WT (27% ± 5%; n=3). Very surprising was the finding that Renilla activity is completely supressed in the presence of a C-terminal

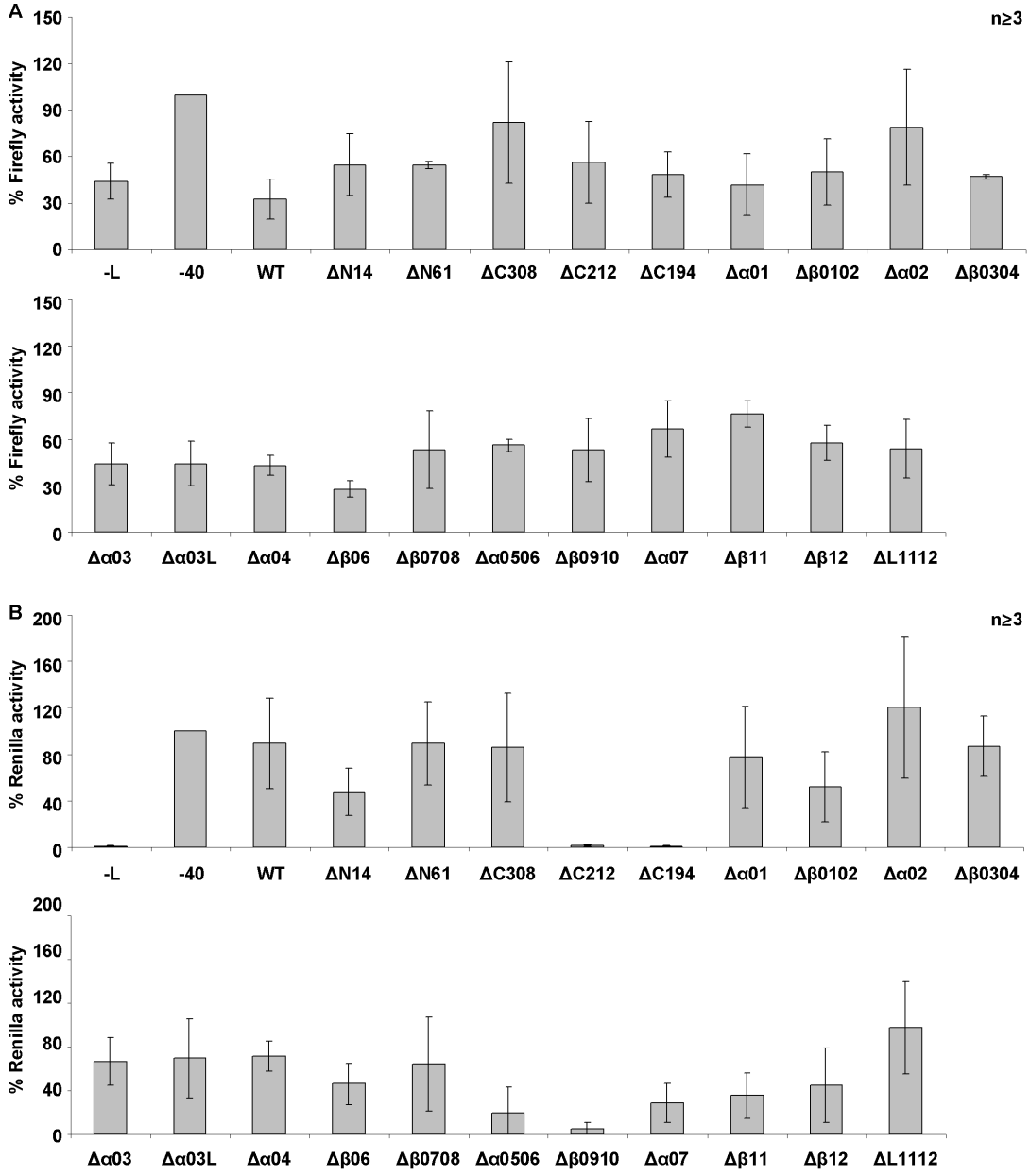

Figure 45: **Influence of VP40 deletion mutants on transcription and replication.** 293T cells were transfected with plasmids enocding a T7-driven minigenome, T7 RNA polymerase, Firefly luciferase to allow for normalization of transfection efficiency, and all viral proteins. Either no VP40, VP40-WT or a VP40 deletion mutant was included. As a negative control, L was omitted. 72 hours p.t., reporter activity was measured. Activity in cells without VP40 was defined as 100%. (A) Firefly reporter activity. (B) Renilla reporter activity.

deletion mutant (0.8% ± 0.4% for VP40-ΔC194; n=4) (Figure 45B). Also, deletions in the C-terminal domain caused a similar effect, with removal of the β-strands 9 and 10 resulting in a loss of Renilla activity (5.1% ± 5.8%; n=3), as did the removal of α-helices 5 and 6 which immediately precede β-strand 9, although this effect was less pronounced (19.6% ± 23.3%). However, none of these mutants resulted in a loss of Firefly activity to levels below those in the presence of VP40-WT, thus this reduction in Renilla activity is not due to downregulation of cellular transcription or translation, which would lead to lower availability of the minigenome or RNP-components.

3.3.3 Influence of VP40 mutants in an iVLP assay with pretransfected target cells

As a rapid screening assay for VP40-NP interactions we decided to use an iVLP assay with pretransfected target cells. We sought to identify VP40 mutants that do produce iVLPs that are not able to transfer minigenome into target cells, presumably as a result of their inability to incorporate RNP complexes. Based on the assumption that VP40-NP interactions are crucial for recruitment of RNP complexes into iVLPs, it should be, therefore, possible to identify regions that are important for VP40-NP interactions using this approach.

None of the VP40 deletion mutants were able to produce iVLPs, which could transfer minigenome into target cells (Figure 46). To check for VLP production, supernatant of p0 was cleared from cellular debris, subjected to a proteinase K protection assay and analysed by SDS-PAGE and western-blotting. Unfortunatley, none of the VP40-mutants, with exception of VP40-ΔN14 was detectable in the supernatant in a proteinase K resistant form (Figure 47A and 47B), so that the negative result of the iVLP assay is most likely due to impaired VLP formation, and does not allow any conclusions about VP40-NP interactions. Interestingly, both C-terminal deletion mutants VP40-ΔC194 and VP40-ΔC212 were detectable in the supernatant, but not resistant to proteinase K digestion, suggestion that they are not protected by a lipid envelope. Also, it is interesting to note that the banding pattern of VP40-WT inside VLPs was different from the banding pattern of intracellular VP40 (Figure 43B and 47B)

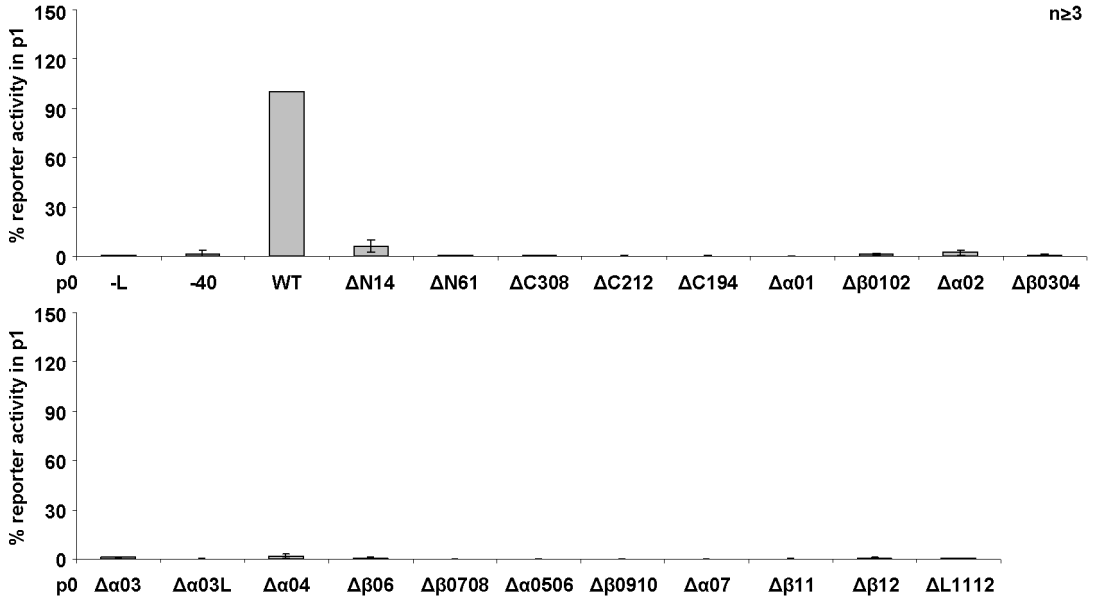

Figure 46: **VP40 deletion mutants in an iVLP assay with pretransfected target cells.** iVLPs were produced and used to infect pretransfected 293T cells. 72 hours p.i., reporter activity was measured. As a negative control, VP40 was omitted in p0.

3.3.4 Coimmunoprecipitation of VP40 and NP

As a second approach to detect and examine VP40-NP interactions we decided to use coimmunoprecipitation. C-terminally flag-tagged NP was coexpressed with VP40 deletion mutants, and precipitated using an agarose-coupled α-flag antibody. Coprecipitated VP40 was then detected using SDS-PAGE and western blotting. Pilot experiments performed by Natsha Krowchuk, an undergraduiate student under my supervision, indicated that the N-terminal domain of VP40 is responsible for interactions with NP. Therefore, only deletion mutants in this region were analyzed.

Coprecipitation of VP40 by NP-flag was dependent on the presence of both NP-flag and VP40, showing that there is no unspecific precipitation of VP40 (Figure 48). All VP40 constructs tested with the exception of VP40-$\Delta\beta$0102 and VP40-ΔC194 were coprecipitated with NP, suggesting a role of the first two β-strands of the N-terminal domain for interactions between VP40 and NP. However, based on these results, and contrary to the findings of the pilot experiment, we cannot longer exclude a contribution of the C-terminal domain of VP40 to interaction with NP. Therefore, additional C-terminal deletion mutants will need to be included in further experiments, to address this possibility.

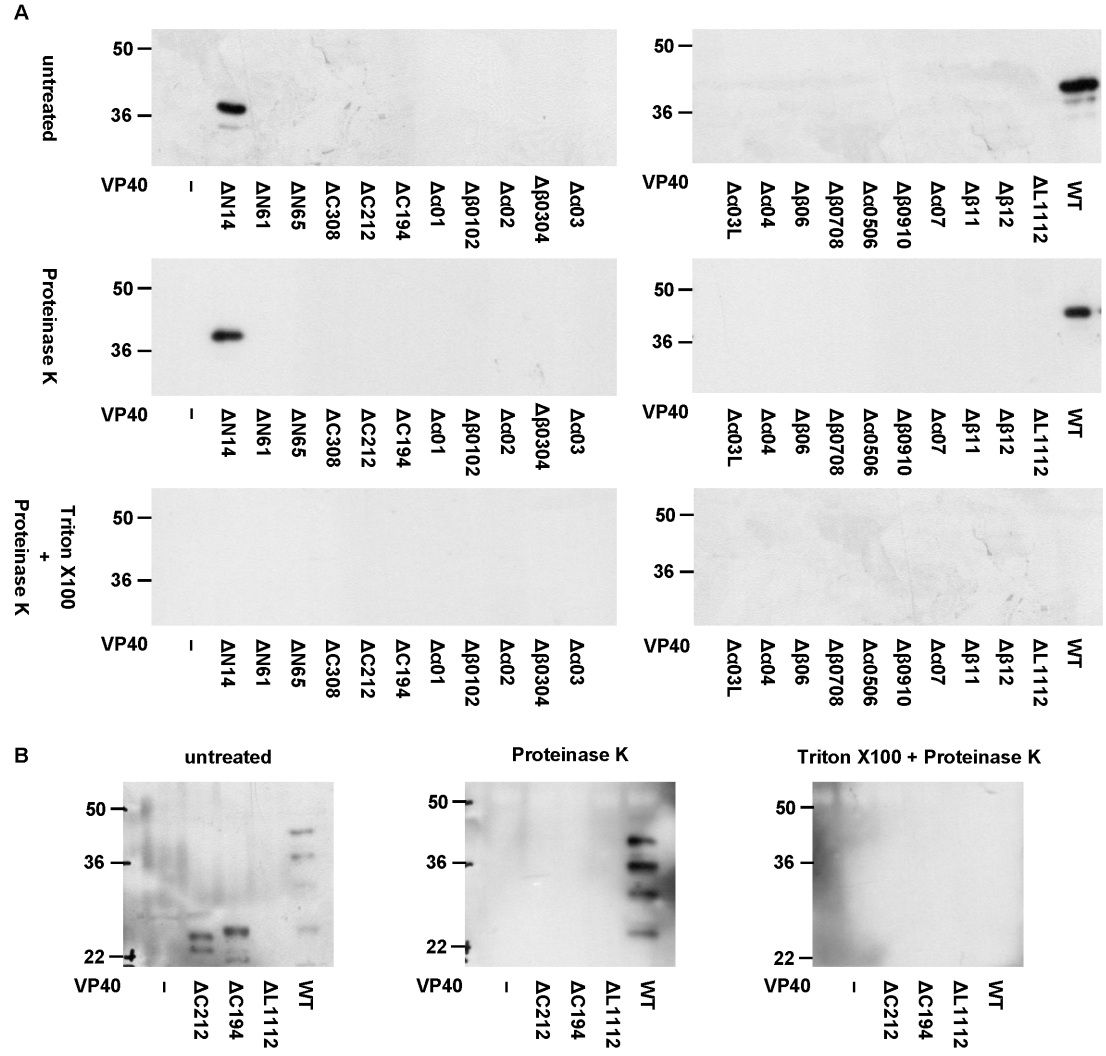

Figure 47: **iVLPs produced by VP40 deletion mutants.** Western blot analysis of iVLPs produced by VP40 mutants. Cell supernatant was cleared of cellular debris and subjected to protease K protection assay followed by SDS-PAGE and western blotting. (A) VP40 was detected using a monoclonal antibody (2C4). (B) VP40 was detected using a polyclonal goat anti ZEBOV serum.

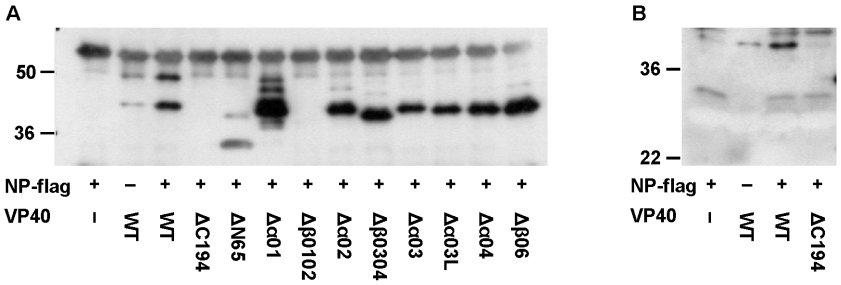

Figure 48: **CoIP of NP and VP40.** NP-flag and VP40 were coexpressed in 293T cells. 1 day p.t., cells were harvested, lysed and coimmunoprecipitation was performed using an agarose-coupled α-flag antibody. (A) Precipitated VP40 was detected using a monoclonal antibody (2C4). (B) Precipitated VP40 was detected using a polyclonal goat anti ZEBOV serum.

3.3.5 Analysis of VP40 3D-structure for future studies

To further analyze the interactions between NP and VP40 in future studies, we decided to take a closer look at the crystal structure of VP40 [40]. Of special interest was whether we can identify single charged amino acids which are accessible on the surface of VP40, since such charged residues are often involved in protein-protein interactions [220]. Using DeepView [80] the electrostatic potential and molecular surface of the VP40 monomer was computed and visualized (Figure 49). The top of the protein is mostly negatively charged, however, we were unable to find individual amino acids responsible for this charge. One side of the the protein is dominated by a positively charged patch made up by the amino acids R134 and K137. The other side is dominated by a smaller positively charged region consisting of the amino acids R52 and R137. At the bottom of the molecule are four isolated charged residues, D45, D175, K90 and K86. Interestingly, two of these residues (K86 and K90) are located in the first two β-strands of VP40 which, together with the CoIP-data (see section 3.3.4), might suggest a role of these residues in interactions with NP.

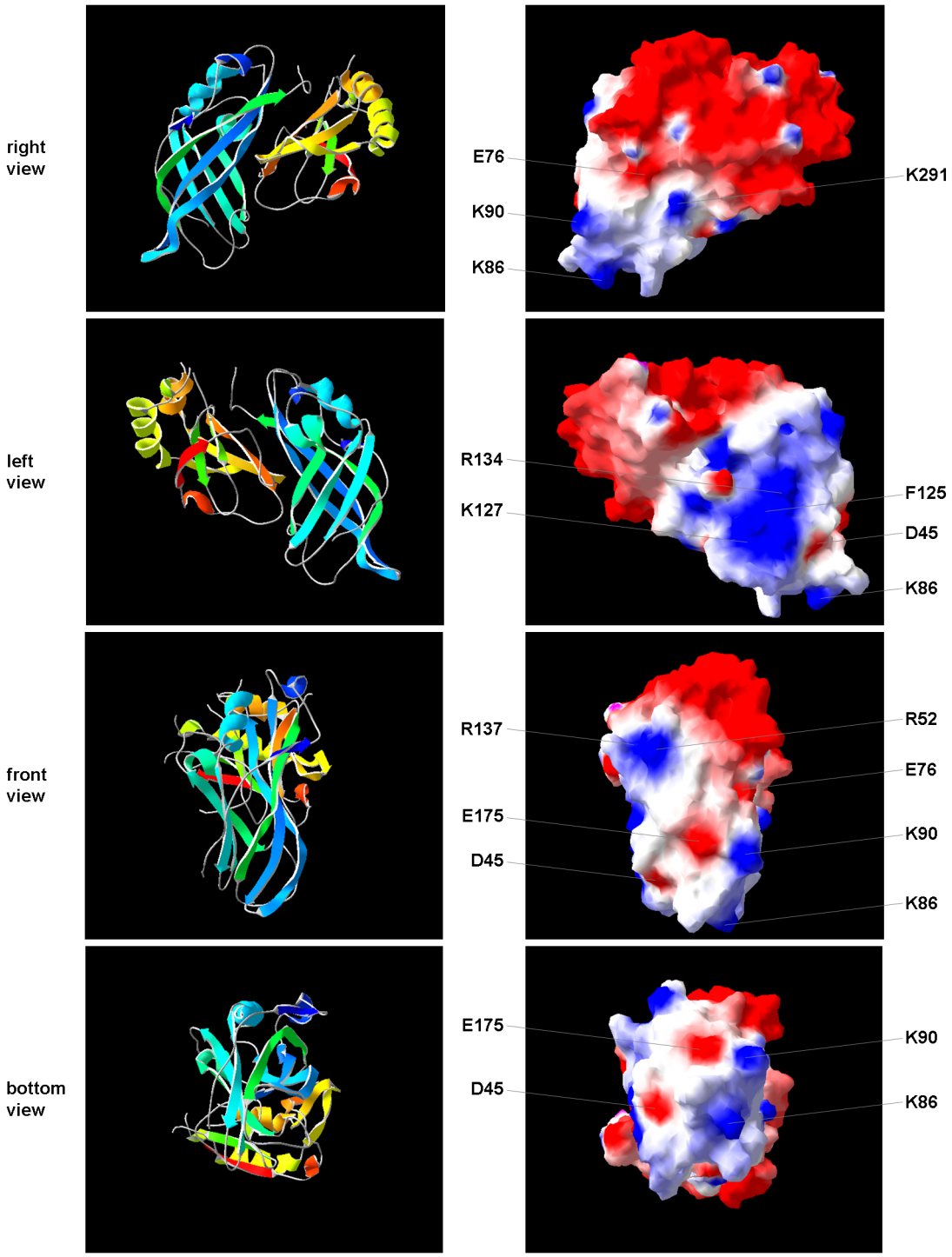

Figure 49: **Electrostatic potential of the VP40-surface.** The electrostatic potential at the surface of VP40 was calculated using DeepView. Selected charged surface residues are labeled.

3.4 Role of VP24 in the viral life cycle

With several systems available to study individual aspects of the viral life cycle, we decided to analyze the role of VP24 for morphogenesis and budding, since this role is so far only very poorly understood (see section 1.4.6).

3.4.1 Role of VP24 in an iVLP assay with pretransfected target cells

As a first step in analyzing the function of VP24 we decided to confirm results reported by Watanabe *et al.*, that VP24 is not necessary for minigenome transfer in an iVLP assay with pretransfected target cells [212].

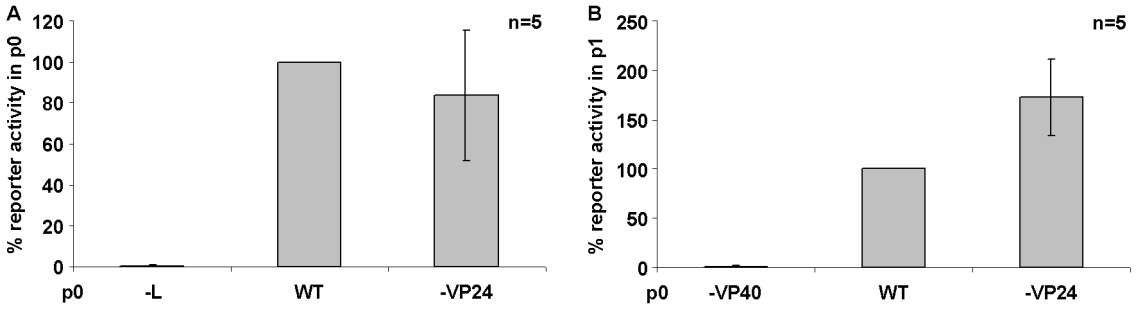

Figure 50: **VP24 in an iVLP assay with pretransfected target cells.** (A) Reporter activity in p0. As negative control, L was omitted in p0. (B) Reporter acitivity in p1. As a negative control VP40 was omitted in p0.

The established iVLP assay with pretransfected target cells (see section 3.1.4) was performed with and without VP24 in p0 (Figure 50). Reporter activity in p0 did not differ significantly between samples with and without VP24. However, in p1 a slightly higher reporter activity (172% ± 39%; n=5) was observed if VP24 was omitted in p0, in line with the previously reported results from Watanabe *et al.*

3.4.2 Role of VP24 in an iVLP assay with naïve target cells

To investigate whether VP24 has a function in morphogenesis that can not be detected in an iVLP assay with pretransfected target cells, an iVLP assay with naïve target cells was performed as described in section 3.1.5.

Surprisingly, in this assay reporter activity in p1 dropped to 14% ± 11% (n=9). Since VP24-deficient iVLPs obviously contain a minigenome, as they are able to transfer it to

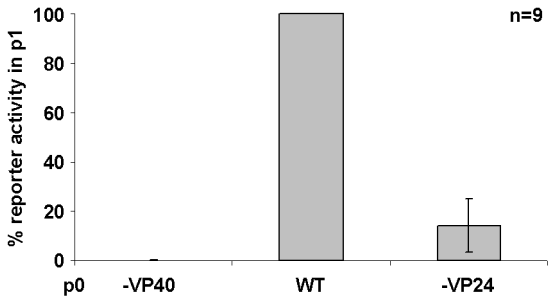

Figure 51: **VP24 in an iVLP assay with naïve target cells.** An iVLP assay with naïve target cells was performed as described in section 3.1.5. Reporter acitivity in p1 is shown. As a negative control VP40 was omitted in p0.

pretransfected target cells (see section 3.4.1), this means that initital transcription of the minigenome in target cells must be impaired.

3.4.3 Heterologous substitution of VP24 in an iVLP assay with naïve target cells

For many RNP components it has been reported that heterologous combinations, from different species as well as different genera of filoviruses, still remain functional in reverse genetics systems [20, 77, 191]. It was, therefore, analyzed whether this is also the case for VP24. Analysis of reporter activity in p1 showed that neither VP24 from MARV strain Angola nor from strain Musoke were able to substitute for missing ZEBOV VP24 (Figure 52). This indicates that heterologous substitution across genus borders is not possible for VP24, and supports a specific function for ZEBOV VP24.

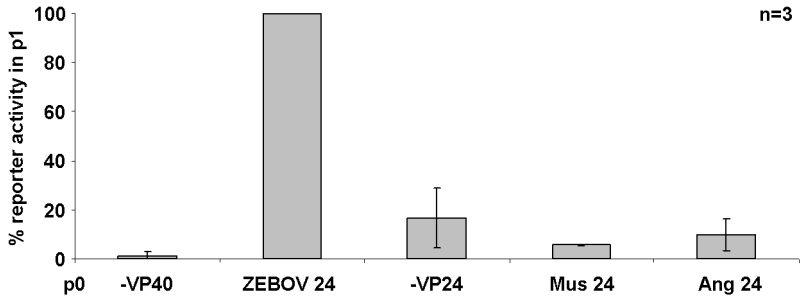

Figure 52: **Heterologous substitution of VP24.** An iVLP assay with naïve target cells was performed as described in section 3.1.5 with ZEBOV VP24, without VP24, or with MARV VP24 strain Musoke (Mus) or Angola (Ang). Reporter acitivity in p1 is displayed. As a negative control VP40 was omitted in p0.

3.4.4 Rescue of infectivity of VP24-deficient iVLPs by pretransfection

Since VP24-deficient iVLPs are not able to perform initial transcription in target cells, we hypothesized that VP24 is necessary to recruit one or several RNP components into the iVLPs. To test this hypothesis, we decided to provide single RNP-components as well as combinations of components in p1 *in trans* by pretransfection.

3.4.4.1 Optimization of electroporation of VeroE6 cells As it is difficult to achieve a high transfection efficiency in VeroE6 cells, which are the best cell line for iVLP assay tested by us (see section 3.1.5.2), with chemical compounds, and transfection with Fugene was not optimized in our laboratory for this cell line at the time we performed this part of our studies, we decided to test electroporation as another method for transfection of VeroE6 cells, since this method has been described to be highly efficient in these cells [9].

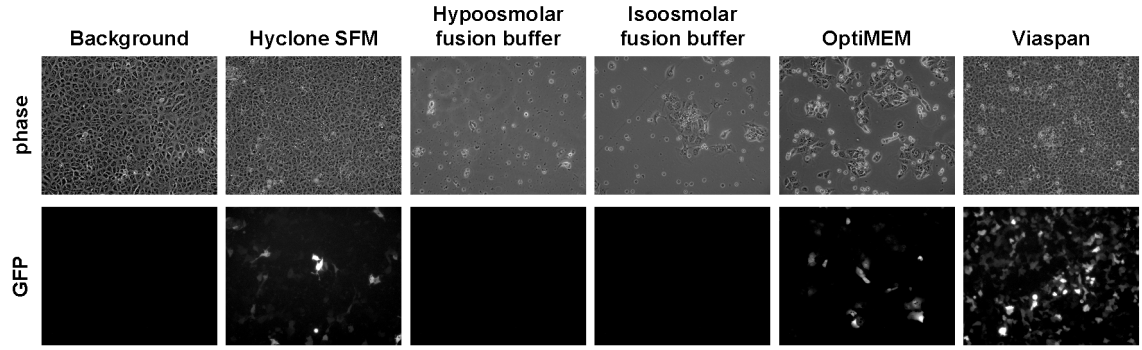

Figure 53: **Electorporation of VeroE6 cells.** 10 μg pCAGGS-GFP was electroporated as described in section 2.2.7, but using serum free Vero medium (Hyclone SFM), hypo- and isoosmolar electrofusion buffer, OptiMEM and Viaspan as electroporation media. One T75 flask VeroE6 cells was electroporated, and $1/8^{\text{th}}$ of the cells were seeded out in 1 well of a 6-well plate. GFP expression was determined 24 hours p.t. by fluorescence microscopy. As a background control cells electroporated in Viaspan without pCAGGS-GFP were examined.

Electroporation was optimized with respect to the medium used, while the parameters for electroporation were adopted form *Baron et al.* [9]. In particular, we tested OptiMEM (Invitrogen), ViaSpan (Barr Laboratories), serum-free Vero medium (Hyclone), and hypoosmolar as well as isoosmolar electrofusiuon buffer (Eppendorf). Almost none of the cells electroporated with hypo- or isoosmolar electrofusion buffer survived electroporation, and also with OptiMEM cell viability was poor (Figure 53). With both Hyclone serum free Vero medium and Viaspan viability was high, and Viaspan showed the highest transfection

efficiency and was, therefore, used for further experiments.

3.4.4.2 Rescue of infectivity of VP30-deficient iVLPs by pretransfection Since it was not clear whether RNP-components provided *in trans* could replace RNP-components missing in iVLPs, it was decided to first test this procedure using VP30, whose function is better understood than VP24 (see section 1.4.5). Since VP30 is only necessary for transcription, but not replication, it should be possible to generate iVLPs without VP30, and reporter activity in VP30 should only occur if VP30 provided *in trans* is able to replace the missing VP30 in the iVLPs.

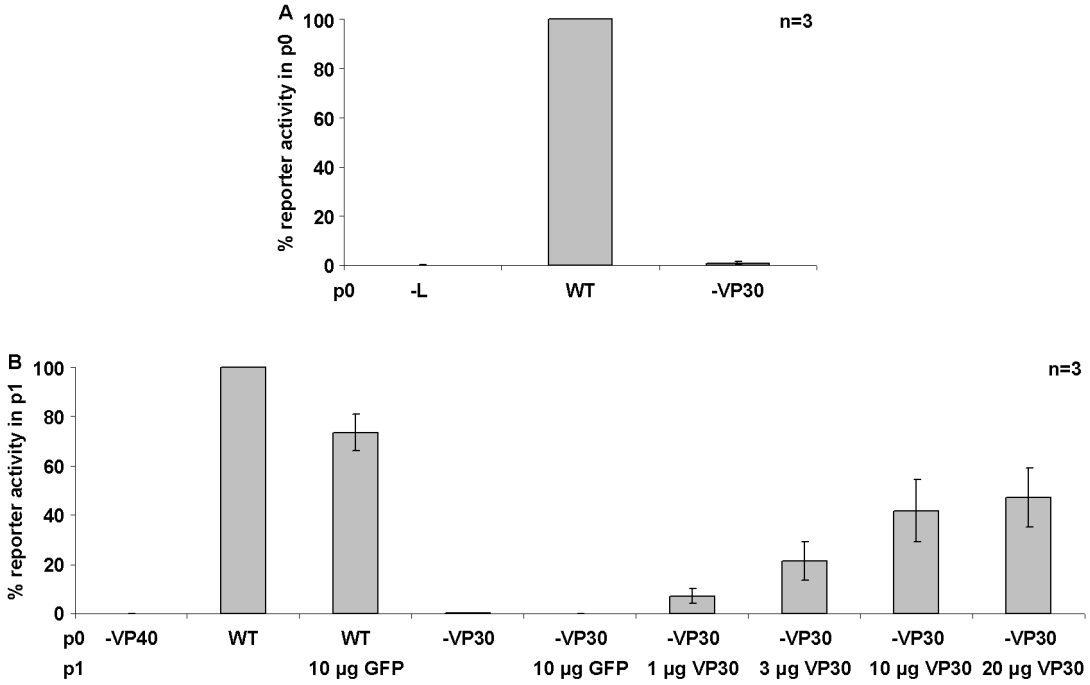

Figure 54: **Rescue of VP30-deficient iVLP infection.** (A) Dependence of reporter activity in p0 on VP30. An iVLP assay with naïve target cells was performed as described in section 3.1.5. As a negative control, L was omitted. (B) WT or VP30-deficient iVLPs were produced and used to infect VeroE6 target cells. To rescue infectivity, target cells were electroporated with 1 to 20 μg of pCAGGS-VP30. As a negative control target cells were transfected with 10 μg pCAGGS-GFP. As a negative control for iVLP production VP40 was omitted in p0.

As expected, reporter activity in p0 was dependent on VP30, conbsistent with the reported function of VP30 as transcriptional activator (Figure 54A) [139]. Also, VP30-deficient particles were not able to produce any reporter activity in naïve target cells (Figure 54B). When VP30 was pretransfected into target cells, we observed a recovery of reporter activity up to 47% ± 12% (n=3) in a dose dependent manner, indicating that it is possible to

provide missing RNP components *in trans*.

3.4.4.3 Rescue of infectivity of VP24-deficient iVLPs by pretransfection To check whether RNP components are missing in VP24-deficient iVLPs, the previous experiment was repeated using VP24-deficient iVLPs and pretransfection of target cells with single RNP components, as well as with combinations of RNP components.

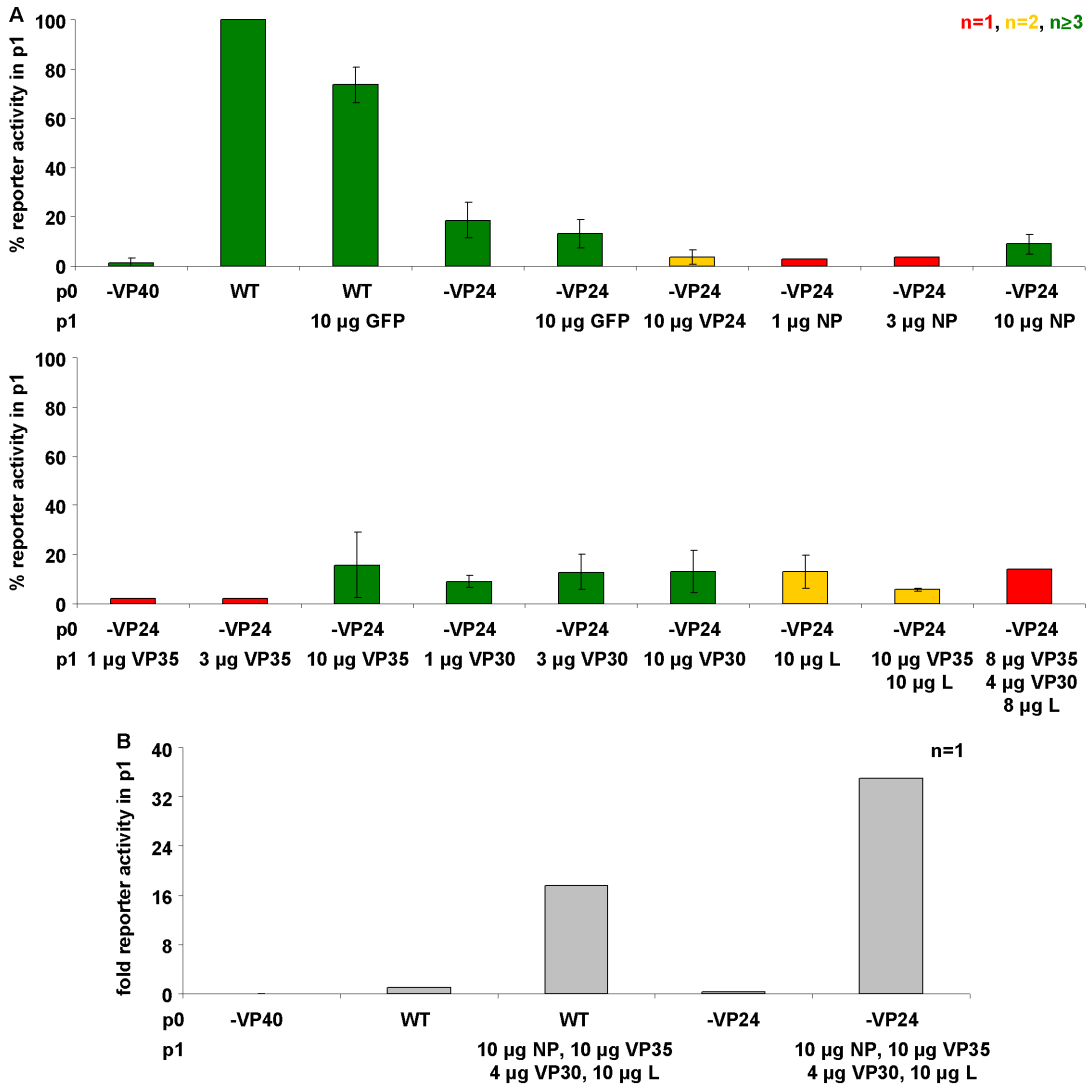

Figure 55: **Rescue of VP24-deficient iVLP infection.** (A) WT or VP24-deficient iVLPs were produced as described in section 3.1.5 and used to infect VeroE6 target cells. To rescue infectivity, target cells were electroporated with the indicated plasmids. As a negative control target cells were transfected with 10 μg pCAGGS-GFP. As a negative control for iVLP production VP40 was omitted in p0. Bars represent the average of 1 (red), 2 (yellow) or $\geq$3 (green) experiments. (B) WT or VP24-deficient iVLPs were produced and used to infect VeroE6 target cells pretransfected with all RNP components.

Neither single RNP components nor VP24 were able to restore reporter activity in p1

(Figure 55A). Also, the combinations NP/VP35 and NP/VP35/VP30 were not able to restore reporter activity. When all RNP components were transfected into target cells, reporter activity was restored at a level more than 17 × higher than reporter activity in naïve target cells infected with WT-iVLPs (Figure 55B). Similar to an iVLP assay with 293T pretransfected with all RNP components, we observed a higher activity for VP24-deficient iVLPs (3496% vs. 1762% of WT activity in naïve cells; n=1).

3.4.5 Analysis of iVLP morphology

Since no single RNP component or VP24 was able to restore reporter activity in p1, we decided to further analyze VP24-deficient iVLPs for their morphology. WT and VP24-deficient iVLPs were, therefore, purified over a 20% sucrose cushion and analyzed using electron microscopy as well as proteinase K protection assay and western blotting or silverstaining (see sections 2.4.4, 2.4.6, 2.3.2 and 2.3.4).

3.4.5.1 Electron microscopy Electron microscopic analysis was performed by Dr. Larissa Kolesnikova at the Robert-Koch Institute in Berlin, Germany. There were no major differences in size or structure of WT and VP24-deficient iVLPs (Figure 56). Also, in both types of particles RNP complex-like structures could be found. It seems that the RNP-like structures in VP24-deficient particles are somewhat less regular than in WT particles; however, the relevance of this finding have to be further investigated.

3.4.5.2 Silver staining and western blot analysis To further confirm that the impaired infectivity of VP24-deficient iVLPs was not due to the absence of a single or several RNP components, iVLPs were analyzed by either silver staining or western blotting.

Untreated WT particles showed bands corresponding to all viral proteins except L, which could not be detected due to its high molecular weight and/or low abundance (Figure 57A, lane 1-3). Treatment with Proteinase K resulted in loss of the band for GP which, in contrast to the other viral proteins, is not protected by the lipid envelope of the iVLPs (Figure 57A, lane 4-6). The remaining signals correspond to proteins inside the iVLPs, which are protected by the envelope. Triton X-100 is able to destroy this envelope, and, therefore, subsequent treatment with proteinase K resulted in digestion of all proteins (Figure 57A, lane 7-9). Only one band remained visible in the gel (labeled with *), which

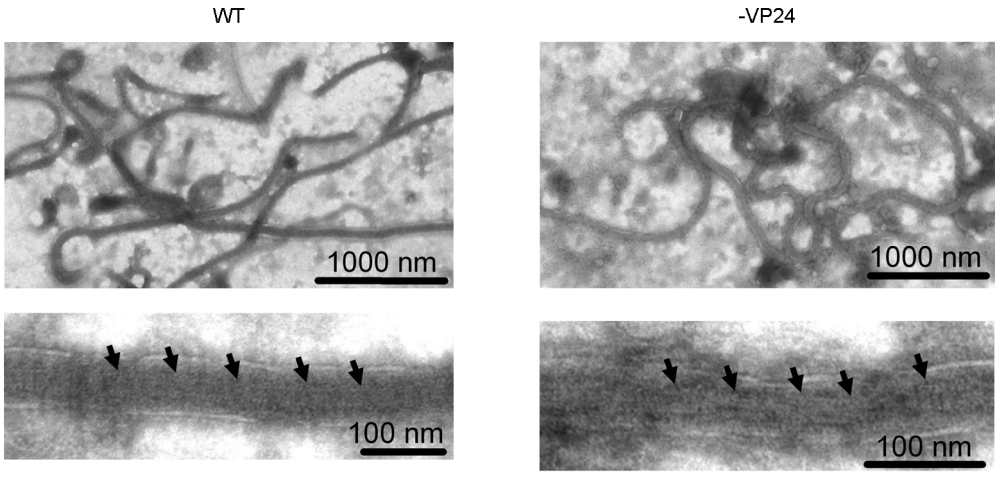

Figure 56: **Electron microscopic analysis of VP24-deficient iVLPs.** WT or VP24-deficient iVLPs were produced, concentrated and purified by centrifugation over a 20% sucrose cushion and fixed in paraformaldehyde. Electron microscopic analysis was performed after negative staining. Arrows indicate RNP-like structures. Pictures kindly provided by Dr. Larissa Kolesnikova.

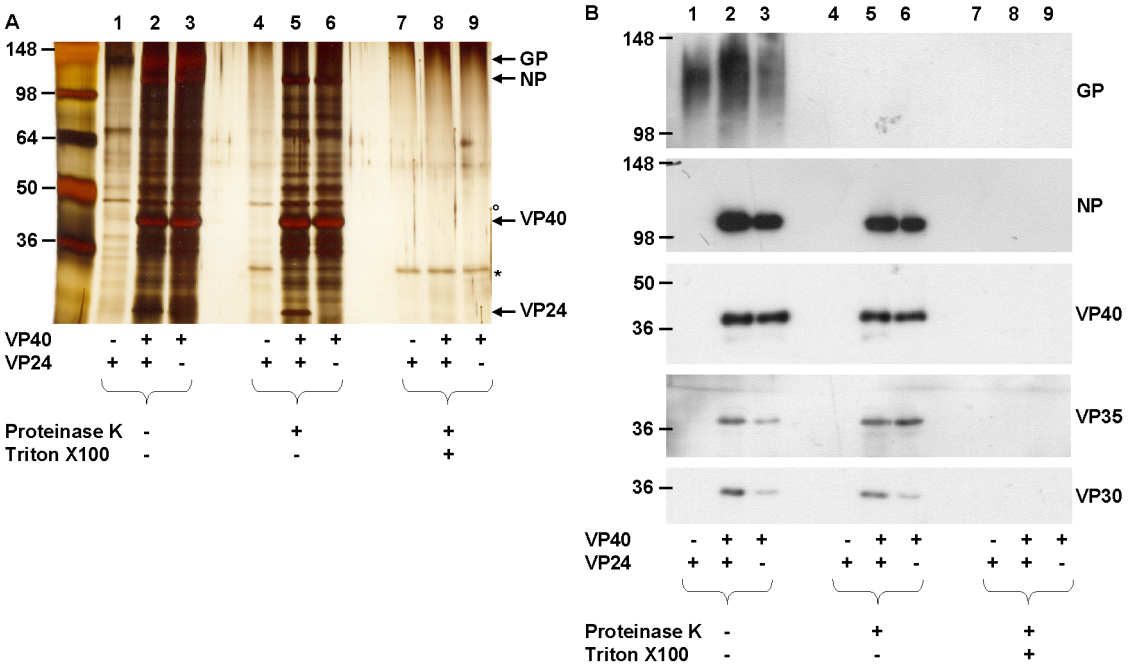

Figure 57: **Analysis of VP24-deficient iVLPs by silver staining and western blotting.** WT or VP24-deficient iVLPs were produced, concentrated and purified by centrifugation over a 20% sucrose cushion and subjected to a proteinase K protection assay. (A) Silver staining. The approximate sizes of GP, NP, VP40 and VP24 are indicated. * indicates a band that most likely corresponds to proteinase K. ° indicates a band that corresponds to a non-viral protein inside iVLPs and GP-only particles. (B) Western blot anaylsis with specific antibodies as indicated on the right.

represents either a digestion product of a protein present outside the VLPs or proteinase K itself, as it shows up in both the Proteinase K and the proteinase K/Triton X-100 treated samples, but not in the untreated samples. The bands for VP40 and NP showed no apparent difference between WT and VP24-deficient iVLPs, whereas VP24 was only present in WT particles (Figure 57A, lanes 5 and 6). Also, the amount of GP incorporated into these particles was not visibly altered (Figure 57A, lanes 2 and 3). It has been reported that expression of GP in mammalian cells in the absence of VP40 leads to the production of pleomophic particles, which show GP spikes on their surface [148]. Interestingly, we were able to detect these GP-only particles which, beside the bands for GP, showed also one band (labeled with °) which did not correspond to any of the known viral proteins, but appeared to be inside the particles as it was resistant to proteinase K digestion (Figure 57A, lanes 1 and 4). It has recently been reported that actin can be found inside EBOV VLPs, which could correspond to this band [85]. With the exception of GP we were unable to detect any of the viral proteins in these GP-only particles.

Western blot analysis confirmed the results obtained with silver staining. We did not observe differences in the amount of NP or VP40 between WT and VP24-deficient particles after proteinase K digest (Figure 57B, lanes 5 and 6), and only a small difference in the amount of NP in the untreated samples was observed (Figure 57B, lanes 2 and 3). Also, VP35 showed no clear differences between WT and VP24-deficient particles (Figure 57B, lanes 5 and 6). However, the amount of VP30 was clearly diminished in the VP24-deficient particles, although VP30 was not completely absent in them, suggesting changes in the composition and/or the structure of the nucleocapsids.

3.4.6 Analysis of VP24 function in an packaging assay

In order to confirm that VP24 is not necessary for packaging of viral RNA, and to assess the importance of other RNP components for packaging, a variation of an iVLP assay with pretransfected cells was established. In this packaging assay L was omitted from p0, so that no transcription or replication of the minigenome could take place, and minigenome transcripts were only produced by T7-driven transcription. Therefore, the presence or absence of RNP components should not influence the amount of minigenome available for packaging. iVLPs produced without L were then purified over a sucrose cushion to increase the signal in p1, and used to infect VeroE6 cells pretransfected with all the RNP

components, as described in section 2.4.3.

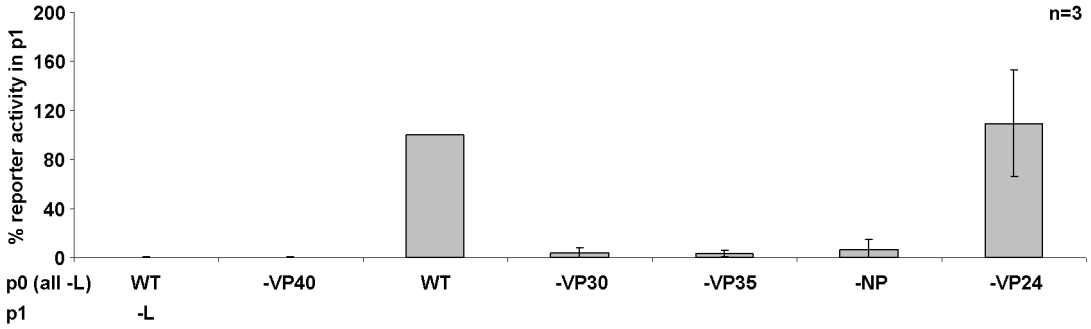

Figure 58: **Packaging assay.** iVLPs were produced without L in p0, so that no replication/transcription took place. To allow for reporter activity in p1, target cells were pretransfected with all RNP-components. This allowed the study of minigenome packaging into iVLPs. L-deficient iVLPs were used to infect p1 cells, and the pretransfected RNP components were able to replicate and transcribe the packaged minigenome, thus producing reporter activity. As negative controls, either VP40 was omitted in p0 or L was omitted in p1.

As expected, both L in p1 and VP40 in p0 were necessary for reporter activity in p1 (Figure 58). The positive signal for iVLPs produced in the presence of all viral proteins except L (in this assay called WT particles) was about 200 × higher than the signal of the negative control (-VP40 in p0). VP24 was not necessary for reporter activity in p1, suggesting again that VP24 is not involved in packaging, whereas both NP and VP35 were indispensable. Surprisingly, VP30 was also necessary for efficient transfer of minigenomes, in contrast to an iVLP assay with naïve target cells, where it did not seem to play a role for minigenome transfer (see section 3.4.4.2).

4 Discussion

4.1 Development of an iVLP assay with naïve target cells

The classification of EBOV as a BSL4 agent has restricted research on it to a few facilities worldwide, and in those facilities research under BSL4 conditions is time-consuming and intricate. Therefore, systems that model individual aspects of the virus life cycle and allow the study of EBOV under BSL2 conditions are highly desirable. Minigenome systems allow the analysis of viral transcription and replication and have been available for more than 10 years, during which they have provided tremendous insight into these processes [42, 145]. However, systems to study other parts of the viral life cycle such as morphogenesis, packaging, budding and entry have been developed for EBOV in form of iVLP systems only relatively recently [212].

iVLP systems have been established for a number of negative strand RNA viruses, among them Lymphocytic Choriomenigitis virus, Influenza virus, Uukuniemi virus, Borna disease virus, VSV, Thogoto virus and EBOV [118, 144, 149, 151, 182, 207, 212]. In these systems iVLPs are produced in cells (p0) after transfection of cDNA encoding for the viral proteins, a minigenome and non-viral accessory proteins (e.g. T7). iVLP-containing supernatant from these cells is then used to infect target cells (p1), and thereby deliver the minigenome. In all of these systems, RNP components are provided in p1 *in trans* by means of either helper-virus infection or through transfection. The provided RNP components are able to replicate and transcribe the delivered minigenome, so that these systems model vRNA replication, transcription and packaging as well as particle formation and budding in p0 and entry and genome delivery in p1. However, they do not model the formation of functional and packaging competent nucleocapsids in p0 or initial transcription of the vRNA in p1 by the nucleocapsids, a step indispensable in the life cycle of negative strand viruses.

The iVLP system with naïve target cells which we developed, overcomes this limitation by using a reporter detectable in minute amounts [226], and a modified protocol for transfer of particles. It allows us, for the first time for any negative strand RNA virus, to assess the formation of functional nucleocapsids and intitial transcription in target cells. We believe that infection of naïve target cells was not detectable in the previously published iVLP systems due to the very low signal strength after iVLP infection; a positive signal in an

iVLP assay with naïve target cells is in the same range as a negative signal in an iVLP assay with pretransfected target cells (Table 3). This huge difference in signal strength between pretransfected and naïve target cells can be explained by the fact that in an infection of naïve target cells, like in a natural infection, only very small amounts of RNP components are availabe. Watanabe *et al.* have shown that they obtain an iVLP titer of 600 iVLPs per ml, which in our system would correspond to an MOI of 2.5×10^{-3} per cell, under the assumption that we achieved similar titers [212]. Also, there is no production of new NP, which prohibits replication of the minigenome according to the current models of replication and transcription for nonsegmented negative RNA viruses [216]. The limited amounts of both viral proteins and minigenome contribute to the low signal strength observed. In an iVLP system with pretransfected target cells these limitations do not apply. High amounts of RNP components available in the target cells probably not only transcribe the incoming minigenome, but also support replication, which further increases the signal strength.

There are, however, several points that need to be addressed with respect to the specificity of the reporter signal observed in p1. In particular, one could argue that these signals are either due to unspecific transfer of reporter protein inside the iVLPs, or due to unspecific transfer of plasmids encoding the minigenome and/or RNP proteins. This is especially true since McCarthy *et al.* have shown that functional luciferase can be detected in VP40-only VLPs [132]. However, both arguments can be rebutted by the observation that infection with VP24-deficient iVLPs results in a 90% reduction of reporter activity in p1. Since VP24 clearly is not necessary for packaging (see section 4.2) and the amount of produced VLPs is unchanged (Figure 57), one would expect reporter levels to be similar in infection with WT iVLPs and VP24-deficient iVLPs, if reporter activity is due transfer of plasmids or reporter protein, unless VP24 specifically recruits Renilla luciferase or plasmid DNA into iVLPs. Such a function for VP24 has never been described, or even suggested, and would not appear to make sense in the context of the viral life cycle. Further, when we performed a control experiment in which we provided both plasmid encoded Firefly luciferase and minigenome encoded Renilla luciferase in p0 and then determined the ratio of Firefly to Renilla activity in both p0 and p1, we found that this ratio is 12 × reduced in p1, which shows that the reporter activity in p1 is not, or only to a small extent, due to unspecific transfer of reporter protein, since this should occur equally for both Firefly and Renilla luciferase (Figure 28). Finally, the timecourse of reporter activity in p1 showed a maximum

at day 2 and declined again (Figure 26), following a pattern one would expect for transfer of a minigenome, where a lag time is required to allow for transcription and translation of the reporter. Over time the minute amounts of minigenome and RNP complex components are likely degraded by the target cell, so that no new reporter protein is produced. Together with the turnover of the already existing reporter protein this explains the decrease of activity that we observed between day 2 and 3. In contrast, if reporter protein, but no minigenome, would be transferred one would expect that no new reporter protein is produced in the target cells, so that the signal is strongest shortly after the infection, and then continuously declines.

Interestingly, the level of luciferase activity present in VLPs due to unspecific packaging of luciferase reported by McCarthy *et al.* is 14 × the background level obtained without VP40 [132]. In an iVLP system with naïve target cells the reporter signal in p1 is about 180 × the background level obtained without VP40 (Table 3). Taken together this means that about 8% of p1 reporter activity in an iVLP system with naïve target cells is due to unspecific transfer of reporter signal, which corresponds well to the 12 × reduction in the ratio of Firefly to Renilla observed in the control experiment. Interestingly, this level of background activity corresponds to the level of reporter activity we observe after infection with spherical particles, when we separate spherical and filamentous particles (Figure 29). It is, therefore, reasonable to conclude that these spherical particles do not contain functional nucleocapsids, and that the reporter activity detected in p1 after infection with these particles is due to unspecific transfer of reporter protein.

When we infected different cell lines with iVLPs, we observed that both human primary macrophages and 293T cells were much less infectable than VeroE6 cells (Figure 27). For 293T cells this result is not surprising, since they are much less susceptible to infection with EBOV than VeroE6 cells [A. Groseth, personal comunication]. However, human macrophages are thought to be the primary target cells of EBOV [94], and can be infected with EBOV *in vitro* [184]. There are several possibilities why we were unable to infect macrophages with iVLPs. First, only macrophages from one donor were tested, and it can not be excluded that donor-specific factors contributed to the low infectivity observed. This possibility will be addressed in future studies by performing control infections with EBOV in parallel to infection with iVLPs. Second, it is possible that EBOV VLPs induce an antiviral state in macrophages, but not in VeroE6 cells, which are deficient in IFN

production [46]. EBOV as well as inactivated EBOV and EBOV VLPs are able to activate human macrophages, resulting in increased levels of cytokine production, e.g. TNF-α, being detectable within 3 hours hours [184, 208]. TNF-α has been shown to be able to induce an antiviral state [22], which might interfere with EBOV-infection. Indeed, EBOV replication in macrophages is impaired by the induction of an antiviral state through IFN-α/β [43]; however, whether TNF-α has a similar effect has not yet been studied. It is, therefore, possible, that the iVLPs induce an antiviral state either directly or by autocrine or paracrine action of mediators produced by macrophages, which then interferes with transcription or subsequent translation of the reporter protein; especially since no viral proteins are produced in the target cells which could inhibit such an antiviral state. VeroE6 cells, on the other hand, are derived from African green monkey epithelial kidney cells; they are not known to produce proinflammatory cytokines and have a defect in production of IFN [46], which probably contributes to their susceptibility to both EBOV and EBOV iVLPs.

4.2 Role of VP24 in the viral life cycle

The newly developed iVLP system using naïve target cells provided the basis to analyze the role of the second matrix protein of EBOV, VP24. A role for VP24 has long been enigmatic. Recently, it has been implicated in blocking IFN signaling at various points in the signaling pathway (see also section 1.4.6) [11, 82, 159]. Further, VP24 has been shown to be important for host adaptation, a property that has also been linked to IFN antagonism [43].

In contrast, a function of VP24 in budding and morphogenesis has been controversial. Han *et al.* reported that VP24 is released in membrane enclosed particles upon singular expression in mammalian cells [84], while Licata *et al.* published results showing that in their system VP24 was not released in the form of VLPs in the absence of other viral proteins, and did not influence the release of VLPs produced by the expression of VP40 [121]. However, they observed a small increase in VLP production due to VP24 in the case of VLPs produced by coexpression of VP40 and NP, which led to the suggestion that VP24 may serve as a bridging or linking protein between VP40 and NP. For MARV it was recently reported that VP24 does not influence the release of VLPs, although silencing of VP24 in MARV-infected cells reduced the amount of released viral particles, suggesting a

role of VP24 in the assembly of virions [8].

Our own results support the previous findings by Licata *et al.*, since we did not observe big differences in the amount of iVLPs produced in presence or absence of VP24 (Figure 57). Also, we were able to confirm the finding of Watanabe *et al.*, that VP24 is not necessary for the production of iVLPs or the incorporation of minigenomes into these iVLPs [212], as shown by both an iVLP assay with pretransfected target cells (Figure 50) and a packaging assay (Figure 58). We were able to detect nucleocapsid-like structures in both WT and VP24-deficient iVLPs (Figure 56), which is in conflict with reports from both Huang *et al.* and Watanabe *et al.*, who observed that VP24 is necessary for the formation of nucleocapsid-like structures [97, 211]. However, these experiments were done in the absence of a viral genome or genome analogue, which might contribute to the formation of nucleocapsids. Also, it is not quite clear how relevant the minor differences we observed in the morphologies of VP24-deficient and WT nucleocapsid-like structures are (see section 3.4.5.1). It is possible that VP24-deficient nucleocapdsid-like structures can be only identified in iVLPs, while they are not prominent in the cytoplasm of cells (e.g. as a result of a more diffuse distribution).

Surprisingly, we detected a reduction of reporter signal in p1 after infection of naïve target cells with VP24-deficient iVLPs to 14% of the WT-signal (Figure 51), which is only slightly higher than the expected background due to unspecific reporter protein transfer (see also section 4.1). This suggests that VP24 plays a role in assembly and/or packaging of functional nucleocapsids in p0 or initial transcription in p1, since these are the only processes that are modelled in an iVLP assay with naïve target cells, but not in an iVLP assay with pretransfected target cells. However, VP24 is not directly necessary for replication and transcription, since reporter activity in p0 in absence of VP24 is not diminuished, but rather increased (Figure 50A), which is in line with previous findings by and Watanabe *et al.* [212]. Proteinase K protection assays showed that VP24-deficient iVLPs still contain all viral proteins analyzed (Figure 57), although VP30 levels are decreased; and our attempts to provide missing RNP components *in trans* suggest that it is not a single RNP component that is missing. This means that the role of VP24 is not to recruit a single RNP component into the nucleocapsids. Instead, we propose that VP24 is necessary for the assembly of fully functional nucleocapsids that can be incorporated into iVLPs, by ensuring a correct spacial arrangement of the individual components with respect to each

other. Interestingly, Carbonelle *et al.* have recently presented data that support a role of VP24 in virus assembly and suggest a structural relationship between VP24 and NP [28].

We further propose that reporter activity in p1 in an iVLP assay with target cells pretransfected with all RNP components is independent of VP24 because VP24-deficient misarranged nucleocapsids are still able to support replication of the minigenome, while they are incompetent for transcription. With an excess of NP present replication can be triggered, and the newly synthezised RNA is then able to form replication- and transcription-competent RNP complexes in p1, since all RNP components are available in excess. From our current data it is impossible to conclude whether or not additional RNP components have to be recruited into the misarranged RNP complexes to allow for initial replication.

Two questions that remain to be answered are how exactly VP24 influences nucleocapsid formation, and why VP24 is necessary for the formation of functional nucleocapsids that can be packaged into particles, but not for the formation of transcriptionally and replicationally active RNP-complexes in the cytoplasm. A possible answer to the first question is that VP24 might be important in the condensation of RNP complexes. For rhabdoviruses it has been shown that RNP complexes condense into tightly coiled structures called skeletons at the plasma membrane during budding, and that this process is driven by the rhabdovirus matrix protein M [105]. For EBOV such tightly coiled nucleocapsids, similar to the ones found in virions, are already formed in the cytoplasm in inclusion bodies [70]. VP24, which has been found in these inclusion bodies, has been shown to be important for the formation of such structures [97, 211]. It is, therefore, reasonable to suggest that VP24, the minor matrix protein of EBOV, fulfills this condensation function by a process analogous to that involving the matrix protein of rhabdoviruses. To explain our results one would have to assume that uncondensed nucleocapsids also can be packaged into iVLPs, but that these nucleocapsids are no longer transcriptionally active, after they have been packaged in an uncondensed form. Whether the differences we observed in nucleocapsid-like structures inside iVLPs produced in presence and absence of VP24 correspond to condensed and uncondensed forms of nucleocapsids, remains to be investigated. Condensation of nucleocapsids in the presence of VP24 would also explain why no VP24 is necessary for formation of transcriptionally and replicationally active RNP-complexes in the cytoplasm, since it is possible that active RNP-complexes do not necessarily exist of condensed nucleocapsids.

4.3 Role of NP, VP35, VP30 and L for packaging

After having studied the role of VP24 for morphogenesis, packaging and budding, we were also interested in the role of the RNP components NP, VP35, VP30 and L for these processes. Recently it has been published by Johnson *et al.* that VP35 alone is sufficient for packaging of minigenomes into VP40-only VLPs [108]. This finding was rather surprising, since NP is known to encapsidate the viral genome [131] and, therefore, should be indispensable for packaging. We, therefore, decided to examine the roles of NP, VP35, VP30 and L in morphogenesis, packaging and budding by using an iVLP assay. However, these investigations were complicated by the fact that these proteins take part in transcription and/or replication of the minigenome and, therefore, production of reporter activity. As a result, we decided to use a modified iVLP assay that only assesses packaging, and is independent of transcription and replication of the minigenome in p0.

For this packaging assay p0 cells were transfected with all plasmids necessary for the production of iVLPs, with the exception of L. Therefore, production of minigenomes should only be driven by T7, and not the viral proteins, which allowed us to leave out single RNP components in p0 to study the effect on the packaging of minigenomes, without altering the level of minigenomes available for this process. p1 target cells were pretransfected with all RNP components in order to allow for replication and transcription of the delivered minigenomes independent of the RNP components inside the iVLPs. Infection with particles deficient only in L produced a strong reporter signal in p1, which showed that packaging is not dependent on L (Figure 58). This result also suggests that L-deficient RNP complexes are able to recruit L protein present in the target cells. This was also the case if we additionally ommited VP24 in p0, further showing that VP24 is not necessary for packaging. In contrast, when we left out either NP or VP35 in p0, we were not able to detect any reporter activity in p1, suggesting that both these proteins are necessary for packaging, contrary to the results by Johnson *et al.* This difference in findings might be due to the fact that the readout method used in the study by Johnson *et al.* was RT-PCR, which is able to detect extremely small amount of RNA. Therefore, it is possible that the observed signals are due to an unspecific packaging of minigenome.

When we analyzed the role of VP30 for formation of functional nucleocapsids using an iVLP assay with target cells pretransfected with VP30, we observed that minigenome activity after infection of these cells with VP30-deficient iVLPs reached levels of about 50%

of activity obtained after infection with WT-iVLPs. This indicates that the nucleocapsids in these iVLPs are functional if VP30 is provided *in trans*, and that these iVLPs contain a minigenome; which suggests that VP30 does not play a role for nucleocapsid morphogenesis and packaging. This is in line with findings by Huang *et al.* and Watanabe *et al.*, who show that NP, VP35 and VP24 are sufficient for the formation of nucleocapsid-like structures [97, 211].

However, when we performed a packaging assay we were unable to detect reporter activity in target cells pretransfected with all RNP components and infected with iVLPs produced in the absence of L and VP30. This indicates that VP30 is necessary for minigenome packaging, which clearly contradicts the conclusions drawn from the iVLP assay. It is very unlikely that the negative result in the packaging assay is due to differences in availability of minigenome in p0 caused by the absence of VP30, since VP30 has been shown to be dispensable for replication of minigenomes [139]; further, minigenomes should only be produced by T7-driven transcription, since no viral polymerase is present. An effect of VP30 on this T7-driven production of minigenomes is unlikely, since this should also be detectable in the iVLP assays with VP30-deficient iVLPs.

More likely is that one of the two assumptions made in the packaging assay are wrong. The first assumption is that the amount of minigenome available in p0 is not influenced by the presence or absence of other RNP components if no L is provided. Since L has been shown to be the viral polymerase [138, 139], no replication of minigenome by viral RNP components should occur, and the minigenome should be exclusively produced by the T7 polymerase. However, it is possible that T7-driven minigenome production is influenced by expression of EBOV proteins. The viral protein T7 lysozyme has been shown to directly inhibit T7 RNA polymerase by locking it in an "initiation conformation" [225]. Also, it is possible that expression of T7 polymerase, which is provided under the control of a mammalian promoter, is influenced by expression of viral proteins. The influence of viral matrix proteins on cellular transcription and replication will be discussed below (see scetion 4.4.3). However, since VP40 is always present at the same level in the assay, its presence, while potentially impairing T7 expression, should have equal effects in all samples and, therefore, not skew the results. In contrast to this, if one of the RNP components enhances T7 expression, this could affect the results. It has been shown that viral proteins are able to enhance expression of cellular genes. For example, human immunodeficiency

virus tat protein is able to enhance the activity of the human transcription factor TFIIIC [102]. However, for filoviruses such a phenomenom has not been shown.

The second assumption made is that the lack of reporter activity in p1 is due to the absence of minigenome, which is the most obvious, but not the only explaination. It is not clear to what extent it is possible to provide components in p1 *in trans*. It is obviously possible to provide missing VP30 *in trans* (see section 3.4.4.2). Also, singly missing L is recruited into nucleocapsids after being provided *in trans*, since in the packaging assay replication of the minigenome delivered by L-deficient iVLPs takes place. However, it is not clear by what mechanisms this recruitment occurs, and it is possible that nucleocapsids which are deficient in L as well as VP30 are no longer able to recruit L. This would mean that the negative result obtained with iVLPs deficient in VP30 and L is not due to a deficiency in packaging, but to the fact that the minigenome is locked inside a dysfunctional nucleocapsid which is unable to recover functionality by recruiting L when both L and VP30 are missing at the same time. To address these issues further experiments will be necessary to quantitate the amount of minigenome in the iVLPs and p0 cells.

4.4 Role of VP40 in the viral life cycle

Unlike VP24, the role of VP40 in the viral life cycle is comparatively well understood. In particular, it has been shown to be the driving force for the budding of progeny virions [104, 148, 194]. However, one aspect of VP40 that is almost completely not understood is the role of the different oligomers. While two oligomeric forms of EBOV VP40 have been shown to exist, namely hexamers [162, 179] and octamers [76, 192], both of which made up of antiparallel dimers, and the existance of stable free dimers has been suggested [192], no data about their function is available; however, we were able to show that octamerization is essential for the viral life cycle [96]. We, therefore, decided to further investigate the role of the different oligomeric forms of VP40 using our newly established systems.

4.4.1 Dominant negative effect of VP40-R134A on octamerization

The first question we addressed was whether or not the mutation R134A is dominant negative with respect to octamerization. VP40 octamers consist of four VP40 dimers in antiparallel orientation which are connected by short RNA strands [76, 96]. In a theoret-

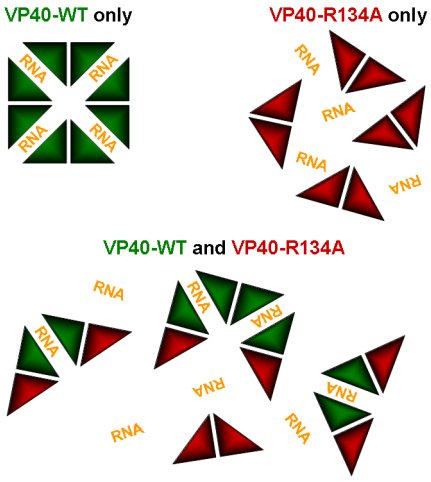

Figure 59: **Model of the dominant negative effect of VP40-R134A.** VP40-WT forms dimers, which are bridged by RNA to from octamers. Disruption of RNA binding in VP40-R134A leads to a loss of octamerization. Upon coexpression of VP40-WT and VP40-R134A, heterodimers form and disrupt octamerization even of VP40-WT.

ical model, upon coexpression of VP40-WT and VP40-R134A heterodimers should form, which would abolish octamerization (Figure 59). Indeed, we observed upon coexpression of VP40-WT and VP40-R134A that increasing amounts of VP40-R134A abolished octamerization of VP40-WT (Figure 23). Thus, the mutation R134A seems to be dominant negative with respect to ocamterization *in vitro*, in line with our model. If such an effect can also be demonstrated *in vivo*, it would allow us to address the question of a role of VP40 octamerization in future, since it should then be possible to inhibit octamerization of VP40 in EBOV infected cells by transfection of VP40-R134A. However, overexpression of matrix proteins has been shown to be able to dysregulate the viral life cycle, a consideration that will have to be addressed when performing such experiments [17, 58].

4.4.2 Design and characterization of a dimerization incompetent VP40

While we had previously designed and characterized a VP40 mutant unable to octamerize [96], at the beginning of our studies no dimerization incompetent VP40 mutant was available. Analysis of the crystall structure revealed two residues (W95 and E160) that appeared to be critical for interaction between VP40 monomers in the dimeric structure. Thus, mutation of these residues would be expected to impair dimerization and, therefore, also formation of hexamers and octamers (see section 3.2.1) [76, 192]. To test the mutants

designed based on this finding, we decided to use a mammalian two hybrid assay which is a powerful tool for analyzing protein interactions [117]. Surprisingly, we were unable to detect interaction of VP40-WT with itself using this assay. We believe that this might be due to the membrane binding activity of VP40 oligomers [179], which may prevent the relocalization of the oligomers into the nucleus, a step necessary for reporter gene activity in a mammalian two hybrid assay. Since the C-terminal domain is responsible for membrane binding [104, 162], while the N-terminal has been shown to be the oligomerization domain, we decided to repeat the experiments with C-terminal truncated forms of VP40. Indeed, we were able to detect interaction of these VP40-mutants (Figure 38). While the additional point mutation of one of the residues identified still allowed interaction to occur, mutation of both W95 and E160 residues rendered VP40 dimerization incompetent. This can be explained by the fact that W95 and E160 interact independently of each other with amino acids of the adjacent VP40 monomer, and that one of these interactions is sufficient to stabilize dimers to an extent that is detectable in a mammalian two hybrid assay.

The observation that VP40-WT interaction is not detectable in a mammalian two hybrid assay has important implications for the use of this assay. In particular, it is not feasible to use VP40-WT as a positive control in such an assay, as has been done in the past [108]. Using a mammalian two hybrid assay it has been reported that VP35 and VP40 are able to interact with each other, and that this interaction results in reporter levels comparable to those for VP40-WT interactions [108]. Taking our own results into consideration, we believe that this finding does not support an interaction between VP35 and VP40.

After having shown that the W95A-E160A-VP40 mutant is indeed oligomerization and, therefore, dimerization incompetent, we decided to use this mutant, as well as the octamerization deficient mutant, to assess their role in the viral life with the new iVLP assay with naïve target cells.

4.4.3 Role in cellular and viral transcription, translation and vRNA replication

It is known that matrix proteins of *Mononegavirales* can influence cellular and/or viral transcription, translation and/or vRNA replication. For example, VSV M has been shown to inhibit cellular transcription and export of host mRNA from the nucleus [125], to block translation of cellular mRNAs by inhibiting the translation initiation factor eIF4E [34]

and to enhance translation of viral mRNAs [35]. Inhibition of cellular transcription occurs for transcription by all three cellular RNA polymerases by inhibition of the transcription factors TFIID (necessary for RNA polymerase II dependent transcription), TFIIIC (necessary for RNA polymerase III dependent transcription) and a yet unidentified transcription factor in the case of RNA polymerase I dependent transcription [125]. Further, inhibition of gene expression is independent of the promoter used [126]. The matrix protein of respiratory syncytial virus (RSV) has also been suggested to inhibit host cell transcription [75], and both RSV M2-2 and rabies M have been shown to influence the balance of viral transcription and replication [17, 58].

We, therefore, analysed the influence of VP40 on expression of a cotransfected luciferase reporter, as well as on minigenome transcription and replication. The luciferase reporter construct used consisted of the ORF for Firefly luciferase under the control of an SV40 early promoter/enhancer, which is RNA polymerase II dependent [27], while the viral proteins as well as T7 polymerase were cloned under the control of a RNA polymerase II dependent chicken β-actin derived promoter. We observed a 3 $\times$ reduction in Firefly reporter activity in the presence of VP40 (Figure 24B), suggesting that expression of the reporter protein is reduced. The presence or absence of other viral proteins, for example L, did not further influence reporter activity. Interestingly, dimerization seemed to be important for this effect, since dimerization incompetent VP40 reduced Firefly activity by only 1.5 $\times$ (Figure 39B), while octamerization seems to be much less important for this effect (2.5 $\times$ reduction of Firefly reporter activity) (Figure 24B).

Surprisingly, both VP40-WT and dimerization incompetent VP40 did not influence the minigenome encoded Renilla reporter activity (Figure 39C). If VP40 has a general effect on protein expression, one would expect that also expression of T7 polymerase as well as the RNP proteins would be reduced, which should result in lower reporter activity. Therefore, either VP40 does not affect expression driven by the chicken β-actin promoter, or the presence of VP40 compensates for the reduced levels of minigenome and RNP proteins.

Since the building blocks of VP40 octamers are dimers [192], dimerization incompetent VP40 should not longer be able to build either dimers or octamers. Therefore, the phenotype of octamerization deficient VP40 should not be more pronounced than that of dimerization incompetent (and, therefore, also octamerization incompetent) VP40; assuming octamers and dimers have not opposing effects on transcription. Contrary to this,

minigenome encoded Renilla reporter activity was significantly higher in the presence of octamerization-deficient VP40 (Figure 24C) than in the presence of either VP40-WT or the dimerization incompetent VP40. This can only be explained if VP40-dimers and VP40-octamers have positive and negative regulatory effects on minigenome encoded Renilla luciferase activity, repectively, and these effects counterbalance each other.

Interestingly, C-terminal deletion mutants of VP40 show a very drastic alteration in phenotype where minigenome encoded reporter activity is completely abolished (Figure 45B). Since C-terminal deletion mutants of VP40 have been shown to spontaneously form nucleic acid containing octamers and hexamers [192], this further supports the hypothesis that VP40 octamers have a negative effect on minigenome encoded Renilla luciferase activity.

We, therefore, propose the following model (Figure 60A): Octamerization has a negative effect on reporter activity derived from minigenome transcription/replication, for example by shifting the ratio of transcription and replication, as described for RSV and Rabies [17, 58], in a way that the overall production of Renilla luciferase mRNA is reduced. This negative effect is counterbalanced by VP40 dimers or another VP40 species made up of dimers, but other than octamers, which have a positive effect on minigenome-derived Renilla reporter activity. If VP40 has an effect on chicken β-actin promoter driven expression, this would lead to a lower expression of RNP proteins and T7, and therefore of minigenome. Such an effect might also be counteracted by the same mechanism (Figure 60B).

Although this model does explain the current data, further experiments will be necessary to confirm it. In particular, future experiments will have to address the question expression of which promoters are affected by VP40, by using a control plasmid encoding Firefly luciferase under the control of a chicken β-actin promoter. Also, it will be helpful to analyse the amount of RNP proteins inside cells, as well as to quantitate Renilla luciferase mRNA and antigenome copies in order to distinguish between effects on viral transcription and replication.

4.4.4 Role in budding and morphogenesis

The role of VP40 in budding has been the subject of extensive studies. In particular, the role of the overlapping late domain motifs has been investigated [89, 103], and VP40 has been shown to be the primary force for the formation of VLPs with the characteristic

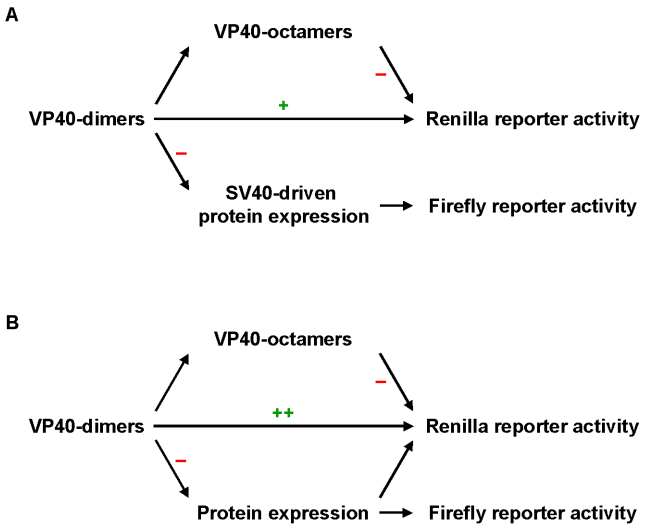

VP40 species	Firefly	Renilla
none		
all	–	+ –
no octamers	–	+
no dimers / octamers		

VP40 species	Firefly	Renilla
none		
all	–	+ + – –
no octamers	–	+ + –
no dimers / octamers		

Figure 60: **Proposed model for the influence of VP40 on viral and cellular replication, transcription and replication.** Positive and negative influences on protein expression and reporter protein production are indicated by + or -. The tables beside the graphs show an overview of which phenotype is to be expected in the presence of the indicated VP40 species. (A) Model if VP40 only impairs SV40 driven protein expression, but not chicken β-actin driven protein expression. (B) Model if VP40 generally impairs protein expression independent of the promoter used.

thread-like appearance of EBOV particles [148]. While it has been hypothesized that VP40 oligomerization is important for budding activity [193], this has not been systematically studied. The only data currently available are our own previous findings which showed that VP40 octamerization is not important for VLP formation [96].

When we analysed the influence of oligomerization on budding using an iVLP assay, we could confirm our previous results that VP40 octamerization does not seem to play any role in budding (Figures 25 and 30). Also, we were unable to detect differences in packaging or the morphogenesis of fully functional nucleocapsids, all of which would be detectable in an iVLP assay with naïve target cells. However, when we analyzed the influence of VP40 dimerization on these processes, we observed that VP40 dimerization is indeed necessary for budding. This is the first time that the oligomerization of a matrix protein of *Mononegavirales* could be directly shown to be important for budding. Oligomerization has also been reported for the matrix protein of Borna disease virus [115], another members of *Mononegavirales*, but no functional significance has yet been identified.

When we analyzed the influence of deletions in VP40 on budding, we observed that all mutants with the exception of VP40-ΔN14 were budding incompetent. This suggests

that both the N-terminal oligomerization domain and the C-terminal membrane binding domain are essential for budding. Further, it indicates that the deletions within the β-sandwiches destroy the tertiary structure of the sandwich and, thereby, the function of the respective domain. Interestingly, most of the deletion mutants were still able to bind NP (see section 4.4.5). The finding that VP40-ΔN14 was still able to drive budding of VLPs was very surprising for us, since this mutant does not contain the two overlapping late domains that have been shown to be crucial for VLP budding [104, 122]. However, while in those studies VLPs were purified over a sucrose cushion prior to western blotting, for screening of the VP40 deletion mutants we only clarified cell supernatant from cellular debris and performed a proteinase K protection assay to ensure that detected VP40 is surrounded by a lipid envelope. Preliminiary results indicate that we as well see a drastic reduction in VLP production by VP40-ΔN14, if we analyze particles purified over a sucrose cushion (data not shown). This suggests that VP40-ΔN14 might lead to the production of particles with a very low density which cannot be centrifuged through a sucrose cushion. While further analysis of these particles will be necessary to assess the relevance of this finding, it is interesting to note that it has been shown by Neumann *et al.* that late domains are not essential for virus replication in cell culture [142]. This suggests that different late domain independent budding mechanisms for EBOV exist, and might be contributing to the particle formation we observe with VP40-ΔN14.

4.4.5 Interaction with NP

Since VP40 is the major contributor to virion morphogenesis, and NP the major structural nucleocapsid component, they have been suggested to interact with each other during morphogenesis [89, 113]. Similar interactions have been reported for paramyxoviruses [38] and rhabdoviruses [217]. A possible interaction between NP and VP40 has been supported by the finding that NP is recruited into VP40-only VLPs, and it has been suggested that the interacting domain on NP is located in the last 50 amino acids of NP, since a deletion mutant missing these amino acids could not be found in VP40-only VLPs [121]. However, the data for this finding are not convincing, since immunoprecipitation using an α-NP antibody was used as a readout. The inability to detect a deletion mutant of NP in VP40-only VLPs with this method was interpreted as evidence for abolished VP40-NP interaction, without controls for proper folding of the NP mutant or interaction of this

mutant with the antibody. Also, it is possible that the recruitment of NP into VP40-only VLPs is unspecific, since it has been reported that other proteins are also unspecifically incorporated into those VLPs [132], or that cellular or viral proteins facilitate a indirect interaction between VP40 and NP. We, therefore, analysed a possible interaction of VP40 and NP, with special emphasis on the questions of whether there is a direct interaction between VP40 and NP, and which region of VP40 is responsible for this interaction.

Our first strategy to characterize an interaction of VP40 and NP was to produce VLPs with different deletion mutants of VP40, and to check these VLPs for NP incorporation. While this strategy does not allow any definite conclusion about a direct interaction of VP40 and NP to be drawn, it can serve as a quick screening method to identify regions involved in the interaction of VP40 and NP. Unfortunately, none of the VP40 deletions mutants were able to produce VLPs (see also section 4.4.4). As a second strategy we, therefore, decided to analyze the interaction of VP40 and NP using coimmunoprecipitation. With this method we were able to show a direct interaction of NP and VP40 (Figure 48). Also, most of the deletion mutants analyzed were able to coimmunoprecipitate with NP, with the exception of VP40-$\Delta\beta$0102 and VP40-ΔC194. Although preliminary results had suggested that the C-terminal domain is not important for VP40-NP interactions, based on our findings we cannot exclude a role of this domain for these interactions. However, it is also possible that VP40-oligomerization, which has been shown to be triggered by C-terminal deletions [192], inhibits interaction with NP. The finding, that VP40-$\Delta\beta$0102 does not support NP-VP40 interactions, suggests that this region is important for these interactions. Although it has to be considered that the lack of interactions might also be caused by misfolding of the N-terminal domain of this VP40 mutant, the fact that all other deletion mutants support interaction with NP suggests that the overall structure of this domain is not important for NP-VP40 interactions, but a rather small region in this domain. When we analyzed the surface of VP40 for charged residues, which have been shown to be often involved in protein-protein interactions [220], we were able to identify two residues (K86 and K90) between the β-strands 1 and 2, which might be important for interaction with NP (Figure 49). Further experiments involving mutagenesis of these residues will allow us to determine their importance for NP-VP40 interactions in future.

4.4.6 Role of VP40 *in vivo*

The results of the iVLP assays suggest that there might be an influence of octamerization on transcription and/or replication of vRNA, as has been shown for the matrix protein of Rabies virus [58]. While it was possible for Rabies virus to rescue recombant virues in which this function was inhibited by introducing a point mutation into M [57], for EBOV similar efforts have been unsuccessful, since recombinant octamerization-deficient viruses are non-viable [96]. To circumvent this problem, we decided to develope a system that allows us to exchange the viral VP40 against mutated VP40 without the need to design, clone and rescue a recombinant virus. Such a system would not only allow us to analyze the effect of VP40 octamerization in a virus infection, it would also be an attractive alternative to an infectious clone system since it allows the analysis of the effect of many mutations in a short amount of time without cloning and rescuing recombinant viruses, which can be a long and difficult process. As an apporach we chose to silence virus derived VP40 by using an siRNA directed against the VP40-NCR, and to supply plasmid-driven VP40 lacking the siRNA target sequence *in trans*. For filoviruses, siRNAs have been successfully used to reduce the infectious titer in tissue culture after infection with EBOV by 1 to 1.5 $\log_{10}$ [68, 79], and to protect 60% of infected guinea pigs against a otherwise lethal dose of guinea pig adapted EBOV [68]. Groseth *et al.* reported the successful use of siRNAs delivered in form of plasmid-encoded small hairpin RNAs under the control of a RNA polymerase III promoter [79], and we decided to adopt this approach since it allowed us to create a cell line that constitutively expresses the siRNA, which provides a homogenous level of siRNAs in the cells and and therefore avoids the problem of relatively low transfection efficiency in VeroE6 cells.

After screening and selection of a suitable cell line clone we observed a reduction in viral titers of $\sim$ 1.5 $\log_{10}$ (Figure 34), as previously reported [68, 79]. This reduction indicates that the chosen target might be suitable for protecting animals, since for guinea pigs an even lower reduction in tissue culture titers led to promising results *in vivo* [68]. Also, the fact that the VP40 is the most abundant protein in virions [45] and, therefore, needed in high amounts during the viral life cycle, as well as the fact that VP40 might be important for several steps in the viral life cycle (see section 4.4.3), support the feasability of VP40 as siRNA target. The chosen siRNA target is genus and species specific, as shown by surpression of recombinantly expressed MARV VP40 (Figure 31C) and of infection with REBOV

(Figure 34). This is not surprising, since siRNAs are known to be very sequence specific, with a small number of nucleotide changes in their target sequence usually rendering them inactive [2]. When we infected the established stable cell line and transfected it with VP40 lacking the siRNA target, we observed a recovery of infection (Fiure 35). Unfortunately, this effect seems to be unspecific, since transfection of empty plasmid also achieved similar results. We believe that this might be due to effects of the transfection reagent used, which was not removed from the tissue culture supernatant in these experiments. Undesired side effects when using chemical transfection reagents, including upregulation of cellular genes [3] and disruption of membrane microdomains important for the uptake of certain viruses [218], have been previously reported. Although we were not able to find any reports about increased susceptility of cells to virus infection due to chemical transfection, one can speculate that this could occur either by upregulation of a cellular gene important for the viral life cycle (e.g. the cellular receptor), or by promoting unspecific fusion of viral and cellular membranes [44]. Further optimization will be necessary to reduce this side effect; possibilities herefore include exchanging the medium after transfection, or the use of different transfection reagents. Nevertheless, we believe that this system shows great promise for the analysis of mutated proteins in an infection without the need to design, clone and resuce recombinant viruses. This will not only allow the study of the effect of mutations that render EBOV non-viable and, therefore, non-rescueable, but also enable us to screen a great number of mutations in a short time.

4.5 Model for the functions of the matrix proteins VP40 and VP24 in the viral life cycle

Based on our findings, we have developed a modell for the different roles for the viral matrix proteins in the viral life cycle, which is depicted in Figure 61. Dimeric VP40 impairs cellular transcription and/or translation, while it has a positive effect on viral transcription and/or translation. It might also enhance viral replication. In contrast, octameric VP40 has a negative effect on viral replication and/or transcription. VP24 is essential for the assembly and packaging of fully functional nucleocapsids into budding virions, and dimeric VP40 together with cellular factors plays a crucial role during this budding process. Although this modell does explain our experimental results, it is at the present time neither complete, nor necessarily true in all points. Further studies will be

necessary to validate the proposed functions of the viral matrix proteins, which will not only increase our knowlegde of the viral life cycle of EBOV, but will also help to develop new countermeasures for EBOV infections by interfering with these functions.

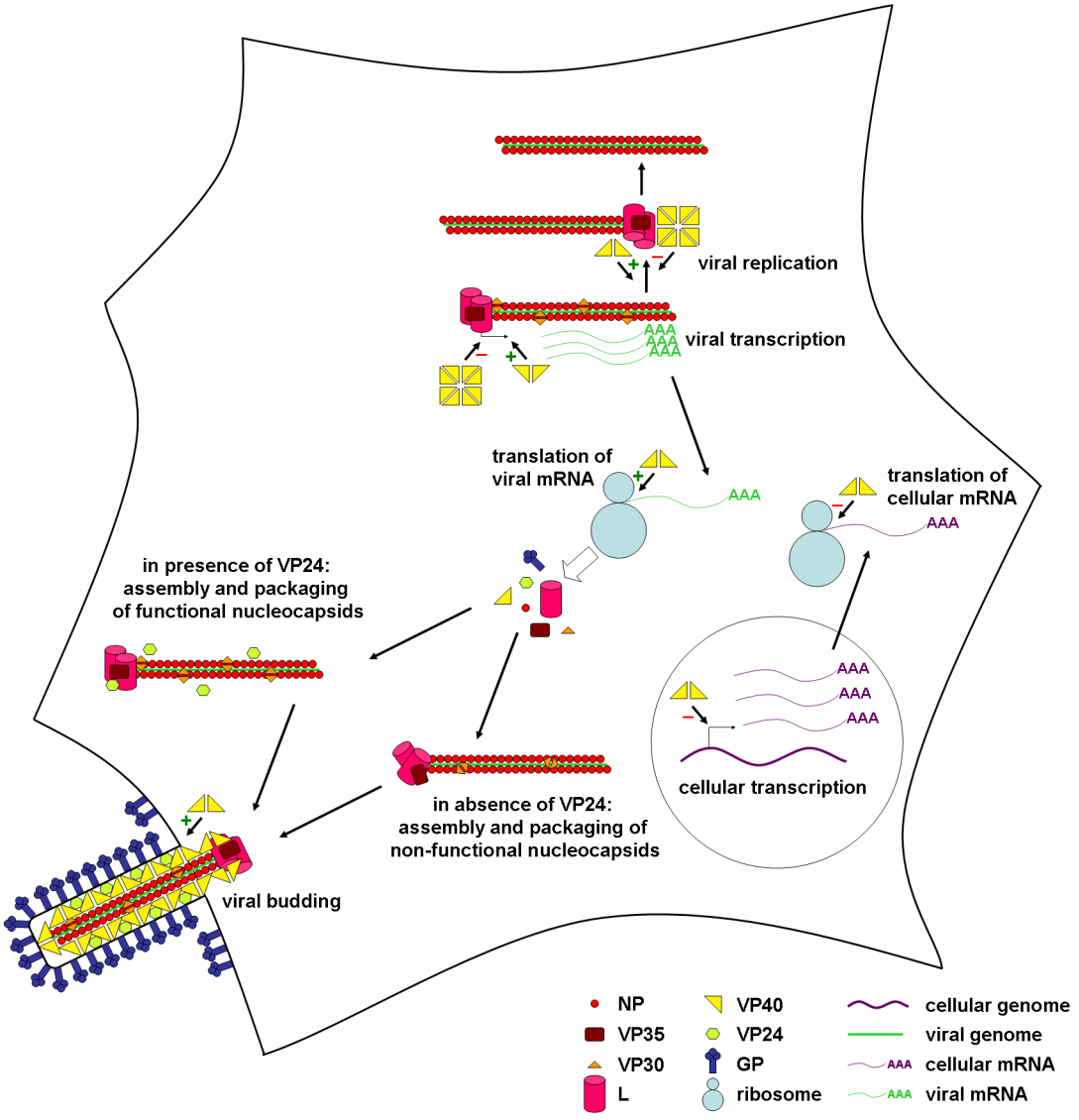

Figure 61: **Proposed model for the role of the matrix proteins VP24 and VP40 in the viral life cycle.** Dimeric VP40 impairs cellular transcription and/or translation, while it has a positive effect on viral transcription and/or translation. It might also enhance viral replication. In contrast, octameric VP40 has a negative effect on viral replication and/or transcription. VP24 is essential for the assembly and packaging of fully functional nucleocapsids into budding virions, and dimeric VP40 together with cellular factors plays a crucial role during this budding process.

5 Summary

Ebola virus (EBOV), a member of the family *Filoviridae* in the order *Mononegavirales*, is the causative agent of a severe haemorrhagic fever. Due to its high case fatality rate of up to 90% and to the fact that no approved vaccination or treatment is available for EBOV infection, it is classified as a biosafety level 4 (BSL4) agent, which restricts reasearch on it to a few facilities worldwide. Systems that model individual aspects of the viral life cycle under BSL2 conditions are, therefore, highly desirable. Based on available reverse genetics systems we have developed several new systems that allow the analysis of viral genome transcription, replication and packaging, as well as nucleocapsid morphogenesis, particle formation, budding, entry and initial transcription in target cells under BSL2 conditions. We were able to model two of these steps, morphogenesis of a fully functional nucleocapsid and inititial transcription in target cells, for the first time for a negative strand RNA-virus, which is a significant advantage in reverse genetics systems for these viruses. The established systems were then used to analyze the role of EBOV proteins, particularly the matrix proteins VP24 and VP40, in the viral life cycle.

The role of VP24, the minor matrix protein of EBOV, has long been enigmatic. Recently, it has been shown to be involved in interferon antagonism; however, data regarding a possible involvement of VP24 in nucleocapsid morphogenesis and particle formation have remained controversial. Using a newly developed infectious virus-like particle assay with naïve target cells we were able to show that VP24 is not necessary for budding of particles or genome packaging, but that it is indispensable for the formation of functional nucleocapsids. This is the first functional evidence for a role of VP24 in nucleocapsid formation.

Although the role of the major matrix protein, VP40, is much better understood, virtually nothing is known about the function of the different oligomeric forms of VP40, namely dimers, hexamers and octamers. Previously, we have been able to show that VP40 octamerization is indispensable for the viral life cycle. As part of this work we have further analyzed the role of VP40 octamerization. Also, based on the available crystal structures for VP40 we designed and characterized a dimerization incompetent VP40 mutant and included this mutant in our studies. We were able to show that VP40 dimerization is a prerequisite for budding, while octamerization does not play a role in this process. Also, VP40 octamerization is not important for packaging or the formation of a functional nucleocapsid. However, VP40 octamers seem to influence transcription and/or replication of

viral genomes, a phenomenon that has been previously described for the matrix protein of Rabies virus, another member of *Mononegavirales*. Also, our data suggest that VP40 is involved in inhibition of cellular transcription and/or translation, a phenomenon widely known for matrix proteins of *Mononegavirales*, and that VP40 dimerization is important for this function. Finally, we analyzed the interactions of the nucleocapsid protein NP with VP40. We were, for the first time, able to directly show an interaction between these two proteins, and have mapped the interaction domain on VP40 to two β-strands in the N-terminal domain. Based on the crystal structure of VP40 we have identified two residues in this region that may be crucial for the interaction with NP.

This work has increased our understanding of the role of EBOV matrix proteins in the viral life cycle, and has revealed several new functions for these proteins. The obtained results will allow us to specifically target individual aspects of the viral life cycle in order to develop new countermeasures against EBOV, but also to further investigate molecular details of these processes.

6 Zusammenfassung

Ebola virus (EBOV) gehört zur Familie *Filoviridae* in der Ordnung *Mononegavirales* und verursacht im Menschen ein schweres hämmorhagisches Fieber. Wegen der hohen Letalität und der Tatsache, dass es weder eine zugelassene Impfung noch Therapie für EBOV-Infektionen gibt, ist es als ein Erreger der höchsten biologischen Sicherheitsstufe L4 eingestuft, weswegen die Erforschung dieses Virus nur in sehr wenigen Laboratorien in der Welt möglich ist. Es ist daher sehr erstrebenswert, Modellsysteme zu entwickeln, die es erlauben, einzelne Aspekte des Lebenszyklus von EBOV unter L2-Bedingungen zu untersuchen. Ausgehend von verfügbaren "Reverse Genetik"-Systemen haben wir mehrere solche Modellsysteme entwickelt, die es erlauben, Transkription, Replikation und Verpackung von viralen Genomen, die Morphogenese von Nukleokapsiden und Formierung von Viruspartikeln, und Abknospung und Zelleintritt sowie initiale Transkription in Zielzellen unter L2-Bedingungen zu erforschen. Erstmals für ein RNA Virus mit einem Genom in Negativ-Orientierung war es uns möglich, zwei Schritte des viralen Lebenszyklus, nämlich die Entstehung eines voll funktionsfähigen Nukleokapsides und die inititale Transkription in Zielzellen, zu modellieren. Dies stellt einen wesentlichen Fortschritt für "Reverse Genetik"-Systeme für diese Viren dar. Die entwickelten Systeme wurden dann dazu verwendet, um die Rolle von EBOV-Proteinen, insbesondere den Matrixproteinen VP40 und VP24, im viralen Lebenszyklus zu erforschen.

Insbesondere die Rolle von VP24 ist für lange Zeit rätselhaft gewesen, bis kürzlich gezeigt werden konnte, dass es als Interferon-Antagonist fungiert. Daten bezüglich einer möglichen Beteiligung von VP24 in der Morphogenese von Nukleokapsiden und der Formierung von Viruspartikeln sind jedoch widersprüchlich geblieben. Mithilfe eines von uns neu entwickelten "infectious virus-like particle" Systems (iVLP-System) konnten wir zeigen, dass VP24 nicht notwendig für die Abknospung von Viruspartikeln oder Verpackung von Genomen ist, jedoch eine wesentliche Rolle in der Entstehung eines voll funktionsfähigen Nukleokapsides spielt. Dies ist der erste funktionelle Nachweis einer Rolle von VP24 in der Entstehung von Nukleokapsiden.

Die Funktion von VP40 ist wesentlich besser verstanden, aber fast nichts ist über die Rolle der verschiedenen oligomeren Formen von VP40 (Dimere, Hexamere, Oktamere) bekannt. Wir konnten kürzlich zeigen, dass die Oktamerisierung von VP40 unerlässlich im viralen Lebenszyklus ist. Als Teil dieser Doktorarbeit haben wir diese Rolle weiter un-

tersucht. Desweiteren haben wir ausgehend von der 3D-Struktur von VP40 dimerisierungsunfähige VP40 Mutanten entworfen und charakterisiert. Wir konnten zeigen, dass die Dimerisierung von VP40 notwendig für das Abknospen von neuen Viruspartikeln ist, während Oktamerisierung von VP40 keine Rolle in diesem Prozess zu spielen scheint. Weiterhin scheint VP40-Oktamerisierung nicht wichtig für das Verpacken oder die Formierung von voll funktionsfähigen Nukleokapsiden zu sein. Allerdings scheint die Oktamerisierung von VP40 einen Einfluss auf die Transkription und Replikation von viralen Genomen zu haben, ein Phänomen, das bereits früher für Rabies, einen anderen Vertreter der Ordnung *Mononegavirales*, gezeigt werden konnte. Außerdem scheint VP40, insbesondere VP40-Dimere, die zelluläre Transkription und/oder Translation zu inhibieren, eine Funktion, die für eine Reihe von Matrixproteinen von Viren der Ordnung *Mononegavirales* bekannt ist. Darüber hinaus haben wir die Interaktionen von VP40 mit dem Nukleokapsidprotein NP untersucht. Wir konnten erstmals eine direkte Interaktion dieser beiden Proteine nachweisen, und haben die Interaktionsdomäne auf zwei β-Stränge in der N-terminalen Domäne eingrenzen können. Mithilfe der bekannten 3D-Struktur von VP40 haben wir zwei Aminosäuren identifiziert, die eine entscheidende Rolle für diese Interaktionen spielen könnten.

Aufgrund dieser Studien haben wir nun ein besseres Verständnis der Funktionen der EBOV-Matrixproteine im viralen Lebenszyklus, und wir konnten mehrere neue Funktionen für diese Proteine zeigen. Diese Ergebnisse werden uns erlauben, einzelne Aspekte des viralen Lebenszyklus spezifisch zu inhibieren, um die molekularen Details dieser Prozesse besser zu verstehen, aber auch um neue Therapeutika für EBOV-Infektionen zu entwicklen.

References

[1] N. Alazard-Dany, V. Volchkova, O. Reynard, C. Carbonnelle, O. Dolnik, M. Ottmann, A. Khromykh, and V. E. Volchkov. Ebola virus glycoprotein gp is not cytotoxic when expressed constitutively at a moderate level. *J Gen Virol*, 87(Pt 5):1247–57, 2006.

[2] M. Amarzguioui, T. Holen, E. Babaie, and H. Prydz. Tolerance for mutations and chemical modifications in a sirna. *Nucleic Acids Res*, 31(2):589–95, 2003.

[3] R. Arulanandam, A. Vultur, and L. Raptis. Transfection techniques affecting stat3 activity levels. *Anal Biochem*, 338(1):83–9, 2005.

[4] M. Babst. A protein's final escrt. *Traffic*, 6(1):2–9, 2005.

[5] A. Bairoch, R. Apweiler, C. H. Wu, W. C. Barker, B. Boeckmann, S. Ferro, E. Gasteiger, H. Huang, R. Lopez, M. Magrane, M. J. Martin, D. A. Natale, C. O'Donovan, N. Redaschi, and L. S. Yeh. The universal protein resource (uniprot). *Nucleic Acids Res*, 33(Database issue):D154–9, 2005.

[6] S. Baize, E. M. Leroy, A. J. Georges, M. C. Georges-Courbot, M. Capron, I. Bedjabaga, J. Lansoud-Soukate, and E. Mavoungou. Inflammatory responses in ebola virus-infected patients. *Clin Exp Immunol*, 128(1):163–8, 2002.

[7] S. Baize, E. M. Leroy, M. C. Georges-Courbot, M. Capron, J. Lansoud-Soukate, P. Debre, S. P. Fisher-Hoch, J. B. McCormick, and A. J. Georges. Defective humoral responses and extensive intravascular apoptosis are associated with fatal outcome in ebola virus-infected patients. *Nat Med*, 5(4):423–6, 1999.

[8] S. Bamberg, L. Kolesnikova, P. Moller, H. D. Klenk, and S. Becker. Vp24 of marburg virus influences the formation of infectious particles. *J Virol*, 79(21):13421–33, 2005.

[9] S. Baron, J. Poast, D. Rizzo, E. McFarland, and E. Kieff. Electroporation of antibodies, dna, and other macromolecules into cells: a highly efficient method. *J Immunol Methods*, 242(1-2):115–26, 2000.

[10] C. F. Basler, A. Mikulasova, L. Martinez-Sobrido, J. Paragas, E. Muhlberger, M. Bray, H. D. Klenk, P. Palese, and A. Garcia-Sastre. The ebola virus vp35 protein inhibits activation of interferon regulatory factor 3. *J Virol*, 77(14):7945–56, 2003.

[11] C. F. Basler and P. Palese. Modulation of innate immunity by filoviruses. *In H. D. Klenk, H. Feldmann (ed.), Ebola and Marburg viruses. Horizon Bioscience, Norfolk, U.K.*, pages 305–349, 2004.

[12] C. F. Basler, X. Wang, E. Muhlberger, V. Volchkov, J. Paragas, H. D. Klenk, A. Garcia-Sastre, and P. Palese. The ebola virus vp35 protein functions as a type i ifn antagonist. *Proc Natl Acad Sci U S A*, 97(22):12289–94, 2000.

[13] S. Bavari, C. M. Bosio, E. Wiegand, G. Ruthel, A. B. Will, T. W. Geisbert, M. Hevey, C. Schmaljohn, A. Schmaljohn, and M. J. Aman. Lipid raft microdomains: a gateway for compartmentalized trafficking of ebola and marburg viruses. *J Exp Med*, 195(5):593–602, 2002.

[14] S. Becker, S. Huppertz, H. D. Klenk, and H. Feldmann. The nucleoprotein of marburg virus is phosphorylated. *J Gen Virol*, 75 (Pt 4):809–18, 1994.

[15] S. Becker and E. Muhlberger. Co- and posttranslational modifications and functions of marburg virus proteins. *Curr Top Microbiol Immunol*, 235:23–34, 1999.

[16] S. Becker, C. Rinne, U. Hofsass, H. D. Klenk, and E. Muhlberger. Interactions of marburg virus nucleocapsid proteins. *Virology*, 249(2):406–17, 1998.

[17] A. Bermingham and P. L. Collins. The m2-2 protein of human respiratory syncytial virus is a regulatory factor involved in the balance between rna replication and transcription. *Proc Natl Acad Sci U S A*, 96(20):11259–64, 1999.

[18] M. P. Bevilacqua, J. S. Pober, G. R. Majeau, W. Fiers, R. S. Cotran, and Jr. Gimbrone, M. A. Recombinant tumor necrosis factor induces procoagulant activity in cultured human vascular endothelium: characterization and comparison with the actions of interleukin 1. *Proc Natl Acad Sci U S A*, 83(12):4533–7, 1986.

[19] A. S. Bjorndal, L. Szekely, and F. Elgh. Ebola virus infection inversely correlates with the overall expression levels of promyelocytic leukaemia (pml) protein in cultured cells. *BMC Microbiol*, 3(1):6, 2003.

[20] Y. Boehmann, S. Enterlein, A. Randolf, and E. Muhlberger. A reconstituted replication and transcription system for ebola virus reston and comparison with ebola virus zaire. *Virology*, 332(1):406–17, 2005.

[21] L. Borio, T. Inglesby, C. J. Peters, A. L. Schmaljohn, J. M. Hughes, P. B. Jahrling, T. Ksiazek, K. M. Johnson, A. Meyerhoff, T. O'Toole, M. S. Ascher, J. Bartlett, J. G. Breman, Jr. Eitzen, E. M., M. Hamburg, J. Hauer, D. A. Henderson, R. T. Johnson, G. Kwik, M. Layton, S. Lillibridge, G. J. Nabel, M. T. Osterholm, T. M. Perl, P. Russell, and K. Tonat. Hemorrhagic fever viruses as biological weapons: medical and public health management. *Jama*, 287(18):2391–405, 2002.

[22] S. Bose, N. Kar, R. Maitra, J. A. DiDonato, and A. K. Banerjee. Temporal activation of nf-kappab regulates an interferon-independent innate antiviral response against cytoplasmic rna viruses. *Proc Natl Acad Sci U S A*, 100(19):10890–5, 2003.

[23] C. M. Bosio, M. J. Aman, C. Grogan, R. Hogan, G. Ruthel, D. Negley, M. Mohamadzadeh, S. Bavari, and A. Schmaljohn. Ebola and marburg viruses replicate in monocyte-derived dendritic cells without inducing the production of cytokines and full maturation. *J Infect Dis*, 188(11):1630–8, 2003.

[24] C. M. Bosio, B. D. Moore, K. L. Warfield, G. Ruthel, M. Mohamadzadeh, M. J. Aman, and S. Bavari. Ebola and marburg virus-like particles activate human myeloid dendritic cells. *Virology*, 326(2):280–7, 2004.

[25] M. Bray. The role of the type i interferon response in the resistance of mice to filovirus infection. *J Gen Virol*, 82(Pt 6):1365–73, 2001.

[26] M. A. Bwaka, M. J. Bonnet, P. Calain, R. Colebunders, A. De Roo, Y. Guimard, K. R. Katwiki, K. Kibadi, M. A. Kipasa, K. J. Kuvula, B. B. Mapanda, M. Massamba, K. D. Mupapa, J. J. Muyembe-Tamfum, E. Ndaberey, C. J. Peters, P. E.

Rollin, and E. Van den Enden. Ebola hemorrhagic fever in kikwit, democratic republic of the congo: clinical observations in 103 patients. *J Infect Dis*, 179 Suppl 1:S1–7, 1999.

[27] B. J. Byrne, M. S. Davis, J. Yamaguchi, D. J. Bergsma, and K. N. Subramanian. Definition of the simian virus 40 early promoter region and demonstration of a host range bias in the enhancement effect of the simian virus 40 72-base-pair repeat. *Proc Natl Acad Sci U S A*, 80(3):721–5, 1983.

[28] C. Carbonnelle, V. Volchkova, H. Contamin, P. Loth, O. Reynard, N. Alazard-Dany, O. Dolnik, M. Ottmann, L. Kolesnikova, and V. Volchkov. Structural protein vp24 is a key determinant of ebola virus virulence. *In Abstracts of the XIII International Conference on Negative Strand Viruses, Salamanca, Spain*, page 156, 2006.

[29] W. B. Cardenas, Y. M. Loo, Jr. Gale, M., A. L. Hartman, C. R. Kimberlin, L. Martinez-Sobrido, E. O. Saphire, and C. F. Basler. Ebola virus vp35 protein binds double-stranded rna and inhibits alpha/beta interferon production induced by rig-i signaling. *J Virol*, 80(11):5168–78, 2006.

[30] S. Y. Chan, M. C. Ma, and M. A. Goldsmith. Differential induction of cellular detachment by envelope glycoproteins of marburg and ebola (zaire) viruses. *J Gen Virol*, 81(Pt 9):2155–9, 2000.

[31] S. Y. Chan, R. F. Speck, M. C. Ma, and M. A. Goldsmith. Distinct mechanisms of entry by envelope glycoproteins of marburg and ebola (zaire) viruses. *J Virol*, 74(10):4933–7, 2000.

[32] K. Chandran, N. J. Sullivan, U. Felbor, S. P. Whelan, and J. M. Cunningham. Endosomal proteolysis of the ebola virus glycoprotein is necessary for infection. *Science*, 308(5728):1643–5, 2005.

[33] C. T. Chung, S. L. Niemela, and R. H. Miller. One-step preparation of competent escherichia coli: transformation and storage of bacterial cells in the same solution. *Proc Natl Acad Sci U S A*, 86(7):2172–5, 1989.

[34] J. H. Connor and D. S. Lyles. Vesicular stomatitis virus infection alters the eif4f translation initiation complex and causes dephosphorylation of the eif4e binding protein 4e-bp1. *J Virol*, 76(20):10177–87, 2002.

[35] J. H. Connor, M. O. McKenzie, and D. S. Lyles. Role of residues 121 to 124 of vesicular stomatitis virus matrix protein in virus assembly and virus-host interaction. *J Virol*, 80(8):3701–11, 2006.

[36] K. K. Conzelmann. Nonsegmented negative-strand rna viruses: genetics and manipulation of viral genomes. *Annu Rev Genet*, 32:123–62, 1998.

[37] K. K. Conzelmann. Reverse genetics of mononegavirales. *Curr Top Microbiol Immunol*, 283:1–41, 2004.

[38] E. C. Coronel, K. G. Murti, T. Takimoto, and A. Portner. Human parainfluenza virus type 1 matrix and nucleoprotein genes transiently expressed in mammalian cells induce the release of virus-like particles containing nucleocapsid-like structures. *J Virol*, 73(8):7035–8, 1999.

[39] A. Dessen, E. Forest, V. Volchkov, O. Dolnik, H. D. Klenk, and W. Weissenhorn. Crystallization and preliminary x-ray analysis of the matrix protein from ebola virus. *Acta Crystallogr D Biol Crystallogr*, 56 (Pt 6):758–60, 2000.

[40] A. Dessen, V. Volchkov, O. Dolnik, H. D. Klenk, and W. Weissenhorn. Crystal structure of the matrix protein vp40 from ebola virus. *Embo J*, 19(16):4228–36, 2000.

[41] O. Dolnik, V. Volchkova, W. Garten, C. Carbonnelle, S. Becker, J. Kahnt, U. Stroher, H. D. Klenk, and V. Volchkov. Ectodomain shedding of the glycoprotein gp of ebola virus. *Embo J*, 23(10):2175–84, 2004.

[42] H. Ebihara, A. Groseth, G. Neumann, Y. Kawaoka, and H. Feldmann. The role of reverse genetics systems in studying viral hemorrhagic fevers. *Thromb Haemost*, 94:240–53, 2005.

[43] H. Ebihara, A. Takada, D. Kobasa, S. Jones, G. Neumann, S. Theriault, M. Bray, H. Feldmann, and Y. Kawaoka. Molecular determinants of ebola virus virulence in mice. *PLoS Pathog*, 2(7):e73, 2006.

[44] A. El Ouahabi, M. Thiry, V. Pector, R. Fuks, J. M. Ruysschaert, and M. Vandenbranden. The role of endosome destabilizing activity in the gene transfer process mediated by cationic lipids. *FEBS Lett*, 414(2):187–92, 1997.

[45] L. H. Elliott, M. P. Kiley, and J. B. McCormick. Descriptive analysis of ebola virus proteins. *Virology*, 147(1):169–76, 1985.

[46] J. M. Emeny and M. J. Morgan. Regulation of the interferon system: evidence that vero cells have a genetic defect in interferon production. *J Gen Virol*, 43(1):247–52, 1979.

[47] M. Enami, W. Luytjes, M. Krystal, and P. Palese. Introduction of site-specific mutations into the genome of influenza virus. *Proc Natl Acad Sci U S A*, 87(10):3802–5, 1990.

[48] S. Enterlein, V. Volchkov, M. Weik, L. Kolesnikova, V. Volchkova, H. D. Klenk, and E. Muhlberger. Rescue of recombinant marburg virus from cdna is dependent on nucleocapsid protein vp30. *J Virol*, 80(2):1038–43, 2006.

[49] H. Feldmann, H. Bugany, F. Mahner, H. D. Klenk, D. Drenckhahn, and H. J. Schnittler. Filovirus-induced endothelial leakage triggered by infected monocytes/macrophages. *J Virol*, 70(4):2208–14, 1996.

[50] H. Feldmann, T. Geisbert, P. Jahrling, H. D. Klenk, S. V. Netesov, C. Peters, A. Sanchez, R. Swanepoel, and V. Volchkov. Filoviridae. *In C. M. Fauqet et al. (ed.), Virus Taxonomy, Eighth Report of the International Committee on Taxonomy of Viruses, Elsevier Academic Press, San Diego, CA*, pages 645–53, 2004.

[51] H. Feldmann, S. Jones, H. D. Klenk, and H. J. Schnittler. Ebola virus: from discovery to vaccine. *Nat Rev Immunol*, 3(8):677–85, 2003.

[52] H. Feldmann, S. M. Jones, H. J. Schnittler, and T. Geisbert. Therapy and prophylaxis of ebola virus infections. *Curr Opin Investig Drugs*, 6(8):823–30, 2005.

[53] H. Feldmann and M. P. Kiley. Classification, structure, and replication of filoviruses. *Curr Top Microbiol Immunol*, 235:1–21, 1999.

[54] H. Feldmann, E. Muhlberger, A. Randolf, C. Will, M. P. Kiley, A. Sanchez, and H. D. Klenk. Marburg virus, a filovirus: messenger rnas, gene order, and regulatory elements of the replication cycle. *Virus Res*, 24(1):1–19, 1992.

[55] H. Feldmann, S. T. Nichol, H. D. Klenk, C. J. Peters, and A. Sanchez. Characterization of filoviruses based on differences in structure and antigenicity of the virion glycoprotein. *Virology*, 199(2):469–73, 1994.

[56] H. Feldmann, V. E. Volchkov, V. A. Volchkova, U. Stroher, and H. D. Klenk. Biosynthesis and role of filoviral glycoproteins. *J Gen Virol*, 82(Pt 12):2839–48, 2001.

[57] S. Finke and K. K. Conzelmann. Dissociation of rabies virus matrix protein functions in regulation of viral rna synthesis and virus assembly. *J Virol*, 77(22):12074–82, 2003.

[58] S. Finke, R. Mueller-Waldeck, and K. K. Conzelmann. Rabies virus matrix protein regulates the balance of virus transcription and replication. *J Gen Virol*, 84(Pt 6):1613–21, 2003.

[59] S. P. Fisher-Hoch, G. S. Platt, G. H. Neild, T. Southee, A. Baskerville, R. T. Raymond, G. Lloyd, and D. I. Simpson. Pathophysiology of shock and hemorrhage in a fulminating viral infection (ebola). *J Infect Dis*, 152(5):887–94, 1985.

[60] K. Flick, J. W. Hooper, C. S. Schmaljohn, R. F. Pettersson, H. Feldmann, and R. Flick. Rescue of hantaan virus minigenomes. *Virology*, 306(2):219–24, 2003.

[61] R. Flick, K. Flick, H. Feldmann, and F. Elgh. Reverse genetics for crimean-congo hemorrhagic fever virus. *J Virol*, 77(10):5997–6006, 2003.

[62] P. Formenty, C. Boesch, M. Wyers, C. Steiner, F. Donati, F. Dind, F. Walker, and B. Le Guenno. Ebola virus outbreak among wild chimpanzees living in a rain forest of cote d'ivoire. *J Infect Dis*, 179 Suppl 1:S120–6, 1999.

[63] E. O. Freed. Mechanisms of enveloped virus release. *Virus Res*, 106(2):85–6, 2004.

[64] T. R. Fuerst, E. G. Niles, F. W. Studier, and B. Moss. Eukaryotic transient-expression system based on recombinant vaccinia virus that synthesizes bacteriophage t7 rna polymerase. *Proc Natl Acad Sci U S A*, 83(21):8122–6, 1986.

[65] W. R. Gallaher. Similar structural models of the transmembrane proteins of ebola and avian sarcoma viruses. *Cell*, 85(4):477–8, 1996.

[66] T. W. Geisbert, L. E. Hensley, T. R. Gibb, K. E. Steele, N. K. Jaax, and P. B. Jahrling. Apoptosis induced in vitro and in vivo during infection by ebola and marburg viruses. *Lab Invest*, 80(2):171–86, 2000.

[67] T. W. Geisbert, L. E. Hensley, P. B. Jahrling, T. Larsen, J. B. Geisbert, J. Paragas, H. A. Young, T. M. Fredeking, W. E. Rote, and G. P. Vlasuk. Treatment of ebola virus infection with a recombinant inhibitor of factor viia/tissue factor: a study in rhesus monkeys. *Lancet*, 362(9400):1953–8, 2003.

[68] T. W. Geisbert, L. E. Hensley, E. Kagan, E. Z. Yu, J. B. Geisbert, K. Daddario-DiCaprio, E. A. Fritz, P. B. Jahrling, K. McClintock, J. R. Phelps, A. C. Lee, A. Judge, L. B. Jeffs, and I. MacLachlan. Postexposure protection of guinea pigs against a lethal ebola virus challenge is conferred by rna interference. *J Infect Dis*, 193(12):1650–7, 2006.

[69] T. W. Geisbert, L. E. Hensley, T. Larsen, H. A. Young, D. S. Reed, J. B. Geisbert, D. P. Scott, E. Kagan, P. B. Jahrling, and K. J. Davis. Pathogenesis of ebola hemorrhagic fever in cynomolgus macaques: evidence that dendritic cells are early and sustained targets of infection. *Am J Pathol*, 163(6):2347–70, 2003.

[70] T. W. Geisbert and P. B. Jahrling. Differentiation of filoviruses by electron microscopy. *Virus Res*, 39(2-3):129–50, 1995.

[71] T. W. Geisbert and P. B. Jahrling. Exotic emerging viral diseases: progress and challenges. *Nat Med*, 10(12 Suppl):S110–21, 2004.

[72] T. W. Geisbert, P. Pushko, K. Anderson, J. Smith, K. J. Davis, and P. B. Jahrling. Evaluation in nonhuman primates of vaccines against ebola virus. *Emerg Infect Dis*, 8(5):503–7, 2002.

[73] T. W. Geisbert, H. A. Young, P. B. Jahrling, K. J. Davis, E. Kagan, and L. E. Hensley. Mechanisms underlying coagulation abnormalities in ebola hemorrhagic fever: overexpression of tissue factor in primate monocytes/macrophages is a key event. *J Infect Dis*, 188(11):1618–29, 2003.

[74] T. W. Geisbert, H. A. Young, P. B. Jahrling, K. J. Davis, T. Larsen, E. Kagan, and L. E. Hensley. Pathogenesis of ebola hemorrhagic fever in primate models: evidence that hemorrhage is not a direct effect of virus-induced cytolysis of endothelial cells. *Am J Pathol*, 163(6):2371–82, 2003.

[75] R. Ghildyal, C. Baulch-Brown, J. Mills, and J. Meanger. The matrix protein of human respiratory syncytial virus localises to the nucleus of infected cells and inhibits transcription. *Arch Virol*, 148(7):1419–29, 2003.

[76] F. X. Gomis-Ruth, A. Dessen, J. Timmins, A. Bracher, L. Kolesnikowa, S. Becker, H. D. Klenk, and W. Weissenhorn. The matrix protein vp40 from ebola virus octamerizes into pore-like structures with specific rna binding properties. *Structure (Camb)*, 11(4):423–33, 2003.

[77] A. Groseth, H. Feldmann, S. Theriault, G. Mehmetoglu, and R. Flick. Rna polymerase i-driven minigenome system for ebola viruses. *J Virol*, 79(7):4425–33, 2005.

[78] A. Groseth, U. Stroher, S. Theriault, and H. Feldmann. Molecular characterization of an isolate from the 1989/90 epizootic of ebola virus reston among macaques imported into the united states. *Virus Res*, 87(2):155–63, 2002.

[79] A. Groseth, S. Theriault, R. Flick, and H. Feldmann. sirna strategies for the control of ebola virus infection. *In Abstracts of the 24th Annual Meeting of the American Society for Virology, University Park, PA*, page 74, 2005.

[80] N. Guex and M. C. Peitsch. Swiss-model and the swiss-pdbviewer: an environment for comparative protein modeling. *Electrophoresis*, 18(15):2714–23, 1997.

[81] M. Gupta, S. Mahanty, R. Ahmed, and P. E. Rollin. Monocyte-derived human macrophages and peripheral blood mononuclear cells infected with ebola virus secrete mip-1alpha and tnf-alpha and inhibit poly-ic-induced ifn-alpha in vitro. *Virology*, 284(1):20–5, 2001.

[82] P. J. Halfmann and Y. Kawaoka. Ebola vp24 inhibits type i interferon signaling. *In Abstracts of the XIII International Congress of Virology. American Society for Microbiology, Washington, DC*, page 81, 2005.

[83] O. Haller, G. Kochs, and F. Weber. The interferon response circuit: induction and suppression by pathogenic viruses. *Virology*, 344(1):119–30, 2006.

[84] Z. Han, H. Boshra, J. O. Sunyer, S. H. Zwiers, J. Paragas, and R. N. Harty. Biochemical and functional characterization of the ebola virus vp24 protein: implications for a role in virus assembly and budding. *J Virol*, 77(3):1793–800, 2003.

[85] Z. Han and R. N. Harty. Packaging of actin into ebola virus vlps. *Virol J*, 2:92, 2005.

[86] B. H. Harcourt, A. Sanchez, and M. K. Offermann. Ebola virus inhibits induction of genes by double-stranded rna in endothelial cells. *Virology*, 252(1):179–88, 1998.

[87] B. H. Harcourt, A. Sanchez, and M. K. Offermann. Ebola virus selectively inhibits responses to interferons, but not to interleukin-1beta, in endothelial cells. *J Virol*, 73(4):3491–6, 1999.

[88] B. Hartlieb, J. Modrof, E. Muhlberger, H. D. Klenk, and S. Becker. Oligomerization of ebola virus vp30 is essential for viral transcription and can be inhibited by a synthetic peptide. *J Biol Chem*, 278(43):41830–6, 2003.

[89] B. Hartlieb and W. Weissenhorn. Filovirus assembly and budding. *Virology*, 344(1):64–70, 2006.

[90] A. L. Hartman, J. S. Towner, and S. T. Nichol. A c-terminal basic amino acid motif of zaire ebolavirus vp35 is essential for type i interferon antagonism and displays high identity with the rna-binding domain of another interferon antagonist, the ns1 protein of influenza a virus. *Virology*, 328(2):177–84, 2004.

[91] R. N. Harty, M. E. Brown, G. Wang, J. Huibregtse, and F. P. Hayes. A ppxy motif within the vp40 protein of ebola virus interacts physically and functionally with a ubiquitin ligase: implications for filovirus budding. *Proc Natl Acad Sci U S A*, 97(25):13871–6, 2000.

[92] L. E. Hensley, S. M. Jones, H. Feldmann, P. B. Jahrling, and T. W. Geisbert. Ebola and marburg viruses: Pathogenesis and development of countermeasures. *Curr Mol Med*, 5:777–788, 2005.

[93] L. E. Hensley, H. A. Young, P. B. Jahrling, and T. W. Geisbert. Proinflammatory response during ebola virus infection of primate models: possible involvement of the tumor necrosis factor receptor superfamily. *Immunol Lett*, 80(3):169–79, 2002.

[94] T. Hoenen, A. Groseth, D. Falzarano, and H. Feldmann. Ebola virus: unravelling pathogenesis to combat a deadly disease. *Trends Mol Med*, 12(5):206–15, 2006.

[95] T. Hoenen, A. Groseth, L. Kolesnikova, S. Theriault, H. Ebihara, B. Hartlieb, S. Bamberg, U. Stroher, H. Feldmann, and S. Becker. Infection of naive target cells with virus-like partices - implications for the function of ebola virus vp24. *J Virol*, 80(14):7260–4, 2006.

[96] T. Hoenen, V. Volchkov, L. Kolesnikova, E. Mittler, J. Timmins, M. Ottmann, O. Reynard, S. Becker, and W. Weissenhorn. Vp40 octamers are essential for ebola virus replication. *J Virol*, 79(3):1898–905, 2005.

[97] Y. Huang, L. Xu, Y. Sun, and G. J. Nabel. The assembly of ebola virus nucleocapsid requires virion-associated proteins 35 and 24 and posttranslational modification of nucleoprotein. *Mol Cell*, 10(2):307–16, 2002.

[98] G. M. Ignatyev. Immune response to filovirus infections. *Curr Top Microbiol Immunol*, 235:205–17, 1999.

[99] G. M. Ignatyev, V. Volchkov, V. M. Blinov, V. V. Samukov, A. P. Agafonov, M. A. Streltsova, and E. A. Kashentseva. Phenomenom of immunosuppression by filoviruses. *Inter J Immunorehabil*, 1 Suppl:138, 1994.

[100] H. Ito, S. Watanabe, A. Sanchez, M. A. Whitt, and Y. Kawaoka. Mutational analysis of the putative fusion domain of ebola virus glycoprotein. *J Virol*, 73(10):8907–12, 1999.

[101] H. Ito, S. Watanabe, A. Takada, and Y. Kawaoka. Ebola virus glycoprotein: proteolytic processing, acylation, cell tropism, and detection of neutralizing antibodies. *J Virol*, 75(3):1576–80, 2001.

[102] K. L. Jang, M. K. Collins, and D. S. Latchman. The human immunodeficiency virus tat protein increases the transcription of human alu repeated sequences by increasing the activity of the cellular transcription factor tfiiic. *J Acquir Immune Defic Syndr*, 5(11):1142–7, 1992.

[103] L. D. Jasenosky and Y. Kawaoka. Filovirus budding. *Virus Res*, 106(2):181–8, 2004.

[104] L. D. Jasenosky, G. Neumann, I. Lukashevich, and Y. Kawaoka. Ebola virus vp40-induced particle formation and association with the lipid bilayer. *J Virol*, 75(11):5205–14, 2001.

[105] H. R. Jayakar, E. Jeetendra, and M. A. Whitt. Rhabdovirus assembly and budding. *Virus Res*, 106(2):117–32, 2004.

[106] S. A. Jeffers, D. A. Sanders, and A. Sanchez. Covalent modifications of the ebola virus glycoprotein. *J Virol*, 76(24):12463–72, 2002.

[107] Z. Jezek, M. Y. Szczeniowski, J. J. Muyembe-Tamfum, J. B. McCormick, and D. L. Heymann. Ebola between outbreaks: intensified ebola hemorrhagic fever surveillance in the democratic republic of the congo, 1981-1985. *J Infect Dis*, 179 Suppl 1:S60–4, 1999.

[108] R. F. Johnson, S. E. McCarthy, P. J. Godlewski, and R. N. Harty. Ebola virus vp35-vp40 interaction is sufficient for packaging 3e-5e minigenome rna into virus-like particles. *J Virol*, 80(11):5135–44, 2006.

[109] S. M. Jones, H. Feldmann, U. Stroher, J. B. Geisbert, L. Fernando, A. Grolla, H. D. Klenk, N. J. Sullivan, V. E. Volchkov, E. A. Fritz, K. M. Daddario, L. E. Hensley, P. B. Jahrling, and T. W. Geisbert. Live attenuated recombinant vaccine protects nonhuman primates against ebola and marburg viruses. *Nat Med*, 11(7):786–90, 2005.

[110] M. P. Kiley, R. L. Regnery, and K. M. Johnson. Ebola virus: identification of virion structural proteins. *J Gen Virol*, 49(2):333–41, 1980.

[111] A. L. Kindzelskii, Z. Yang, G. J. Nabel, 3rd Todd, R. F., and H. R. Petty. Ebola virus secretory glycoprotein (sgp) diminishes fc gamma riiib-to-cr3 proximity on neutrophils. *J Immunol*, 164(2):953–8, 2000.

[112] L. Kolesnikova, S. Bamberg, B. Berghofer, and S. Becker. The matrix protein of marburg virus is transported to the plasma membrane along cellular membranes: exploiting the retrograde late endosomal pathway. *J Virol*, 78(5):2382–93, 2004.

[113] L. Kolesnikova and S. Becker. Virus maturation. *In H. D. Klenk, H. Feldmann (ed.), Ebola and Marburg viruses. Horizon Bioscience, Norfolk, U.K.*, pages 171–201, 2004.

[114] L. Kolesnikova, B. Berghofer, S. Bamberg, and S. Becker. Multivesicular bodies as a platform for formation of the marburg virus envelope. *J Virol*, 78(22):12277–87, 2004.

[115] I. Kraus, E. Bogner, H. Lilie, M. Eickmann, and W. Garten. Oligomerization and assembly of the matrix protein of borna disease virus. *FEBS Lett*, 579(12):2686–92, 2005.

[116] D. W. Landry and J. A. Oliver. The pathogenesis of vasodilatory shock. *N Engl J Med*, 345(8):588–95, 2001.

[117] J. W. Lee and S. K. Lee. Mammalian two-hybrid assay for detecting protein-protein interactions in vivo. *Methods Mol Biol*, 261:327–36, 2004.

[118] K. J. Lee, M. Perez, D. D. Pinschewer, and J. C. de la Torre. Identification of the lymphocytic choriomeningitis virus (lcmv) proteins required to rescue lcmv rna analogs into lcmv-like particles. *J Virol*, 76(12):6393–7, 2002.

[119] E. M. Leroy, S. Baize, V. E. Volchkov, S. P. Fisher-Hoch, M. C. Georges-Courbot, J. Lansoud-Soukate, M. Capron, P. Debre, J. B. McCormick, and A. J. Georges. Human asymptomatic ebola infection and strong inflammatory response. *Lancet*, 355(9222):2210–5, 2000.

[120] M. Levi. Current understanding of disseminated intravascular coagulation. *Br J Haematol*, 124(5):567–76, 2004.

[121] J. M. Licata, R. F. Johnson, Z. Han, and R. N. Harty. Contribution of ebola virus glycoprotein, nucleoprotein, and vp24 to budding of vp40 virus-like particles. *J Virol*, 78(14):7344–51, 2004.

[122] J. M. Licata, M. Simpson-Holley, N. T. Wright, Z. Han, J. Paragas, and R. N. Harty. Overlapping motifs (ptap and ppey) within the ebola virus vp40 protein function independently as late budding domains: involvement of host proteins tsg101 and vps-4. *J Virol*, 77(3):1812–9, 2003.

[123] A. Lucht, R. Grunow, P. Moller, H. Feldmann, and S. Becker. Development, characterization and use of monoclonal vp40-antibodies for the detection of ebola virus. *J Virol Methods*, 111(1):21–8, 2003.

[124] W. Luytjes, M. Krystal, M. Enami, J. D. Pavin, and P. Palese. Amplification, expression, and packaging of foreign gene by influenza virus. *Cell*, 59(6):1107–13, 1989.

[125] D. S. Lyles. Cytopathogenesis and inhibition of host gene expression by rna viruses. *Microbiol Mol Biol Rev*, 64(4):709–24, 2000.

[126] D. S. Lyles, M. O. McKenzie, M. Ahmed, and S. C. Woolwine. Potency of wild-type and temperature-sensitive vesicular stomatitis virus matrix protein in the inhibition of host-directed gene expression. *Virology*, 225(1):172–80, 1996.

[127] S. Mahanty and M. Bray. Pathogenesis of filoviral haemorrhagic fevers. *Lancet Infect Dis*, 4(8):487–98, 2004.

[128] S. Mahanty, K. Hutchinson, S. Agarwal, M. McRae, P. E. Rollin, and B. Pulendran. Cutting edge: impairment of dendritic cells and adaptive immunity by ebola and lassa viruses. *J Immunol*, 170(6):2797–801, 2003.

[129] B. Manicassamy, J. Wang, H. Jiang, and L. Rong. Comprehensive analysis of ebola virus gp1 in viral entry. *J Virol*, 79(8):4793–805, 2005.

[130] J. Martin-Serrano, T. Zang, and P. D. Bieniasz. Hiv-1 and ebola virus encode small peptide motifs that recruit tsg101 to sites of particle assembly to facilitate egress. *Nat Med*, 7(12):1313–9, 2001.

[131] M. Mavrakis, L. Kolesnikova, G. Schoehn, S. Becker, and R. W. Ruigrok. Morphology of marburg virus np-rna. *Virology*, 296(2):300–7, 2002.

[132] S. E. McCarthy, J. M. Licata, and R. N. Harty. A luciferase-based budding assay for ebola virus. *J Virol Methods*, 2006.

[133] J. Modrof, S. Becker, and E. Muhlberger. Ebola virus transcription activator vp30 is a zinc-binding protein. *J Virol*, 77(5):3334–8, 2003.

[134] J. Modrof, E. Muhlberger, H. D. Klenk, and S. Becker. Phosphorylation of vp30 impairs ebola virus transcription. *J Biol Chem*, 277(36):33099–104, 2002.

[135] P. Moller, N. Pariente, H. D. Klenk, and S. Becker. Homo-oligomerization of marburgvirus vp35 is essential for its function in replication and transcription. *J Virol*, 79(23):14876–86, 2005.

[136] E. Muhlberger. Genome organization, replication, and transcription of filoviruses. *In H. D. Klenk, H. Feldmann (ed.), Ebola and Marburg viruses. Horizon Bioscience, Norfolk, U.K.*, pages 1–26, 2004.

[137] E. Muhlberger, B. Lotfering, H. D. Klenk, and S. Becker. Three of the four nucleocapsid proteins of marburg virus, np, vp35, and l, are sufficient to mediate replication and transcription of marburg virus-specific monocistronic minigenomes. *J Virol*, 72(11):8756–64, 1998.

[138] E. Muhlberger, A. Sanchez, A. Randolf, C. Will, M. P. Kiley, H. D. Klenk, and H. Feldmann. The nucleotide sequence of the l gene of marburg virus, a filovirus: homologies with paramyxoviruses and rhabdoviruses. *Virology*, 187(2):534–47, 1992.

[139] E. Muhlberger, M. Weik, V. E. Volchkov, H. D. Klenk, and S. Becker. Comparison of the transcription and replication strategies of marburg virus and ebola virus by using artificial replication systems. *J Virol*, 73(3):2333–42, 1999.

[140] K. B. Mullis and F. A. Faloona. Specific synthesis of dna in vitro via a polymerase-catalyzed chain reaction. *Methods Enzymol*, 155:335–50, 1987.

[141] P. P. Nawroth and D. M. Stern. Modulation of endothelial cell hemostatic properties by tumor necrosis factor. *J Exp Med*, 163(3):740–5, 1986.

[142] G. Neumann, H. Ebihara, A. Takada, T. Noda, D. Kobasa, L. D. Jasenosky, S. Watanabe, J. H. Kim, H. Feldmann, and Y. Kawaoka. Ebola virus vp40 late domains are not essential for viral replication in cell culture. *J Virol*, 79(16):10300–7, 2005.

[143] G. Neumann, H. Feldmann, S. Watanabe, I. Lukashevich, and Y. Kawaoka. Reverse genetics demonstrates that proteolytic processing of the ebola virus glycoprotein is not essential for replication in cell culture. *J Virol*, 76(1):406–10, 2002.

[144] G. Neumann, T. Watanabe, and Y. Kawaoka. Plasmid-driven formation of influenza virus-like particles. *J Virol*, 74(1):547–51, 2000.

[145] G. Neumann, M. A. Whitt, and Y. Kawaoka. A decade after the generation of a negative-sense rna virus from cloned cdna - what have we learned? *J Gen Virol*, 83(Pt 11):2635–62, 2002.

[146] T. L. Nguyen, G. Schoehn, W. Weissenhorn, A. R. Hermone, J. C. Burnett, R. G. Panchal, C. McGrath, D. W. Zaharevitz, M. J. Aman, R. Gussio, and S. Bavari. An all-atom model of the pore-like structure of hexameric vp40 from ebola: Structural insights into the monomer-hexamer transition. *J Struct Biol*, 2005.

[147] T. Noda, K. Aoyama, H. Sagara, H. Kida, and Y. Kawaoka. Nucleocapsid-like structures of ebola virus reconstructed using electron tomography. *J Vet Med Sci*, 67(3):325–8, 2005.

[148] T. Noda, H. Sagara, E. Suzuki, A. Takada, H. Kida, and Y. Kawaoka. Ebola virus vp40 drives the formation of virus-like filamentous particles along with gp. *J Virol*, 76(10):4855–65, 2002.

[149] A. Overby and R. F. Pettersson. Analysis of bunyaviral ribonucleotide packaging with the help of virus-like particles. *In Abstracts of the XIII International Conference on Negative Strand Viruses, Salamanca, Spain*, page 64, 2006.

[150] A. K. Pattnaik, L. A. Ball, A. W. LeGrone, and G. W. Wertz. Infectious defective interfering particles of vsv from transcripts of a cdna clone. *Cell*, 69(6):1011–20, 1992.

[151] M. Perez and J. C. de la Torre. Identification of the borna disease virus (bdv) proteins required for the formation of bdv-like particles. *J Gen Virol*, 86(Pt 7):1891–5, 2005.

[152] L. C. Platanias. The p38 mitogen-activated protein kinase pathway and its role in interferon signaling. *Pharmacol Ther*, 98(2):129–42, 2003.

[153] O. Poch, B. M. Blumberg, L. Bougueleret, and N. Tordo. Sequence comparison of five polymerases (l proteins) of unsegmented negative-strand rna viruses: theoretical assignment of functional domains. *J Gen Virol*, 71 (Pt 5):1153–62, 1990.

[154] X. Pourrut, B. Kumulungui, T. Wittmann, G. Moussavou, A. Delicat, P. Yaba, D. Nkoghe, J. P. Gonzalez, and E. M. Leroy. The natural history of ebola virus in africa. *Microbes Infect*, 7(7-8):1005–14, 2005.

[155] V. R. Racaniello and D. Baltimore. Cloned poliovirus complementary dna is infectious in mammalian cells. *Science*, 214(4523):916–9, 1981.

[156] D. S. Reed, L. E. Hensley, J. B. Geisbert, P. B. Jahrling, and T. W. Geisbert. Depletion of peripheral blood t lymphocytes and nk cells during the course of ebola hemorrhagic fever in cynomolgus macaques. *Viral Immunol*, 17(3):390–400, 2004.

[157] R. L. Regnery, K. M. Johnson, and M. P. Kiley. Virion nucleic acid of ebola virus. *J Virol*, 36(2):465–9, 1980.

[158] S. P. Reid, W. B. Cardenas, and C. F. Basler. Homo-oligomerization facilitates the interferon-antagonist activity of the ebolavirus vp35 protein. *Virology*, 341(2):179–89, 2005.

[159] S. P. Reid, L. W. Leung, A. L. Hartman, O. Martinez, M. L. Shaw, C. Carbonnelle, V. E. Volchkov, S. T. Nichol, and C. F. Basler. Ebola virus vp24 binds karyopherin alpha1 and blocks stat1 nuclear accumulation. *J Virol*, 80(11):5156–67, 2006.

[160] L. L. Rodriguez, A. De Roo, Y. Guimard, S. G. Trappier, A. Sanchez, D. Bressler, A. J. Williams, A. K. Rowe, J. Bertolli, A. S. Khan, T. G. Ksiazek, C. J. Peters, and S. T. Nichol. Persistence and genetic stability of ebola virus during the outbreak in kikwit, democratic republic of the congo, 1995. *J Infect Dis*, 179 Suppl 1:S170–6, 1999.

[161] T. H. Roels, A. S. Bloom, J. Buffington, G. L. Muhungu, W. R. Mac Kenzie, A. S. Khan, R. Ndambi, D. L. Noah, H. R. Rolka, C. J. Peters, and T. G. Ksiazek. Ebola hemorrhagic fever, kikwit, democratic republic of the congo, 1995: risk factors for patients without a reported exposure. *J Infect Dis*, 179 Suppl 1:S92–7, 1999.

[162] R. W. Ruigrok, G. Schoehn, A. Dessen, E. Forest, V. Volchkov, O. Dolnik, H. D. Klenk, and W. Weissenhorn. Structural characterization and membrane binding properties of the matrix protein vp40 of ebola virus. *J Mol Biol*, 300(1):103–12, 2000.

[163] M. B. Ruiz-Arguello, F. M. Goni, F. B. Pereira, and J. L. Nieva. Phosphatidylinositol-dependent membrane fusion induced by a putative fusogenic sequence of ebola virus. *J Virol*, 72(3):1775–81, 1998.

[164] E. I. Ryabchikova, L. V. Kolesnikova, and S. V. Luchko. An analysis of features of pathogenesis in two animal models of ebola virus infection. *J Infect Dis*, 179 Suppl 1:S199–202, 1999.

[165] R. K. Saiki, S. Scharf, F. Faloona, K. B. Mullis, G. T. Horn, H. A. Erlich, and N. Arnheim. Enzymatic amplification of beta-globin genomic sequences and restriction site analysis for diagnosis of sickle cell anemia. *Science*, 230(4732):1350–4, 1985.

[166] A. Sanchez, A. S. Khan, S. R. Zaki, G. J. Nabel, T. G. Ksiazek, and C. J. Peters. Filoviridae - marburg and ebola viruses. *In D. Knipe, P. Howley (ed.), Fields Virology (4 ed.). Lippincott Williams and Wilkins, Philadelphia, PA*, 1:1279–304, 2001.

[167] A. Sanchez and M. P. Kiley. Identification and analysis of ebola virus messenger rna. *Virology*, 157(2):414–20, 1987.

[168] A. Sanchez, M. P. Kiley, B. P. Holloway, and D. D. Auperin. Sequence analysis of the ebola virus genome: organization, genetic elements, and comparison with the genome of marburg virus. *Virus Res*, 29(3):215–40, 1993.

[169] A. Sanchez, M. P. Kiley, B. P. Holloway, J. B. McCormick, and D. D. Auperin. The nucleoprotein gene of ebola virus: cloning, sequencing, and in vitro expression. *Virology*, 170(1):81–91, 1989.

[170] A. Sanchez, M. Lukwiya, D. Bausch, S. Mahanty, A. J. Sanchez, K. D. Wagoner, and P. E. Rollin. Analysis of human peripheral blood samples from fatal and nonfatal cases of ebola (sudan) hemorrhagic fever: cellular responses, virus load, and nitric oxide levels. *J Virol*, 78(19):10370–7, 2004.

[171] A. Sanchez, S. G. Trappier, B. W. Mahy, C. J. Peters, and S. T. Nichol. The virion glycoproteins of ebola viruses are encoded in two reading frames and are expressed through transcriptional editing. *Proc Natl Acad Sci U S A*, 93(8):3602–7, 1996.

[172] A. Sanchez, Z. Y. Yang, L. Xu, G. J. Nabel, T. Crews, and C. J. Peters. Biochemical analysis of the secreted and virion glycoproteins of ebola virus. *J Virol*, 72(8):6442–7, 1998.

[173] A. P. Schmitt and R. A. Lamb. Escaping from the cell: assembly and budding of negative-strand rna viruses. *Curr Top Microbiol Immunol*, 283:145–96, 2004.

[174] M. J. Schnell, T. Mebatsion, and K. K. Conzelmann. Infectious rabies viruses from cloned cdna. *Embo J*, 13(18):4195–203, 1994.

[175] H. J. Schnittler and H. Feldmann. Marburg and ebola hemorrhagic fevers: does the primary course of infection depend on the accessibility of organ-specific macrophages? *Clin Infect Dis*, 27(2):404–6, 1998.

[176] H. J. Schnittler and H. Feldmann. Viral hemorrhagic fever–a vascular disease? *Thromb Haemost*, 89(6):967–72, 2003.

[177] H. J. Schnittler, U. Stroher, T. A. Afanasieva, and H. Feldmann. The role of endothelial cells in filovirus hemorrhagic fever. *In H. D. Klenk, H. Feldmann (ed.), Ebola and Marburg viruses. Horizon Bioscience, Norfolk, U.K.*, pages 279–303, 2004.

[178] K. Schornberg, S. Matsuyama, K. Kabsch, S. Delos, A. Bouton, and J. White. Role of endosomal cathepsins in entry mediated by the ebola virus glycoprotein. *J Virol*, 80(8):4174–8, 2006.

[179] S. Scianimanico, G. Schoehn, J. Timmins, R. H. Ruigrok, H. D. Klenk, and W. Weissenhorn. Membrane association induces a conformational change in the ebola virus matrix protein. *Embo J*, 19(24):6732–41, 2000.

[180] S. B. Sieczkarski and G. R. Whittaker. Viral entry. *Curr Top Microbiol Immunol*, 285:1–23, 2005.

[181] G. Simmons, R. J. Wool-Lewis, F. Baribaud, R. C. Netter, and P. Bates. Ebola virus glycoproteins induce global surface protein down-modulation and loss of cell adherence. *J Virol*, 76(5):2518–28, 2002.

[182] E. A. Stillman, J. K. Rose, and M. A. Whitt. Replication and amplification of novel vesicular stomatitis virus minigenomes encoding viral structural proteins. *J Virol*, 69(5):2946–53, 1995.

[183] U. Stroher, A. Vaillant, J. M. Juteau, S. Jones, and H. Feldmann. Degenerate phosphorthioate oligodeoxynucleotides as potent antivirals for filoviruses and arenaviruses. *In Abstracts of the XIII International Congress of Virology. American Society for Microbiology, Washington, DC*, page 109, 2005.

[184] U. Stroher, E. West, H. Bugany, H. D. Klenk, H. J. Schnittler, and H. Feldmann. Infection and activation of monocytes by marburg and ebola viruses. *J Virol*, 75(22):11025–33, 2001.

[185] N. J. Sullivan, T. W. Geisbert, J. B. Geisbert, L. Xu, Z. Y. Yang, M. Roederer, R. A. Koup, P. B. Jahrling, and G. J. Nabel. Accelerated vaccination for ebola virus haemorrhagic fever in non-human primates. *Nature*, 424(6949):681–4, 2003.

[186] N. J. Sullivan, A. Sanchez, P. E. Rollin, Z. Y. Yang, and G. J. Nabel. Development of a preventive vaccine for ebola virus infection in primates. *Nature*, 408(6812):605–9, 2000.

[187] P. H. Sureau. Firsthand clinical observations of hemorrhagic manifestations in ebola hemorrhagic fever in zaire. *Rev Infect Dis*, 11 Suppl 4:S790–3, 1989.

[188] R. Swanepoel, P. A. Leman, F. J. Burt, N. A. Zachariades, L. E. Braack, T. G. Ksiazek, P. E. Rollin, S. R. Zaki, and C. J. Peters. Experimental inoculation of plants and animals with ebola virus. *Emerg Infect Dis*, 2(4):321–5, 1996.

[189] A. Takada, K. Fujioka, M. Tsuiji, A. Morikawa, N. Higashi, H. Ebihara, D. Kobasa, H. Feldmann, T. Irimura, and Y. Kawaoka. Human macrophage c-type lectin specific for galactose and n-acetylgalactosamine promotes filovirus entry. *J Virol*, 78(6):2943–7, 2004.

[190] A. Takada, C. Robison, H. Goto, A. Sanchez, K. G. Murti, M. A. Whitt, and Y. Kawaoka. A system for functional analysis of ebola virus glycoprotein. *Proc Natl Acad Sci U S A*, 94(26):14764–9, 1997.

[191] S. Theriault, A. Groseth, G. Neumann, Y. Kawaoka, and H. Feldmann. Rescue of ebola virus from cdna using heterologous support proteins. *Virus Res*, 106(1):43–50, 2004.

[192] J. Timmins, G. Schoehn, C. Kohlhaas, H. D. Klenk, R. W. Ruigrok, and W. Weissenhorn. Oligomerization and polymerization of the filovirus matrix protein vp40. *Virology*, 312(2):359–68, 2003.

[193] J. Timmins, G. Schoehn, S. Ricard-Blum, S. Scianimanico, T. Vernet, R. W. Ruigrok, and W. Weissenhorn. Ebola virus matrix protein vp40 interaction with human cellular factors tsg101 and nedd4. *J Mol Biol*, 326(2):493–502, 2003.

[194] J. Timmins, S. Scianimanico, G. Schoehn, and W. Weissenhorn. Vesicular release of ebola virus matrix protein vp40. *Virology*, 283(1):1–6, 2001.

[195] M. F. Tosi. Innate immune responses to infection. *J Allergy Clin Immunol*, 116(2):241–9; quiz 250, 2005.

[196] J. S. Towner, J. Paragas, J. E. Dover, M. Gupta, C. S. Goldsmith, J. W. Huggins, and S. T. Nichol. Generation of egfp expressing recombinant zaire ebolavirus for analysis of early pathogenesis events and high-throughput antiviral drug screening. *Virology*, 332(1):20–7, 2005.

[197] J. S. Towner, P. E. Rollin, D. G. Bausch, A. Sanchez, S. M. Crary, M. Vincent, W. F. Lee, C. F. Spiropoulou, T. G. Ksiazek, M. Lukwiya, F. Kaducu, R. Downing, and S. T. Nichol. Rapid diagnosis of ebola hemorrhagic fever by reverse transcription-pcr in an outbreak setting and assessment of patient viral load as a predictor of outcome. *J Virol*, 78(8):4330–41, 2004.

[198] F. Villinger, P. E. Rollin, S. S. Brar, N. F. Chikkala, J. Winter, J. B. Sundstrom, S. R. Zaki, R. Swanepoel, A. A. Ansari, and C. J. Peters. Markedly elevated levels of interferon (ifn)-gamma, ifn-alpha, interleukin (il)-2, il-10, and tumor necrosis factor-alpha associated with fatal ebola virus infection. *J Infect Dis*, 179 Suppl 1:S188–91, 1999.

[199] V. E. Volchkov, S. Becker, V. A. Volchkova, V. A. Ternovoj, A. N. Kotov, S. V. Netesov, and H. D. Klenk. Gp mrna of ebola virus is edited by the ebola virus polymerase and by t7 and vaccinia virus polymerases. *Virology*, 214(2):421–30, 1995.

[200] V. E. Volchkov, V. M. Blinov, and S. V. Netesov. The envelope glycoprotein of ebola virus contains an immunosuppressive-like domain similar to oncogenic retroviruses. *FEBS Lett*, 305(3):181–4, 1992.

[201] V. E. Volchkov, A. A. Chepurnov, V. A. Volchkova, V. A. Ternovoj, and H. D. Klenk. Molecular characterization of guinea pig-adapted variants of ebola virus. *Virology*, 277(1):147–55, 2000.

[202] V. E. Volchkov, H. Feldmann, V. A. Volchkova, and H. D. Klenk. Processing of the ebola virus glycoprotein by the proprotein convertase furin. *Proc Natl Acad Sci U S A*, 95(10):5762–7, 1998.

[203] V. E. Volchkov, V. A. Volchkova, A. A. Chepurnov, V. M. Blinov, O. Dolnik, S. V. Netesov, and H. Feldmann. Characterization of the l gene and 5' trailer region of ebola virus. *J Gen Virol*, 80 (Pt 2):355–62, 1999.

[204] V. E. Volchkov, V. A. Volchkova, E. Muhlberger, L. V. Kolesnikova, M. Weik, O. Dolnik, and H. D. Klenk. Recovery of infectious ebola virus from complementary dna: Rna editing of the gp gene and viral cytotoxicity. *Science*, 291(5510):1965–9, 2001.

[205] V. E. Volchkov, V. A. Volchkova, W. Slenczka, H. D. Klenk, and H. Feldmann. Release of viral glycoproteins during ebola virus infection. *Virology*, 245(1):110–9, 1998.

[206] V. A. Volchkova, H. Feldmann, H. D. Klenk, and V. E. Volchkov. The nonstructural small glycoprotein sgp of ebola virus is secreted as an antiparallel-orientated homodimer. *Virology*, 250(2):408–14, 1998.

[207] E. Wagner, O. G. Engelhardt, F. Weber, O. Haller, and G. Kochs. Formation of virus-like particles from cloned cdnas of thogoto virus. *J Gen Virol*, 81(Pt 12):2849–53, 2000.

[208] V. Wahl-Jensen, S. K. Kurz, P. R. Hazelton, H. J. Schnittler, U. Stroher, D. R. Burton, and H. Feldmann. Role of ebola virus secreted glycoproteins and virus-like particles in activation of human macrophages. *J Virol*, 79(4):2413–9, 2005.

[209] V. M. Wahl-Jensen, T. A. Afanasieva, J. Seebach, U. Stroher, H. Feldmann, and H. J. Schnittler. Effects of ebola virus glycoproteins on endothelial cell activation and barrier function. *J Virol*, 79(16):10442–10450, 2005.

[210] K. L. Warfield, D. L. Swenson, G. Demmin, and S. Bavari. Filovirus-like particles as vaccines and discovery tools. *Expert Rev Vaccines*, 4(3):429–40, 2005.

[211] S. Watanabe, T. Noda, and Y. Kawaoka. Functional mapping of the nucleoprotein of ebola virus. *J Virol*, 80(8):3743–51, 2006.

[212] S. Watanabe, T. Watanabe, T. Noda, A. Takada, H. Feldmann, L. D. Jasenosky, and Y. Kawaoka. Production of novel ebola virus-like particles from cdnas: an alternative to ebola virus generation by reverse genetics. *J Virol*, 78(2):999–1005, 2004.

[213] M. Weik, J. Modrof, H. D. Klenk, S. Becker, and E. Muhlberger. Ebola virus vp30-mediated transcription is regulated by rna secondary structure formation. *J Virol*, 76(17):8532–9, 2002.

[214] W. Weissenhorn, A. Carfi, K. H. Lee, J. J. Skehel, and D. C. Wiley. Crystal structure of the ebola virus membrane fusion subunit, gp2, from the envelope glycoprotein ectodomain. *Mol Cell*, 2(5):605–16, 1998.

[215] W. Weissenhorn, A. Dessen, L. J. Calder, S. C. Harrison, J. J. Skehel, and D. C. Wiley. Structural basis for membrane fusion by enveloped viruses. *Mol Membr Biol*, 16(1):3–9, 1999.

[216] S. P. Whelan, J. N. Barr, and G. W. Wertz. Transcription and replication of nonsegmented negative-strand rna viruses. *Curr Top Microbiol Immunol*, 283:61–119, 2004.

[217] T. Wilson and J. Lenard. Interaction of wild-type and mutant m protein vesicular stomatitis virus with nucleocapsids in vitro. *Biochemistry*, 20(5):1349–54, 1981.

[218] J. Wong, J. Zhang, G. Gao, M. Esfandiarei, X. Si, Y. Wang, B. Yanagawa, A. Suarez, B. McManus, and H. Luo. Liposome-mediated transient transfection reduces cholesterol-dependent coxsackievirus infectivity. *J Virol Methods*, 133(2):211–8, 2006.

[219] R. J. Wool-Lewis and P. Bates. Characterization of ebola virus entry by using pseudotyped viruses: identification of receptor-deficient cell lines. *J Virol*, 72(4):3155–60, 1998.

[220] D. Xu, C. J. Tsai, and R. Nussinov. Hydrogen bonds and salt bridges across protein-protein interfaces. *Protein Eng*, 10(9):999–1012, 1997.

[221] Z. Yang, R. Delgado, L. Xu, R. F. Todd, E. G. Nabel, A. Sanchez, and G. J. Nabel. Distinct cellular interactions of secreted and transmembrane ebola virus glycoproteins. *Science*, 279(5353):1034–7, 1998.

[222] Z. Y. Yang, H. J. Duckers, N. J. Sullivan, A. Sanchez, E. G. Nabel, and G. J. Nabel. Identification of the ebola virus glycoprotein as the main viral determinant of vascular cell cytotoxicity and injury. *Nat Med*, 6(8):886–9, 2000.

[223] J. Yasuda, M. Nakao, Y. Kawaoka, and H. Shida. Nedd4 regulates egress of ebola virus-like particles from host cells. *J Virol*, 77(18):9987–92, 2003.

[224] S. R. Zaki, W. J. Shieh, P. W. Greer, C. S. Goldsmith, T. Ferebee, J. Katshitshi, F. K. Tshioko, M. A. Bwaka, R. Swanepoel, P. Calain, A. S. Khan, E. Lloyd, P. E. Rollin, T. G. Ksiazek, and C. J. Peters. A novel immunohistochemical assay for the detection of ebola virus in skin: implications for diagnosis, spread, and surveillance of ebola hemorrhagic fever. commission de lutte contre les epidemies a kikwit. *J Infect Dis*, 179 Suppl 1:S36–47, 1999.

[225] X. Zhang and F. W. Studier. Mechanism of inhibition of bacteriophage t7 rna polymerase by t7 lysozyme. *J Mol Biol*, 269(1):10–27, 1997.

[226] Y. Zhuang, B. Butler, E. Hawkins, A. Paguio, L. Orr, M. G. Wood, and K. V. Wood. A new age of enlightenment. *Promega Notes*, 79:6–11, 2001.

A Materials

A.1 Media, solutions and reagents for cell culture

CMC	Sigma (#C4888-500MG)
Dulbecco's modified Eagle's medium	Sigma (#D4796)
EMEM	Invitrogen (#11430-030)
Fetal bovine serum	Wisent Inc. (#080550) heat inactivated @ 50°C for 30 minutes
Fugene	Roche (#11814443001)
Ficoll-paque plus	Amersham (#17-1440-03)
Genticin	Invitrogen (#10131-027)
Glutamine	Invitrogen (#25030-081)
Human AB serum	Sigma-Aldrich (#H4522) heat inactivated @ 56°C for 30 minutes
non-essential amino acids	Invitrogen (#11140-050)
OptiMEM	Invitrogen (#31985-070)
Penicillin / Streptomycin	Invitrogen (#15140-122)
Poly-D-lysine hydrobromide	Sigma-Aldrich (#P6407-5MG)
RPMI 1640	Invitrogen (#11875-093)
Trypsin / EDTA	Invitrogen (#25200-056)
$DMEM_{10\%FBS}$	500 ml Dulbecco's modified Eagle's medium 50 ml Fetal Bovine Serum 5 ml Glutamine 5 ml Penicillin / Streptomycin
$DMEM_{0\%FBS}$	500 ml Dulbecco's modified Eagle's medium 5 ml Glutamine 5 ml Penicillin / Streptomycin
$DMEM_{5\%FBS}$	50 ml $DMEM_{10\%FBS}$ 50 ml $DMEM_{0\%FBS}$
$DMEM_{2\%FBS}$	20 ml $DMEM_{10\%FBS}$ 80 ml $DMEM_{0\%FBS}$
2 × EMEM	200 ml EMEM 20 ml Glutamine 20 ml non-essential amino acids 100 ml Fetal Bovine Serum ad 1 l dH_2O filter sterilize before use
PBS	8 g NaCl 200 mg KCl 1.4 g Na_2 HPO_4 240 mg KH_2 PO_4 add dH_2O ad 1 l

3% CMC	900 ml dH_2O in a 4l beaker stir at $\sim$ 700 RPM, heat to 50 to 60°C add 30 g CMC in very small amounts add dH_2O ad 1 l autoclave

A.2 Other buffers and solutions

Blocking $Buffer_{IFA}$	5 % Glycerol 2 % Bovine serum albumin 0.2 % Tween20 0.05 % Sodium acide in PBS
6 × DNA sample loading buffer	250 mg Bromophenol blue 40 g Saccharose PBS ad 100 ml
LB medium	20 g LB Broth Lennox powder ad 1 l dH_2O autoclave before use
Lysis buffer	1 mM EDTA 1 % Triton X-100 3 % BSA 1 % Protease inhibitor cocktail
4 × $sample\ buffer_{2\%\ SDS}$	20 ml Glycerol 10 ml 2-Mercaptoethanol 1 g SDS 10 ml 1M Tris-HCl pH 6.8 100 mg Bromophenol blue ad 50 ml dH_2O
4 × $sample\ buffer_{0.5\%\ SDS}$	20 ml Glycerol 10 ml 2-Mercaptoethanol 250 mg SDS 10 ml 1M Tris-HCl pH 6.8 100 mg Bromophenol blue ad 50 ml dH_2O
10 × SDS-PAGE buffer	30.2 g Trizma base 144.13 g Glycine 900 ml dH_2O 100 ml 10% SDS solution filter sterilize before use
50 × TAE buffer	242 g Trizma base 72 ml glacial acetic acid 100 ml 0.5M EDTA pH 8.0 900 ml dH_2O filter sterilize before use

TBS buffer	50 mM Tris-HCl, pH 7.4 150 mM NaCl in dH_2O
TNE buffer	10 mM Tris-HCl, pH 7.4 1 mM EDTA 150 mM NaCl autoclave before use
Transfer buffer	6.05 g Tris base 28.5 Glycine 400 ml Methanol ad 2 l dH_2O
TSS buffer	85 ml LB medium 10 g PEG-8000 5 ml DMSO 1g $MgCl_2$ ad 100 ml dH_2O filter sterilize before use

A.3 Materials for cell culture

0.4 cm gap cuvette	Biorad (#165-2088)
12x75 mm culture tubes	VWR International (#60818-565)
6 well plates	Costar (#3516)
12 well plates	Costar (#3513)
24 well plates	Costar (#3524)
Primaria 10 cm culture dishes	Falcon (#353803)
Primaria 6 well plates	BD Biosciences (#352846)
T25 flasks	Costar (#3056)
T75 flasks	Costar (#3376)
Cell freezing module	Nalgene (#5100-0001)
Vacutainer (Sodium Heparin)	BD Biosciences (#366480)

A.4 Chemicals

Acetic acid, glacial	Fisher (#BP1185-500)
40% Acrylamide	Biorad (#161-0148)
Agarose	Invitrogen (#15510-027)
Ammonium persulfate	Sigma (#A3678-100G)
Deoxycholic acid	Sigma (#D2510-100G)
DMSO	Sigma (#D2650-100ML)

EDTA	Sigma (#E5134-1KG)
Ethidium bromide	Fisher (#BP1302-10)
Formalin	Fisher (#SF100-4)
Glycerol	Sigma (#G5516-100ML)
Glycin	Fisher (#G46-1)
Iodacetamide	Sigma-Aldrich (#I1149-25MG)
LB broth lennox powder	BD (#240230)
2-Mercaptoethanol	Sigma (#M7522-100ML)
Methanol	Fisher (#BP1105-4)
$MgCl_2$	Fisher (#BP214-500)
NaCl	Fisher (#S271-3)
Nonidet P40	Roche (#11754599001)
Nycodenz	Axis-Shield (#1002424)
Paraformaldehyde	Sigma (#P6148-500G)
PEG-8000	Sigma (#P5413-1KG)
SDS	Fisher (#BP166-500)
Skim milk powder	Safeway
Sucrose	Fisher (#B220-1)
TEMED	Sigma (#T9281-50ML)
Tris base	Fisher (#BP152-1)
Triton X-100	Sigma (#T8787-100ML)
Trizma	Sigma (#T1503-100ML)
Tween20	Fisher (#BP337-100)

A.5 Proteins and antibodies

2C4	kindly provided by Dr. Andreas Lucht
2E114	kindly provided by Dr. Andreas Lucht
α-REBOV-VP30	kindly provided by Dr. Allison Groseth
α-REBOV-VP35	kindly provided by Dr. Allison Groseth
α-VSV-GP	kindly provided by Dr. Steven Jones
Alexa goat α-mouse-488	Invitrogen (#A11001)
α-flag agarose	Sigma (#A2220-5ML)
α-goat HRP	Jackson Immunoresearch (#715-035-151)
α-mouse HRP	Jackson Immunoresearch (#715-035-147)
Bovine serum albumin	Sigma (#A3803-100G)
Proteinase K	Worthington (#LS004222)

A.6 Reporter assays

96 well plates white	Sigma Aldrich (#M4811)
Dual luciferase assay kit	Promega (#E1960)
Passive lysis buffer	Promega (#E1941)

A.7 Materials for proteinbiochemistry

Blotting paper (thick)	Biorad (#170-3932)
ECL plus western blotting detection system	GE Healthcare (#RPN2132)
Hyperfilm ECL 18x24cm	GE Healthcare (#RPN3103K)
Kapak sealpak pouch	VWR (#11214-338)
Parafilm	Americannat (#3465576999)
Protease inhibitor cocktail	Sigma (#P8340)
PVDF membrane	GE Healthcare (#RPN303F)
SilverSNAP stain kit II	Pierce (#24612)
Ultra-clear centrifuge tubes	Beckmann (#344059)
sample buffer$_{2\%\ \mathrm{SDS}}$	

A.8 Materials for molecular biology

FastDigest restriction enzymes	Fermentas Life Sciences
High concentration T4 DNA ligase	Invitrogen (#15224-041)
HiSpeed plasmid maxi kit	Qiagen (#12663)
OneStep RT-PCR kit	Qiagen (#210212)
PfuUltra II fusion HS DNA polymerase	Stratagene (#600672)
QIAprep spin miniprep kit	Qiagen (#27106)
QIAquick gel extraction kit	Qiagen (#28706)
QIAquick PCR purification kit	Qiagen (#28106)
Restriction enzymes	New England Biolabs
Shrink alkaline phosphatase	Roche (#11758250001)
T4 DNA ligase	Invitrogen (#15224-025)
T4 polynucleotide kinase	New England Biolabs (#M0201S)

A.9 Equiqment

Axiover 200M microscope	Carl Zeiss Canada
DNA 120 speedvac	Thermo Savant
FACSCalibur flow cytometer	BD Biosciences
Feline 14 X-ray film processor	Fisher
Mikro 20 centrifuge	HettichLab
Mini-PROTEAN 3 system	Biorad (#165-3301)
Mini trans-blot cell	Biorad (#170-3935)
UV screen macro vue UV-25	Hoefer
Veritas luminometer	Turner Biosystems

A.10 Cell lines

Vero E6 cells	CSCHAH, Winnipeg
293DD cells	CSCHAH, Winnipeg
HUH7 cells	Department for Virology, Philipps University Marburg

A.11 Viruses

ZEBOV-GFP	[95]
REBOV	CSCHAH, Winnipeg
VSV-GFP	CSCHAH, Winnipeg

A.12 Computer software

DeepView 3.7 (SP5)	http://www.expasy.org/spdbv
Excel 2000	Microsoft
Flowjo 7.1.0	Tree Star
GraphPad InStat 3.06	GraphPad Software
Swiss-Model	http://swissmodel.expasy.org/SWISS-MODEL

A.13 Plasmids

The following plasmids were used in this PhD thesis. The integrity of each construct was confirmed by sequencing. For each plasmid either a reference, the source or the cloning

strategy is given. For the cloning strategy first the original plasmid is stated and then the operation performed on this plasmid using the following abbreviations:

c(x,y) z	cloning of a DNA-fragment into vector z using the enzymes x and y
dm(x,y)	deletional mutagenesis using primers x and y
dm2s(x,y,z)	type IIs deletional mutagenesis using primers x and y and enzyme z
hyb(x,y)	hybridization of primers x and y
sc(x,y) z	subcloning into vector z using the enzymes x and y
sdm(x,y)	site directed mutagenesis using primers x and y
pcr(x,y)	PCR-amplification using primers x and y
rt(x,y)	RT-PCR-amplification using primers x and y

#	Construct	Cloning Strategy / Reference
508	pTM1-ZEBOV-VP40-WT	see [96]
256	pTM1-ZEBOV-VP40-ΔN14	508 dm(1482,1483)
202	pTM1-ZEBOV-VP40-ΔN61	508 dm(1482,1485)
516	pTM1-ZEBOV-VP40-ΔN65	508 dm(1482,1486)
206	pTM1-ZEBOV-VP40-ΔC308	508 dm(1520,1522)
266	pTM1-ZEBOV-VP40-ΔC212	508 dm(1507,1522)
233	pTM1-ZEBOV-VP40-ΔC194	508 dm(1505,1522)
240	pTM1-ZEBOV-VP40-Δα01	508 dm(1484,1486)
308	pTM1-ZEBOV-VP40-Δα02	508 dm(1489,1490)
235	pTM1-ZEBOV-VP40-Δα03	508 dm(1495,1496)
236	pTM1-ZEBOV-VP40-Δα03L	508 dm(1495,1498)
245	pTM1-ZEBOV-VP40-Δα04	508 dm(1500,1502)
250	pTM1-ZEBOV-VP40-Δα0506	508 dm(1509,1511)
350	pTM1-ZEBOV-VP40-Δα07	508 dm(1513,1514)
223	pTM1-ZEBOV-VP40-Δβ0102	508 dm(1487,1488)
520	pTM1-ZEBOV-VP40-Δβ0304	508 dm(1491,1493)
419	pTM1-ZEBOV-VP40-Δβ06	508 dm(1503,1504)
211	pTM1-ZEBOV-VP40-Δβ0708	508 dm(1506,1508)
343	pTM1-ZEBOV-VP40-Δβ0910	508 dm(1510,1512)
209	pTM1-ZEBOV-VP40-Δβ11	508 dm(1515,1517)
332	pTM1-ZEBOV-VP40-Δβ12	508 dm(1518,1521)
346	pTM1-ZEBOV-VP40-ΔL1112	508 dm(1516,1519)
873	pTM1-ZEBOV-VP40-W95A	508 sdm(1267,1285)
939	pTM1-ZEBOV-VP40-W95A-E160A	873 sdm(1268,1286)
324	pTM1-ZEBOV-flag-VP40	875 pcr(1585,1588); c(EcoRI,XhoI) pTM1

#	Construct	Cloning Strategy / Reference
767	pTM1-ZEBOV-flag-VP40-E160A	324 sdm(1268,1286)
827	pTM1-ZEBOV-flag-VP40-W95A-E160A	767 sdm(1267,1285)
858	pTM1-ZEBOV-HA-VP40	875 pcr(1586,1588); c(EcoRI,XhoI) pTM1
929	pTM1-ZEBOV-HA-VP40-W95A	858 sdm(1267,1285)
936	pTM1-ZEBOV-HA-VP40-E160A	858 sdm(1268,1286)
932	pTM1-ZEBOV-HA-VP40-W95A-E160A	929 sdm(1268,1286)
875	pCAGGS-ZEBOV-VP40-WT	508 sc(EcoRI,XhoI) pCAGGS
353	pCAGGS-ZEBOV-VP40-ΔN14	256 sc(EcoRI,XhoI) pCAGGS
267	pCAGGS-ZEBOV-VP40-ΔN61	202 sc(EcoRI,XhoI) pCAGGS
563	pCAGGS-ZEBOV-VP40-ΔN65	516 sc(EcoRI,XhoI) pCAGGS
272	pCAGGS-ZEBOV-VP40-ΔC308	206 sc(EcoRI,XhoI) pCAGGS
360	pCAGGS-ZEBOV-VP40-ΔC212	266 sc(EcoRI,XhoI) pCAGGS
279	pCAGGS-ZEBOV-VP40-ΔC194	233 sc(EcoRI,XhoI) pCAGGS
364	pCAGGS-ZEBOV-VP40-Δα01	240 sc(EcoRI,XhoI) pCAGGS
334	pCAGGS-ZEBOV-VP40-Δα02	308 sc(EcoRI,XhoI) pCAGGS
281	pCAGGS-ZEBOV-VP40-Δα03	235 sc(EcoRI,XhoI) pCAGGS
283	pCAGGS-ZEBOV-VP40-Δα03L	236 sc(EcoRI,XhoI) pCAGGS
368	pCAGGS-ZEBOV-VP40-Δα04	245 sc(EcoRI,XhoI) pCAGGS
495	pCAGGS-ZEBOV-VP40-Δα0506	250 sc(EcoRI,XhoI) pCAGGS
501	pCAGGS-ZEBOV-VP40-Δα07	350 sc(EcoRI,XhoI) pCAGGS
277	pCAGGS-ZEBOV-VP40-Δβ0102	223 sc(EcoRI,XhoI) pCAGGS
566	pCAGGS-ZEBOV-VP40-Δβ0304	520 sc(EcoRI,XhoI) pCAGGS
463	pCAGGS-ZEBOV-VP40-Δβ06	419 sc(EcoRI,XhoI) pCAGGS
273	pCAGGS-ZEBOV-VP40-Δβ0708	211 sc(EcoRI,XhoI) pCAGGS
467	pCAGGS-ZEBOV-VP40-Δβ0910	343 sc(EcoRI,XhoI) pCAGGS
400	pCAGGS-ZEBOV-VP40-Δβ11	209 sc(EcoRI,XhoI) pCAGGS
491	pCAGGS-ZEBOV-VP40-Δβ12	332 sc(EcoRI,XhoI) pCAGGS
369	pCAGGS-ZEBOV-VP40-ΔL1112	346 sc(EcoRI,XhoI) pCAGGS
429	pCAGGS-ZEBOV-VP40-W95A	873 sc(EcoRI,XhoI) pCAGGS
430	pCAGGS-ZEBOV-VP40-E160A	508 sdm(1268,1286); sc(EcoRI,XhoI) pCAGGS
964	pCAGGS-ZEBOV-VP40-W95A-E160A	939 sc(EcoRI,XhoI) pCAGGS
876	pCAGGS-ZEBOV-VP40-R134A	508 sdm(1273,1274); sc(EcoRI,XhoI) pCAGGS
737	pCAGGS-ZEBOV-flag-VP40	324 sc(EcoRI,XhoI) pCAGGS

#	Construct	Cloning Strategy / Reference
911	pCAGGS-ZEBOV-flag-VP40-W95A	833 sc(EcoRI,XhoI) pCAGGS
444	pCAGGS-ZEBOV-flag-VP40-R134A	324 sdm(1273,1274); sc(EcoRI,XhoI) pCAGGS
900	pCAGGS-ZEBOV-flag-VP40-E160A	767 sc(EcoRI,XhoI) pCAGGS
896	pCAGGS-ZEBOV-flag-VP40-W95A-E160A	827 sc(EcoRI,XhoI) pCAGGS
530	pCAGGS-ZEBOV-HA-VP40	858 sc(EcoRI,XhoI) pCAGGS
954	pCAGGS-ZEBOV-HA-VP40-W95A	929 sc(EcoRI,XhoI) pCAGGS
950	pCAGGS-ZEBOV-HA-VP40-E160A	936 sc(EcoRI,XhoI) pCAGGS
946	pCAGGS-ZEBOV-HA-VP40-W95A-E160A	932 sc(EcoRI,XhoI) pCAGGS
637	pCAGGS-ZEBOV-VP40-STP	ZEBOV-RNA rt(6041,6042); c(AgeI,XhoI) 875
919	pCAGGS-ZEBOV-NP	[95]
924	pCAGGS-ZEBOV-VP35	[95]
427	pCAGGS-ZEBOV-VP30	[95]
921	pCAGGS-ZEBOV-VP24	[95]
877	pCAGGS-ZEBOV-L	[95]
925	pCAGGS-ZEBOV-GP	[95]
920	pCAGGS-T7	[95]
747	pCAGGS-GFP	[95]
966	pCAGGS-MARV-Mus-VP24	kindly provided by Dr. Sandra Bamberg
	pCAGGS-MARV-Ang-VP24	kindly provided by Brittany Balcewich
918	pCAGGS-ZEBOV-NP-flag	919 pcr(6090,6091), c(XhoI,NheI) pCAGGS
734	pCAGGS-ZEBOV-VP35-flag	kindly provided by Dr. Peggy Möller
719	pCAGGS-ZEBOV-VP24-flag	kindly provided by Dr. Sandra Bamberg
	pCAGGS-ZEBOV-VP24-HA	kindly provided by Dr. Sandra Bamberg
923	3E5E-T7-ZEBOV-rluc	[95]
922	pGL2-control	Promega (#E1611)
582	pBind	Promega (#E2440)
581	pBind-id	Promega (#E2440)
585	pAct	Promega (#E2440)
583	pBind-myc	Promega (#E2440)
584	pG5luc	Promega (#E2440)
595	pBind-ZEBOV-VP40	875 pcr(6033,6034); c(BamHI,NotI) 582
688	pBind-ZEBOV-VP40-ΔC194	279 pcr(6033,6034); c(BamHI,NotI) 582

#	Construct	Cloning Strategy / Reference
867	pBind-ZEBOV-VP40-ΔC194-W95A	688 sdm(1267,1285)
789	pBind-ZEBOV-VP40-ΔC194-E160A	688 sdm(1268,1286)
824	pBind-ZEBOV-VP40-ΔC194-W95A-E160A	789 sdm(1267,1285)
608	pBind-NP	919 pcr(6035,6036); c(BamHI,NotI) 582
605	pAct-ZEBOV-VP40	875 pcr(6033,6034); c(BamHI,NotI) 585
694	pAct-ZEBOV-VP40-ΔC194	279 pcr(6033,6034); c(BamHI,NotI) 585
868	pAct-ZEBOV-VP40-ΔC194-W95A	694 sdm(1267,1285)
793	pAct-ZEBOV-VP40-ΔC194-E160A	694 sdm(1268,1286)
821	pAct-ZEBOV-VP40-ΔC194-W95A-E160A	793 sdm(1267,1285)
663	pAct-NP	919 pcr(6035,6036); c(BamHI,NotI) 585
571	pCDNA3.1-ZEBOV-flag-VP40	737 sc(EcoRI,XhoI)
574	pCDNA3.1-ZEBOV-flag-VP40-R134A	444 sc(EcoRI,XhoI)
837	pCDNA3.1-ZEBOV-flag-VP40-F125-R134A	574 sdm(1271,1272)
833	pCDNA3.1-ZEBOV-flag-VP40-W95A	571 sdm(1267,1285)
841	pCDNA3.1-ZEBOV-flag-VP40-E160A	571 sdm(1268,1286)
926	pCDNA3.1-ZEBOV-flag-VP40-W95A-E160A	833 sdm(1268,1286)
851	pCDNA3.1-ZEBOV-flag-VP40-ΔN14	571 dm2s(6155,6156,BsmBI)
	psiRNA-hH1neo	Invivogen (#ksirna2-n11)
653	pSIRNA-ZEBOV-VP40-NCR-0	hyb(6037,6038); c(BbsI) psiRNA-hH1neo
656	psiRNA-ZEBOV-VP40-NCR-1	hyb(6039,6040); c(BbsI) psiRNA-hH1neo
660	psiRNA-MARV-VP40-NCR-0	hyb(6043,6044); c(BbsI) psiRNA-hH1neo

A.14 Primers

Primers were either synthesized in house by the CSCHAH DNA core, or ordered from Operon. The following primers were used:

1267	gcaaattccaattgcgcttcctctaggtgtc
1268	ggttttcctccaggcgttcgttcttccgcc
1271	cactatcacccatgccggcaaggcaac
1272	gttgccttgccggcatgggtgatagtg

1273	caatccacttgtcgcagtcaatcggctggg
1274	cccagccgattgactgcgacaagtggattg
1285	gacacctagaggaagcgcaattggaatttgc
1286	ggcggaagaacgaacgcctggaggaaagcc
1482	catattgaattcccatggtat
1483	gaggccatataccctgtcagg
1484	gtcgatggtgtcatcggcaat
1485	catgccagccacacaccaggc
1486	acaccaggcagtgtgtcatca
1487	gcctggtgtgtggctggcatg
1488	aagacctacagctttgactca
1489	aaagctgtaggtcttttgatc
1490	gcttcatacactatcacccat
1491	agcaagcatgatggcggccgt
1492	tgccttgccgaaatgggtgat
1493	ggtcctggaatcccggatcat
1494	tccaggacccagccgattgac
1495	gggatgatccgggattccagg
1496	attggaaaccaggctttcctc
1497	tccaattcgcaggagcctgag
1498	aaccaggctttcctccaggag
1499	ctccaggagttcgttcttccg
1500	gaggaaagcctggtttccaat
1501	ccagtccaactaccccagtat
1502	ccccagtatttcacctttgat
1503	caaatcaaaggtgaaatactg
1504	gctgcaacatggaccgatgac
1505	gtcatcggtccatgttgcagc
1506	cgctccatttgatcctgttgg
1507	ttttggatgaaatgaaattcc
1508	aacaaaagtgggaagaagggg
1509	ccccttcttcccacttttgtt
1510	gtcctggagtgaagtcattat
1511	tttaagatcgttccaattgat
1512	ccagaaactctggtccacaag
1513	tggcacttcgattcccatgat
1514	aagaaggtgacttctaaaaat

1515	ttgtccatttttagaagtcac
1516	caaaagaacagggatgatggt
1517	ccaaagtacattgggttggac
1518	gtctcctggagccaccgggtc
1519	ctcaccatggtaatcacacag
1520	tgtgattaccatggtgaggtc
1521	caggattgtgacacgtgtcat
1522	taattgcaataattgactcag
1585	ggaattcaatatggactacaaggacgacgatgacaagaagaggcgggttatattgcctactgctc
1586	ggaattcaatatggcttacccttatgatgtgccggattatgccaggcgggttatattgcctactgctc
1587	ggaattcaatatggaacaaaaactcatctcagaagaggatctgaggcgggttatattgcctactgctc
1588	ggtaccctcgagctggatctgag
6033	gcggatccatatgaggcgggttatattgcctac
6034	ctagctaattaagagctcgcg
6035	gcggatccttatggattctcgtcctcagaaaatctg
6036	cagcggccgctcactgatgatgttgcaggattgc
6037	acctcgaatcttctcagggatagtgatcaagagtcactatccctgagaagattctt
6038	caaaaagaatcttctcagggatagtgactcttgatcactatccctgagaagattcg
6039	acctcgcatgcttacatctgaggatatcaagagtatcctcagatgtaagcatgctt
6040	caaaaagcatgcttacatctgaggatactcttgatatcctcagatgtaagcatgcg
6041	catgggaatcgaagtgccagaaac
6042	gactcgagctatcctcagatgtaagcatgc
6043	acctcgtgccctccattgctaagtcatcaagagtgacttagcaatggagggcactt
6044	caaaaagtgccctccattgctaagtcactcttgatgacttagcaatggagggcacg
6157	gctagccgtctcggatggaggccatataccctgtcag
6158	cgctagcgtctctcatcttcttgtcatcgtcgtccttg

B List of Abbrevations

BSC	biosafety cabinet
BSL	biosafety level
CAT	chloramphenicol acetyl transferase
cRNA	antigenomic viral RNA
CSCHAH	Canadian Science Centre for Human and Animal Health
DC	dendritic cell
DIC	disseminated intravascular coagulation
DNA	desoxyribonucleic acid
dsRNA	double stranded RNA
EBOV	Ebola virus
eGFP	enhanced green fluorescent protein
EHF	Ebola hemorrhagic fever
ER	endoplasmic reticulum
ESCRT	endosomal sorting complex required for transport
FACS	flow cytometry assisted cells sorting
FFU	focus forming units
GP	glycoprotein
HDVrib	hepatitis delta virus ribozyme
IFN	interferon
iVLP	infectious virus like particle
kB	kilobases
kDa	kilodalton
MOI	multiplicity of infection
MVB	multivesicular body
NCR	non-coding region
NEB	New England Biolabs
NHP	non-human primate
NK cell	natural killer cell
NO	nitric oxide
ORF	open reading frame
PBS	phosphate buffered saline
PCR	polymerase chain reaction
p.i.	post infection
PLB	passive lysis buffer
Pol-I	RNA polymerase I
p.t.	post transfection
PVDF	polyvinylidene fluoride
RLU	relative light units
RNA	ribonucleic acid
RNP	ribonucleoprotein
RPM	rotations per minute
RSV	respiratory syncytial virus
RT	room temperature
RT-PCR	reverse transcriptase
SDS-PAGE	sodium dodecyl sulfate polyacrylamide gel electrophoresis
STAT	signal transducer and activator of transcription
T7	T7 RNA polymerase

TAE	tris acetate EDTA
TBS	tris buffered saline
TF	tissue factor
TLC	thin layer chromatography
TNF	tumor necrosis factor
VLP	virus like particle
VP	virion protein
vRNA	viral genomic RNA
VSV	vesiculo stomatitis virus
WT	wild-type

Amino acids are given in one letter code as follows:

A	alanine
C	cysteine
D	aspartic acid
E	glutamic acid
F	phenylalanine
H	histidine
I	isoleucine
K	lysine
L	leucine
M	methionine
N	asparagine
P	proline
Q	glutamine
R	arginine
S	serine
T	threonine
V	valine
W	tryptophane
Y	tyrosine

C Curriculum vitae

Personal Details

Name	Thomas Hoenen
Address:	605-55 Garry St., Winnipeg MB, R3C 4H4, Canada
Date of Birth	March 5th, 1979
Place of Birth	Aachen, Germany

Education

since July 2004	stay in the Special Pathogens Program at the Canadian Science Centre for Human and Animal Health, Winnipeg, Canada, as part of my PhD training
since January 2004	PhD training at the Department for Virology, Marburg
July 2003 to December 2003	research training in the Special Pathogens Program at the Canadian Science Centre for Human and Animal Health, Winnipeg, Canada
October 2002 to June 2003	diploma thesis at the Department for Virology, Marburg
August 1999 to September 1999	research training at the Department for Botany and Molecular Biology, RWTH Aachen
October 1998 to June 2003	study of human biology at the Philipps University Marburg
1989 to 1998	Bischöfliches Pius-Gymnasium Aachen (grammar school)
1985 to 1989	Domsingschule Aachen (primary school)

Alternative Service

1997 to 2003	German Federal Agency for Technical Relief (THW), Aachen / Marburg

Support

January 2004 to December 2005	scholarship holder of the German Chemical Industry Association (VCI)
January 1999 to December 2003	scholarship holder of the German National Merit Foundation
since August 2000	scholarship holder of e-fellows.net
July to August 1997	participant at the German Pupils Academy, arranged by "Bildung and Begabung e.V."

Voluntary Service

May 2001 to June 2003	member of the committee for reorganisation of allocation of funds at the faculty of medicine
2001 to 2003	member of several appointment and habilitation committees (C4 professorship Immunology, C4 professorship Virology, habilitation Dr. Herz, Dr. Wolf and Dr. ter Meulen)
October 2000 to February 2001	member of the faculty council of the faculty of medicine
January 2000 to June 2003	member of the student representatives for human biology and medicine
August 1998 to June 2004	member of "Faith and Light", social and religious oriented work with mentally disabled persons

Publications

Papers

July 2006 — **T. Hoenen**, A. Groseth, L. Kolsnikova, S. Theriault, H. Ebihara, B. Hartlieb, S. Bamberg, H. Feldmann, U. Ströher, S. Becker. *Infection of naïve target cells with ZEBOV-iVLPs - implications for the role of VP24.* J. Virol. 80(14):7260-7264

May 2006 — **T. Hoenen**, A. Groseth, D. Falzarano, H. Feldmann. *Ebola virus: Unravelling pathogenesis to combat a deadly disease.* Trends Mol Med. 12(5):206-215

February 2005 — **T. Hoenen**, V. Volchkov, L. Kolesnikova, E. Mittler, J. Timmins, M. Ottmann, O. Reynard, S. Becker, W. Weissenhorn. *VP40 Octamers are essential for Ebola virus replication.* J. Virol. 79(3):1898-1905

Abstracts

September 2006 — **T. Hoenen**, N. Krowchuk, F. Zielecki, H. Feldmann, U. Ströher, S. Becker. *Ebola virus matrix and nucleoprotein interactions.* 3rd International Symposium on Filoviruses, Winnipeg, MB, Canada - poster presentation

September 2006 — A. Groseth, **T. Hoenen**, J. Alimonti, F. Zielecki, H. Ebihara, U. Ströher, S. Becker, H. Feldmann. *Application of minigenome systems for siRNA screening and identification of an NP directed plasmid-driven small hairpin RNA that can inhibit Ebola virus infection.* 3rd International Symposium on Filoviruses, Winnipeg, MB, Canada - poster presentation

June 2006 — A. Groseth, **T. Hoenen**, S. Becker, U. Ströher, H. Feldmann. *Regulation of filovirus transcription by VP30: More than just a hairpin?* 13th International Conference on Negative Strand Viruses, Salamanca, Spain - poster presentation

March 2006	**T. Hoenen**, A. Groseth, B. Hartlieb, H. Feldmann, U. Ströher, S. Becker. *Role of Ebola virus VP24 and VP30 in ribonucleoprotein complex formation.* 1st Annual Public Health Agency of Canada Research Forum, Winnipeg, MB, Canada - poster presentation
March 2006	A. Groseth, **T. Hoenen**, S. Theriault, H. Ebihara, S. Jones, H. Feldmann. *siRNA strategies for the control of Ebola virus infection.* 1st Annual Public Health Agency of Canada Research Forum, Winnipeg, MB, Canada - poster presentation
October 2005	**T. Hoenen**, A. Groseth, U. Ströher, H. Feldmann, S. Becker. *Studying the life cycle of Ebola virus with infectious virus like particles.* 1st Annual International Centre for Infectious Diseases Retreat, Winnipeg, MB, Canada - poster presentation
October 2005	A. Groseth, **T. Hoenen**, S. Theriault, H. Ebihara, H. Feldmann. *siRNA strategies for the control of Ebola virus infection.* 1st Annual International Centre for Infectious Diseases Retreat, Winnipeg, MB, Canada - poster presentation
July 2005	**T. Hoenen**, A. Groseth, U. Ströher, H. Feldmann, S. Becker. *Study of Ebola VP40 octamerization using minigenome virus-like particles.* 13th International Congress of Virology (ICV) / Joint Meeting of the 3 Divisions of the International Union of Microbiological Societies (IUMS), San Francisco, CA, USA - oral presentation
July 2005	A. Groseth, **T. Hoenen**, R. Flick, H. Feldmann. *Using reverse genetics to explore filovirus transcription and replication.* 13th International Congress of Virology (ICV) / Joint Meeting of the 3 Divisions of the International Union of Microbiological Societies (IUMS), San Francisco, CA, USA - oral presentation
June 2005	**T. Hoenen**, L. Kolesnikova, W. Weissenhorn, V. Volchkov, E. Mittler, U. Ströher, H. Feldmann, S. Becker. *Role of VP40 octamerization for the viral life cycle.* 24th annual meeting of the American Society for Virology (ASV), Penn State University, PA, USA - oral presentation
March 2004	**T. Hoenen**, L. Kolesnikova, V. Volchkov, W. Weissenhorn, S. Becker. *Role of RNA binding for Ebola virus VP40 octamerization.* Annual Meeting of the German Society for Virology 2004, Tübingen, Germany - oral presentation

D List of academic teachers

My academic teachers were in Marburg Drs. Aumüller, Becker, Berndt, Daut, Elsäßer, Engelhardt, Frenking, Garten, Grzeschik, Gudermann, Heeg, Jungclas, Kaiser, Kirchner, Klenk, Knöller, Koch, Kuhn, Lenz, Lill, Rogausch, Schäfer, Schulz, Seitz, Tampé, Voigt, von Löw, Weihe, Westermann, and in Winnipeg Drs. Feldmann and Ströher.

E Acknowledgements

This work would not have been possible without the support of many great people. First of all I would like thank my three supervisors, and especially the main supervisor of my thesis, Stephan Becker. He has not only taught me how to become a scientist, but also supported me in all my decision, regardless of his own benefit, and was always there for me, even if we were thousands of kilometers separated. Also I would like to thank my supervisors at the Canadian Science Centre for Human and Animal Health in Winnipeg, Ute Ströher and Heinz Feldmann. Heinz has provided me the opportunity to perform a big part of my practical work in his group at the CSCHAH, and taught me a lot about how the scientific system in North America works, and how to evaluate and write grants and papers. But mostly he is a wonderful person to work for, and provides an incredible amount of care for his students, among them I count myself. Ute hosted me in her lab, she was always there when I had questions or problems, and she taught me a lot about the practical aspects of science. She has been a great supervisor, but maybe even more important a good friend.

In Marburg as well as in Winnipeg I had the privilege to work with some extraordinary people. Among them were three scientists, Hideki Ebihara, Larissa Kolesnikova and Allison Groseth, who impressed me with their skills and knowledge as well as with their dedication towards science, and with whom I had many helpful discussions.

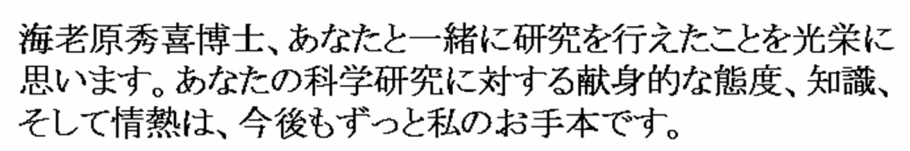

Лариса, мне было очень приятно с Вами работать и я также был бы рад сотрудничать с вами в дальнейшем.

Allison has for the last three years also been the best companion in life I can imagine, and not only carried me through the downs that come with doing ones PhD, but also given and shared with me many of the most wonderful moments of my life.

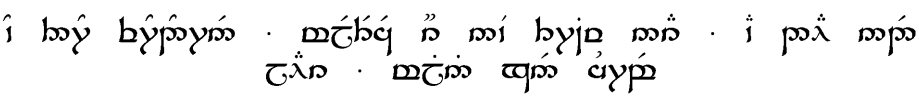

This work would also not have been possible without the help of many others. First

and foremost I want to mention the students who helped me with individual parts of my projects, Anja Klussmeier, Eva Mittler, Florian Zielecki, Natasha Krowchuk and Brittany Balcewich. It has been a pleasure to work with you guys, and I am looking forward to continue working together with you in future. I also want to thank the technicians and scientists both in Winnipeg and in Marburg, who have been extremely supportive. I especially want to thank Angelika Lander for all the constructs she sent me whenever I needed them. Also, Judie Alimonti and Lisa Fernando have been a great help with FACS analysis, and Jim Strong was always there for me when I needed some blood taken. Finally I want to thank all people in the Special Pathogens Program and in the Department for Virology in Marburg, especially the old G23 crew, for an awesome time and all the things you have done for me.

Nicht vergessen möchte ich meine Familie und Freunde. Nach Kanada zu gehen war für mich eine wunderbare Erfahrung, aber auch schwer, weil es mich sehr weit von Euch entfernt hat. Für Eure Unterstützung bin ich unendlich dankbar, und für all die Anrufe, Emails und die Zeit, die Ihr immer für mich hattet, wenn ich zu Besuch in Deutschland war. Besonders danken möchte ich meinen Eltern, für die meine Entscheindung wohl mit am schwersten war, und die mich nichtsdestotrotz in dieser wie auch in allen meinen anderen Entscheidungen immer unterstützt und mich meinen eigenen Weg haben gehen lassen. Ihr könnt Euch nicht nicht vorstellen, wie oft ich mich auch heute noch an die Dinge erinnere, die Ihr für mich getan habt!

Although I would have had good reasons to dedicate this thesis to every single one of the above mentioned, I decided to dedicate it to two persons, who have most influenced me in my decision to become a scientist, and in particular a human biologist. These people are my former biology teacher, Monika Ochel, who has excited my love for medical science, and Wolfgang Reinert, who has reinforced this and steered me in the right direction.

Finally, I want to thank the organizations which have funded my throughout my PhD studies, the German Chemical Industry Association (VCI) and especially Stefanie Kiefer, the German Research Association, the Department for Virology of the Philipps University Marburg and it's head, Dr. Hans Dieter Klenk, and the Public Health Agency of Canada.

F Ehrenwörtliche Erklärung

Ich erkläre ehrenwörtlich, dass ich die dem Fachbereich Medizin Marburg zur Promotionsprüfung eingereichte Arbeit mit dem Titel "Function of the Viral Matrix Proteins VP40 and VP24 for the Life Cycle of Ebola Virus" im Institut für Virologie des Medizinischen Zentrums für Hygiene und Infektionsbiologie unter Leitung von Prof. Dr. Klenk mit Unterstützung durch PD Dr. Becker und am Canadian Science Centre for Human and Animal Health in Winnipeg, Kanada, mit Unterstützung durch Dr. Feldmann und Dr. Ströher ohne sonstige Hilfe selbst durchgeführt und bei der Abfassung der Arbeit keine anderen als die in der Dissertation angeführten Hilfsmittel benutzt habe. Ich habe bisher an keinem in- und ausländischen Medizinischen Fachbereich ein Gesuch um Zulassung zur Promotion eingereicht noch die vorliegende oder eine andere Arbeit als Dissertation vorgelegt. Teile aus der vorliegenden Arbeit wurden in folgenden Publikationsorganen veröffentlicht:

Original-Arbeiten:

T. Hoenen, V. Volchkov, L. Kolesnikova, E. Mittler, J. Timmins, M. Ottmann, O. Reynard, S. Becker, W. Weissenhorn. (February 2005) VP40 Octamers are essential for Ebola virus replication. J. Virol. 79(3):1898-1905

T. Hoenen, A. Groseth, L. Kolsnikova, S. Theriault, H. Ebihara, B. Hartlieb, S. Bamberg, H. Feldmann, U. Ströher, S. Becker. (June 2006) Infection of naïve target cells with ZEBOV-iVLPs - implications for the role of VP24. J. Virol. 80(14):7260-7264

Abstracts:

T. Hoenen, L. Kolesnikova, V. Volchkov, W. Weissenhorn, S. Becker. (March 2004) Role of RNA binding for Ebola virus VP40 octamerization. Annual Meeting of the German Society for Virology 2004, Tübingen, Germany - oral presentation

T. Hoenen, L. Kolesnikova, W. Weissenhorn, V. Volchkov, E. Mittler, U. Ströher, H. Feldmann, S. Becker. (June 2005) Role of VP40 octamerization for the viral life cycle. 24^{th} annual meeting of the American Society for Virology (ASV), Penn State University, PA, USA - oral presentation

T. Hoenen, A. Groseth, U. Ströher, H. Feldmann, S. Becker. (July 2005) Study of Ebola VP40 octamerization using minigenome virus-like particles. 13^{th} International Congress of Virology (ICV) / Joint Meeting of the 3 Divisions of the International Union of Micro-

biological Societies (IUMS), San Francisco, CA, USA - oral presentation

T. Hoenen, A. Groseth, U. Ströher, H. Feldmann, S. Becker. (October 2005) Studying the life cycle of Ebola virus with infectious virus like particles. 1st Annual International Centre for Infectious Diseases Retreat, Winnipeg, MB, Canada - poster presentation

T. Hoenen, A. Groseth, B. Hartlieb, H. Feldmann, U. Ströher, S. Becker. (March 2006) Role of Ebola Virus VP24 and VP30 in ribonucleoprotein complex formation. 1st Annual Public Health Agency of Canada Research Forum, Winnipeg, MB, Canada - poster presentation

T. Hoenen, N. Krowchuk, F. Zielecki, H. Feldmann, U. Ströher, S. Becker. (September 2006) Ebola virus matrix and nucleoprotein interactions. 3rd International Symposium on Filoviruses, Winnipeg, MB, Canada - poster presentation

Winnipeg, den 25. September 2006, _____